Characterization of the Physical and Hydraulic Properties of Peat Impacted by a Temporary Access Road

by

Jenna K. Pilon

A thesis

presented to the University of Waterloo

in fulfillment of the

thesis requirement for the degree of

Master of Science

in

Geography

Waterloo, Ontario, Canada, 2015

Author's Declaration

I hereby declare that I am the sole author of this thesis. This is a true copy of the thesis, including any required final revisions, as accepted by my examiners.

I understand that my thesis may be made electronically available to the public.

Abstract

Due to the disruption of hydrology and water quality, permanent installation of roads and well pads is a practice that is discouraged. It is becoming more common to install temporary structures, which can subsequently be removed. However, little is known regarding the temporary or permanent hydrologic and biogeochemical impacts of temporary structures.

In 2013, a temporary Access Road (at Pad 106) within the Firebag Fen in northeast Alberta was reclaimed to evaluate immediate and longer-term hydrologic and biogeochemical responses within the fen. Prior to its removal, the road hindered the natural water flow, and the restriction of runoff by the road led to vegetation mortality on the up-gradient (wet) side of the road. The long-term goal of the Suncor Firebag Road Removal Reclamation Project was to determine the capacity of the affected fen to naturally self-correct and self-regulate following road removal before intervention attempts. The specific objectives of this thesis are to: (1) compare peat physical characteristics and hydraulic conductivity in disturbed peat and undisturbed peat; and (2) determine the rate of change in water table and hydraulic gradients on both sides of the road immediately following road removal.

Coring locations and groundwater well sites were located along transects running perpendicular to the road and, once the road was removed, on the peat that was underneath the road. Cores were collected for the determination of peat physical characteristics. Groundwater wells were installed for the determination of water table position and hydraulic gradients. Meteorologic conditions were monitored with a on-site station at the Firebag Fen site and showed variability between monitoring stations, and across the road, but consistently over time.

Results indicate that the direction of flow was diagonal to the road. Heads decreased from the east (566.01 m.a.s.l mean) to the west (565.33 m.a.s.l mean) over 179 m and from Transect 1 (565.54 m.a.s.l mean) to Transect 4 (565.86 m.a.s.l mean) over 182 m. Median saturated hydraulic conductivity determined from laboratory measurments did not vary between the road and adjacent peatlands (10^{-3} – 10^{-2} m/s). Significant differences between the road and adjacent peatlands were not found for saturated hydraulic conductivity ($p < 0.05$). Porosity, bulk density, and specific yield varied significantly ($p < 0.05$) between peat on the east side of the road and the peat beneath the removed road. Porosity and bulk density also

differed significantly between the east and west sides of the road ($p < 0.05$). Immediately following road removal, peat subsidence beneath the road was apparent. However, as the summer 2013 field season progressed, measured rates of peat subsidence began to slow 45 days post road removal, suggesting that the peat may have begun to rebound.

Acknowledgements

There are a number of people without whom this thesis might not have been written, and to whom I am greatly indebted.

I want to thank my supervisors, Richard Petrone and Merrin Macrae. I am very appreciative of your support and guidance. Thanks also to Jonathan Price and Mike Stone for serving as members of my Examining Committee.

I am very thankful for all the help I received during fieldwork while working on the project with Suncor Energy at Firebag Village Camp in the summer of 2013. A huge thank you goes out to Corey Vogel, Chuck Symons, Jon Downs, Matt Billadeau, Zac Moody, Kyle Seipert and Lyle Seipert. The University of Waterloo Meteorology Research lab also deserves thanks: Jonathan Price, George Sutherland, James Sherwood, Scott Brown, Alex MacLean, Corey Wells, Vito Lam, Adam Green and Tristan Gingras-Hill. Thank you for your assistance on this project. I would like to acknowledge James McCarthy for his ongoing advice and assistance with GIS: thank you! A huge word of thanks also goes out to Adam Lentz, Thomas Pertassek, Tobias KD Weber, and Richard Elgood; thank you for your help and support! I am specifically grateful for Terry Osko's insightful advice. Your generous feedback and positivity made this project possible!

A HUGE thank you goes out to my mom and dad for their encouragement, love and support throughout all my school years. Thank you for everything!

Dedication

For my parents.

"As we express our gratitude, we must never forget that the highest appreciation is not to utter words, but to live by them." ~*John F. Kennedy*

♥

Table of Contents

List of Figures

List of Tables

List of Appendices

1.0 Introduction

One of the largest intact ecosystems on the planet is Canada's boreal region, which contains a quarter of the world's vast relatively undisturbed forest ecosystems called frontier forests, which are able to maintain all their biodiversity (Bryant et al., 1997). Wetlands are a critical component, accounting for 30 % of the Canadian boreal ecozone. Wetlands dominate the landscape in northeastern Alberta, Canada, making up 50 % of the land base. In addition, over 90 % of Alberta wetlands are considered peatlands (Vitt et al., 1996). Wetlands facilitate invaluable environmental services such as acting as carbon sinks, stabilizing the water cycle, and providing habitat for fauna and flora. Peatlands, in particular, are an important constituent of the global carbon cycle, storing approximately one-third of the world's total soil carbon (Gorham, 1991; Turunen et al., 2002).

Oil sand development in Alberta's Athabasca oil sands region is among the most extensive in the world. It is estimated that Canada's oil sand resources contain approximately 28.3 billion cubic meters of recoverable bitumen (Evans et al., 2002). The Athabasca Basin, located within the Western Boreal Plain (WBP), contains the largest deposit, known as the Athabasca deposit. Approximately 80% of the bitumen located within the Athabasca deposit cannot be reached by surface mining (Alberta Culture and Tourism, n.d.), but rather by in-situ extraction operations. Development began in 1967 by the Great Canadian Oil Sands Company, now known as Suncor Energy Inc. The oil sand development has significantly impacted the wetlands of Alberta through the construction of roads, pipelines, seismic lines, power transmission lines and well pads. For example, a study by Turetsky and St. Louis (2006), though located in Germany, showed that 236 gravel roads and 1,600 well sites crossed a study area of 6,000 km^2. Fragmentation caused by linear disturbances can undermine the integrity of the boreal wetland ecozone. Though the development of the oil sands is certain, the footprint of such disturbances can be mitigated through best management practices and restoration of infrastructure after decommissioning.

The oil sand industry located in Alberta has rapidly developed and grown throughout the last decade. As technological advances continue to lower costs associated with oil sand refining, and global conventional oil supplies decline, the oil sand projects of the Athabasca Basin will continue to expand. Though chemical contamination is, and will remain, an

important concern with the continued development of the oil sands, the direct physical disturbances by infrastructure should also be given considerable attention.

Access infrastructure in the Western Boreal Plain is often constructed through peatlands containing sensitive fauna and flora. Roads, although necessary and important, are damaging to northern peatlands, and in some cases are more detrimental than pipelines. Even temporary access roads act as barriers to surface water and severely disrupt, or prevent groundwater flow at and below the ground surface (Turcheneck, 1990; Clymo and Hayward, 1982). Roads also greatly affect local habitat and nearby vegetation with road dust and chemical contaminants (Howell et al., 2014; Forman and Alexander, 1998; Coffin, 2007), and severely compact the peat column. For all these reasons, roads may profoundly impact hydrological processes, which are vital for surface vegetation and a healthy ecosystem.

The goal of this thesis research is to improve our understanding of the direct effect of roads on peatland hydrology and peat physical characteristics and the recovery of the peat following road removal. There is a paucity of information on this topic, and what research there is has focused largely on ecological processes. This thesis examines peat physical characteristics at upstream, downstream and under-road locations before and after road removal. Specific areas of concern relate to quantifying the immediate impact of the road on the peat column; comparing peat physical characteristics along transects of undisturbed peat and under road locations; and recording changes in the hydrologic environment before and after road removal, as the system shifts to equilibrium.

From a sustainability perspective, it is important to quantify the direct and long-term effects of roads on peatland hydrology. Plans to restore or re-vegetate an area disturbed by roads cannot be implemented without quantifying the state of the peat profile, which serves as the substructure for water transmission and establishment of peatland vegetation.

The specific objectives of this thesis research are:

1. To determine how physical characteristics differ between peat beneath and adjacent to a temporary Access Road, and quantify the distance from the road to which any observed differences can be detected;
2. To determine if hydrologic flow beneath the road was impeded by peat compression;

3. To assess changes in peatland hydrologic gradients over one summer season immediately following road removal to infer how peatland hydrology may be restored following road removal.

1.1 Literature Review

1.1.1 Western Boreal Forest and Athabasca Oil Sands Region

The boreal forest of Canada, one of the world's largest forested biomes, covers nearly 30 % of the landmass of North America (Pojar, 1996). The Western Boreal Plain region extends west from Manitoba, meets the Rocky Mountains, and reaches north to Alaska, ranging in elevations from near sea level to about 1000 meters above sea level (m.a.s.l.) in the northern Rocky Mountains. The ecozone overlaps with sub-alpine forest in northern Alberta and northern British Columbia (Pojar, 1996).

The WBF lies within the rain shadow of the Rocky Mountains creating a subhumid climate where annual precipitation, is generally half to one third that of the eastern boreal regions of Ontario and Quebec (Environment Canada, 1990; Rizzo and Wiken, 1989) and is often exceeded by potential evapotranspiration (Devito et al., 2005). The landscape in the WBP is characterized by gently rolling relief as well as a mosaic of fragmented upland forests, riparian ecosystems, and pond-peatland complexes (Petrone et al., 2008; Rizzo and Wiken, 1989). The uniqueness of the WBP in terms of climate, surficial geology, and terrestrial ecology make it difficult to extrapolate eco-hydrological process studies and impacts of land use on Aspen from other region of the Boreal or Temperate forests.

The present distribution of vegetation zones within the boreal ecozone are largely determined by climate in the circumpolar north of Canada (Hogg, 1994). Evergreen coniferous forest is a function of the climate of the boreal zone. Mature vegetation of the boreal forest thrives in well-drained areas. Coniferous trees are the prevailing mature vegetation within the vast boreal forest region. In addition, deciduous broadleaf and mixed forests are often extensive and common. The dominant coniferous species include *Picea*, *Pinus*, and *Larix*, while dominant deciduous hardwoods consist of the species *Populus* and *Betula*. Productivity is limited by low temperature coupled with high soil moisture, build-up

of forest floor biomass, slow decomposition rates, and acidic soil, low levels of available nitrogen and limited nutrient cycling.

The boreal forest is the biome occupying the region between 50 and 70 degrees north, which is dominated by the Canadian and Siberian landmasses (Baldocchi et al., 2000). The Western Boreal Forest is distinct from other biomes because it experiences a relatively short growing season and extremely cold winter temperatures. There is a steady decrease in incoming solar radiation, a pronounced decrease in mean annual temperatures, an increase in the duration of winter, a marked decline in precipitation, and an increase in wind speeds, all progressing gradually northward from the boreal to the Canadian arctic (Eugster et al., 2000).

Because of its great size (12.0-14.7 million km^2), large biomass, and distinct climate, the boreal forest is of particular importance for climate change researchers. Despite its significance, measurements of mass and energy exchange have been rare. However, Baldocchi et al. (2000) conducted research on how the boreal forest interacts with the atmosphere, which is important in understanding how the interception of solar energy heats the surrounding canopy, air and soil. Further, the Western Boreal Plain region is located within the Mixedwood Boreal Plains Ecozone, at the transition between the Mid- and High Continental Boreal Subregion (National Wetlands Working Group, 1988). Mean normal summer (July) and winter (January) temperatures for the region are 15.7 and –14.6 °C, respectively (Marshall et al., 1999). Normal annual precipitation and potential evapotranspiration in the region nearly balanced at 515 and 517 mm, respectively (Marshall et al., 1999). 50-60 % of the annual precipitation occurs on average between June and August, followed by drier autumn months (Marshall et al., 1999). Thus, the pond-riparian-forest mosaic in the Western Boreal Forest is sustained by infrequent wet years within periods of drought, and while mild within a geological context, potential evapotranspiration (PET) exceeds precipitation (P) in most years with infrequent wet years occurring on a 10 – 15 year cycle (Marshall et al., 1999; Devito et al., 2005). Thus, the wetlands and ponds within this region are vulnerable to any climatic change that may alter patterns of P and actual evapotranspiration (AET). Indeed, air photos show that vegetation succession within changing pond surface areas has varied significantly over the past 60 years (Devito et al., 2005).

1.1.2 Peatland Ecohydrology

Peatlands are the product of complex interactions of biotic and abiotic processes typically occurring over the course of thousands of years. Specific gradients of latitude and longitude account for a distinct pattern of peatland distribution, occurring globally between latitudes of 45 and 65 ° N and S (Price et al., 2003). These gradient margins have been found to control peat accumulation through plant productivity and decomposition as well as moisture availability, which is a direct function of atmospheric water supply and evapotranspiration. When these conditions are amplified and favorable, peatlands may begin to form within the landscape. Fens are peatlands that are less acidic and can be nutrient rich in comparison to ombrotrophic bogs (Pojar, 1996), which are peatlands that receive nutrients only by atmospheric means.

Peatlands cover a relatively small portion of the Earth's land area (~3 %), but these unique ecosystems are a globally important carbon store due to their high carbon density per unit area (50 to > 500 km C m^{-2}) (Frolking et al., 2011). Peatlands cover 12 % (1.136 million km^2) of Canada's land area (mostly within boreal and subarctic regions), with perennially frozen arctic peatlands covering 37 % (Tarnocai et al., 1995). Canadian peatlands contain a vast store of soil organic carbon (147 Gt, 56 % of Canadian soil organic carbon) (Tarnocai et al., 1995). Approximately one-third of the world's soil carbon pool is contained within worldwide peatland ecosystems (Gorham, 1991). The accuracy for peatland estimates presented by Tarnocai et al. (1995) have likely > 66 % probability. The estimates are based on the confidence levels used in the IPCC Fourth Assessment.

Peatlands are ecosystems with a surface layer of partially decomposed organic matter called 'peat,' which is greater than 40 cm in thickness. Peat forms in-situ, and is often saturated from the bottom to the surface (Frolking et al., 2011). Peatlands are unique from an ecological perspective, as these environments provide habitat for specialized and rare plants and animals. Peatlands currently function as a net sink for atmospheric CO_2, and can sequester an estimated 76 Tg yr^{-1} of atmospheric carbon (Turetsky et al., 2000).

The broad influences of regional climate upon peatlands and peatland distribution have been recognized in Canada by previous studies (Rubec, 1988). However, more research is needed to establish specific climatic conditions, such as temperature, precipitation, precipitation/evaporation quotients, etc., for Canadian peatlands (Gorham, 1994), as well as

surface radiation and energy balance, and how microclimatology influences peatland vegetation. Although Roulet (1990) and Heinselman (1963) provide information regarding peat temperature cycles as well as depth and duration of frost (of considerable interest for potential impacts of global warming), Gorham (1994) suggests that long-term monitoring of peat temperature profiles at depths, where seasonal cycling is low, might be a useful way of tracing global warming effects, while avoiding "noise" caused by day to day surface fluctuations. Climate-induced warming effects on peatland microclimates will strongly influence nutrient mineralization, plant growth and species composition, as well as trace gases, such as methane, as shown by previous studies by Van Cleve et al. (1990), Moore and Knowles (1990), Roulet et al. (1992) and Dise et al. (1993). Therefore, it is of the utmost importance that attention is paid to microclimatological research of peatlands.

Sphagnum mosses in North America cover large areas in the form of arctic, alpine, tundra, taiga, boreal and sub-boreal bogs, fens and other peatlands (Quinton et al., 2009). Among these peat deposits, similarities exist in their physical properties as a direct function of the widespread *Sphagnum* mosses (Quinton et al., 2000). Peatlands have distinct microforms: hummock, lawn and hollow, although predominantly hummocks and hollows (Clymo, 1973; Rydin, 1993). Within these microforms, different *sphagnum* species occupy different ecological niches as a function of growth height above the water table (McCarter and Price, 2012). Fibric peat, found near the surface of a peatland, is highly permeable and composed of poorly decomposed peat. In contrast, sapric peat is deeply humified with low hydraulic conductivity. Unlike fibric peat, sapric peat is found near the bottom of the peat column. These two classifications, in conjunction with an intermediate, hemic peat, allow for the characteristic high water table level observed in wetland environments (Letts et al., 2000).

Peat below the lowest annual average water table is referred to as the 'catotelm' and is characterized by relatively small average pore diameter and low hydraulic conductivity. Above this region exists the 'acrotelm,' which is composed of plant structures ranging from lightly to moderately decomposed peat material at depth. In addition, this upper layer consists of living to undecomposed mosses and exhibits a larger average pore diameter (Rezanezhad et al., 2009) and higher hydraulic conductivity at the surface. When peat materials within this region drain, they exhibit poor water retention and subsequently low soil

moisture retention (Price and Whittington, 2008); thus, this region has a very limited ability to sustain upward water transmission (Price and Whittington, 2010).

Peat differs in its hydraulic properties in comparison to mineral soil, which suggests that mineral soil parameters are inadequate for quantifying and modeling wetland environment processes (Letts et al., 2000). The species type and community arrangement, along with the degree of decomposition of the environment, impart a specific and unique pore geometry and tortuosity that controls the water retention capacity of sphagnum mosses (Price et al., 2008; Rezanezhad et al., 2009). These hydraulic properties govern the level of saturation that can be sustained at a given water table (soil-water pressure) and consequently the rate of water flow within the living sphagnum and the decomposed peat. These non-vascular plants lack root structure and are solely dependent on water retention and capillary rise for water supply (Clymo, 1973). In the natural environment, moss grows and is nourished upon its own remains, which results in an abrupt transition from subsurface dead mosses to living mosses near and at the surface. Water retention and capillary rise are generated by the unique structure of the plant and pore size distribution (Quinton et al., 2008). The species living on hummocks have great water retention capacity, possibly experiencing great net water loss by evaporation because of the plants' efficient capillary rise imparted by their pore size distribution and structure. In contrast, hollow species depend on their close proximity to the saturated zone because of their lower water retention characteristics and vulnerability to desiccation (Rydin, 1985b; Hajek and Beckett, 2008; Thompson and Waddington, 2008; Turetsky et al., 2008; McCarter and Price, 2012).

1.1.3 Physical Hydraulic Properties

Although the total porosity, specific yield, and bulk density of peat are well documented (Boelter, 1976; Boelter and Verry, 1977; Ingram, 1978), there is a paucity of data available describing the impact of roads on peat physical properties immediately following the road removal process. Knowledge of basic hydraulic properties including porosity, specific yield and bulk density after the removal of temporary access infrastructure will aid our understanding of the immediate and direct response of peat physical parameters after road removal and if intervention is needed to complete reclamation. The immediate and direct response of site hydrology upon road removal is important because any significant change is

expected to happen immediately following system disturbance, hence the importance of immediate measurements. It would be difficult to confirm the road peat is in a state of improvement if initial conditions were not monitored. Roads act as a hydraulic barrier impeding surface and subsurface water flow, which impacts water and solute fluxes, water storage mechanisms and hydraulic parameters. These components are expected to adjust in response to hydrologic change after road removal.

Knowledge of the unique physical properties of peat requires an understanding of the ability of this porous medium to store and transmit water. For example, bulk density increases as a function of depth because the peat column becomes more decomposed with depth below the ground surface. Particle size and interstitial pore space are an inverse function of peat depth, as these properties decrease in size with depth below the surface (Verry and Boelter, 1978; Quinton et al., 2000). Physical properties (porosity, specific yield, bulk density, water retention, saturated hydraulic conductivity, etc.) of peat-sand mixtures depend on the relation between mineral and organic parts (Walczak et al., 2002). In addition, physical hydraulic properties in hydrologically complex soils vary as a direct function of antecedent moisture conditions of the unique environmental landscape (Iden and Durner, 2008).

1.1.3.1 Porosity

The physical properties of any soil are largely dependent on pore size distribution and porosity. In peat, particle size, structure and porosity are a function of the state of decomposition (Boelter, 1969; Bachmann, 1996; Miatkowski et al., 1999). As peat decomposes, organic particle size decreases, and pores become smaller (Boelter, 1968). Peat soils are usually characterized by their very heterogeneous pore structure, or high proportion of both micropores and mezopores. The surface layer of peat at different development stages may have differing values in porosity (Zuidhoff, 2003). Considerable research has been conducted to determine the pristine, undisturbed physical hydraulic properties of peat (Silins and Rothwell, 1998; Schwarzel et al., 2006; Price et al., 2008). *Sphagnum* mosses are highly porous, contain large pores, and are highly tortuous. The total porosity of peat is approximately 0.90 (Boelter, 1968; Hobbs, 1986), which includes a volume fraction of relatively large, interstitial pore space that actively transmits water. Immobile water in the

small, closed-off pores formed by the remains of plant cells is referred to as 'inactive porosity.' Solute transport is dramatically affected by this complex dual porosity structure comprising the peat matrix (Rezanezhad et al., 2012). Total porosity generally decreases gradually with increased decomposition (Boelter, 1968).

Mineral soil theories are still largely the underlying basis of current research being conducted on peat soils. Peat has a remarkably high structural strength in comparison with mineral soils at similar water content due to its highly fibrous and organic nature (Zhang and O'Kelly, 2013)

The correlation between pore size distribution and particle size distribution is a practical approach taken for mineral soils but cannot be applied to peat deposits, as peat substrate does not consist of easily definable, individual grains. Mineral soil porosities typically range from 0.40 to 0.60 (Dingman, 1994), while the porosity of peat is rarely less than 0.80 (Radforth and Brawner, 1977). In peat, pore size distribution is heterogeneous (McCarter and Price, 2012), and water is absorbed to a high degree (Walczak et al., 2002).

1.1.3.2 Specific Yield

Specific yield (Sy) is the proportion of water yielded by gravitational drainage of a saturated volume of soil (Boelter, 1968; Hillel, 1998); however, it is incorrect to assume that there is a fixed value of drainable porosity and that soils drain instantly due to a change in the water table. For example, poorly decomposed peat, containing approximately 93 % water at saturation, releases up to 80 % of this water to drainage (Radforth and Brawner, 1977). In contrast, herbaceous peat contains less water at saturation and contributes less water during gravity drainage due to reduced pore size. Specific yield is substantially higher in fibric peat than in sapric peat or mineral soils, owing to the larger pore sizes common in fibric peat.

1.1.3.3 Bulk Density

Bulk density (g/cm^3) is defined as the mass of particles and water. It can be used as a measure of decomposition. The volume of peat is reduced substantially when dried (Boelter, 1968). Moreover, peat bulk density varies as a direct function of the load applied to it (Terzaghi, 1943). Kalia (1956) studied several characteristics of peat and concluded bulk

density could be used to approximate the degree of decomposition for peat material. McCarter and Price (2012) showed that bulk density increased with depth for three distinct and widespread species of sphagnum (*Sphagnum fuscum*, *Sphagnum rubellum* and *Sphagnum magellanicum*) while the ρb of the profiles and surface samples did not deviate significantly from each other. In general it is well known that deeper, more decomposed peat is more consolidated (Clymo, 1973; Ingram, 1978; Price et al., 2005). Price et al. (2005) discovered a relationship between bulk density and Von Post Scale of Humification (vP) values . Decomposed peat high on the vP scale generally had a higher bulk density. Price et al. (2005) conclusively established a clear inverse relationship between decreasing compressibility and increasing peat bulk density and vP.

Fibric peat, located at the surface of the peat column, is defined as having: porosity, θp, greater than 0.90 (or, 90 %); bulk density, ρb, less than 75 kg m^{-3}; specific yield, Sy, in excess of 0.42; and volumetric water content, θl, less than 0.48 at 1 m suction, ψ (Boelter, 1968). In contrast, the deeper, more humified sapric peat, is characterized by: $\theta p > 0.85$, $\rho b >$ 195 kg m-3, $Sy < 0.15$ and $\theta l > 0.70$ at $\psi = 1$m. The porosity of peat typically ranges from 0.81 to 0.95, but is greater in fibric peat than in sapric peat (Radforth and Brawner, 1977). Newly available technologies, such as 3-D computer tomography, provide alternative methods to evaluate porosity and the role of geometry in establishing the hydraulic properties of peat. Rezanezhad et al. (2009) found that in using 3-D computer tomography there is, in general, an increase in air-filled porosity and average pore tortuosity as volumetric moisture decreases with a decrease in pressure head.

Soil and peat becomes consolidated when water drains from pores and the peat is compressed. Consolidation occurs due to drainage of water from the macropores, while secondary compression is due to the slow drainage of micropores to macropores (Zhang and O'Kelly, 2013). However, these concepts should be used cautiously as the underlying mechanisms for the compression of peat, which consists of partly decomposed fragmented remains of dead organic material, are much different from the conventional understanding of mineral soils, for which these stages were developed.

1.1.3.4 Soil Moisture Retention

Soil water retention is a key hydraulic property, which affects soil water storage and the availability of water for plants. Understanding the variability and balance of soil moisture retention is fundamental for the quantification and unifying of a region's hydrology, ecology and geology. Furthermore, the patterns in spatial and temporal variability of soil moisture are to an extent the controlling factor of regional vegetation and physiography (Rodriguez-Iturbe, 2000). Water retention characteristics for mineral soils have been well established, but considerable attention more recently has been given to the parameterization of soil water retention curves for organic soils (Goetz and Price, 2015; McCarter and Price, 2012; Rezanezhad et al., 2012). Da Silva et al. (1993) successfully established soil water retention relationships for peat using the van Genuchten equation in a laboratory study; however, this study involved only one type of peat and did not report on all fitted parameters. Thompson and Waddington (2013) also examined water retention in boreal-forested peatlands in Slave Lake, Alberta, Canada, although the focus of their study was the effect of wildfire on peat hydraulic properties and moisture retention.

Water retention and the rate of water movement depend largely on the total porosity and the pore size distribution of the material (Kutilek and Novak, 1998). Increases in organic matter content lead to an increase in water retention (Walczak et al., 2002). Water retention curves make it possible to determine the amount of strongly bound soil water (or residual saturation), which is often characterized as having a pF (a decimal log of tension, expressed as pressure head in the unit of cm) > 4.2, which is an indicator of soil micropores. Water content changing between saturation and pF 2 is indicative of macropores in the soil. In macropores, there is a rapid gravitational efflux of water, often referred to as 'aeration capacity.' Water retention occurring between pF 2.0 and 4.2 is called 'potentially useful' retention, but below pF 4.2, water becomes unavailable to be used by plants (Okruszko, 1993). Water retention curves demonstrate that at saturation, organic soils contain nearly 90 % water (Walczak et al., 2002). Much less suction (ψ) is observed at any given volumetric water content for organic soil compared to mineral soil, except at saturation (Letts et al., 2000).

Water retention curves were adjusted by Letts et al. (2000) using porosity parameters as constants. Their analysis illustrated that suction values can be slightly higher for fibric

peat than for sapric peat or mineral soils. In addition, poorly decomposed sphagnum retains more water at saturation than the more decomposed peats (Boelter, 1969; Boelter, 1968). Water retention characteristics of peat reflect the decreasing pore size that occurs at depth within the peat column.

1.1.3.5 Hydraulic Conductivity

Hydraulic conductivity is defined as the ability for water to flow through a porous medium. The concept of hydraulic conductivity has important implications regarding the runoff characteristics of organic soils. The primary factors affecting the hydraulic conductivity of peat are the shape, interconnectivity (i.e., tortuosity), porosity and the hydraulic radius of pores (Rezanezhad et al., 2009). Measurements of hydraulic properties such as the water retention curve and hydraulic conductivity are among the most difficult and time-consuming tasks in soil physics (Schindler et al., 2010a).

Hydraulic conductivity tends to be high near the surface of peatlands due to the large pore size within uncompressed plant material (Boelter, 1968). Nevertheless, hydraulic conductivity is highly variable and can vary upwards of five orders of magnitude within a mere 0.4 to 0.8 m (Bradley, 1996). Pore size distribution within the peat column decreases with depth, and yet, despite small pores, peat still retains water, resulting in a relatively high conductivity (Price, 1991; Price and Whittington, 2010). The higher water content retained within the lower layers of the peat profile suggests that these lower regions of the peat column are necessary and vital for storing and supplying water to the upper layers, whose demands for water are met with sufficient hydraulic gradients when needed.

Saturated hydraulic conductivity of sphagnum is high (~10^{-3} m/s), and is even higher in the uppermost layers due to macropores. However, the upper layers are rarely if ever saturated under natural conditions (Price and Whittington, 2010). Here again, the striking differences in physical properties with depth may be a function of the differences in pore size distribution for different peat materials. Soil pores decrease in diameter as a function of peat decomposition increasing with depth. This relationship strongly controls flow as the hydraulic conductivity increases with the square of pore diameters (Freeze and Cherry, 1979). Because of the highly anisotropic and heterogeneous nature of peat (Ingram, 1978; Price et al., 2008), estimates to determine hydraulic conductivity are potentially inaccurate

and inapplicable to living and undecomposed mosses. However, recent developments in the literature have shown that saturated hydraulic conductivity of the peat column can be accurately quantified (Goetz and Price, 2015; McCarter and Price, 2013; McCarter and Price, 2012).

Undecomposed mosses exhibit an inability to hold water in the primary interstitial pore space, greatly increasing the flow path tortuosity within the peat substrate as air-filled pores coalesce (Quinton et al., 2009), producing a low hydraulic conductivity, except in saturated conditions. Boelter (1968) found a wide range of values for hydraulic conductivity at various depths. Water movement was found to be rapid near surface horizons and was quite variable, but this may have been due to the piezometer method of in-situ sampling. In attempted near-surface measurements by Boelter (1968), water movement was often found to be too rapid for precise measurement, while successful measurements, on the other hand, were highly variable. Colley (1950) reported horizontal peat hydraulic conductivity to be greater than vertical; however, Boelter (1968) found the vertical peat hydraulic conductivity to be greater than the horizontal hydraulic conductivity.

In pristine environments, the reduction of active porosity and decreased pore size with depth typically means that the saturated hydraulic conductivity of peat decreases by several orders of magnitude between the ground surface and a depth of ~0.5 m (Hoag and Price, 1995; Quinton et al., 2008; Rezanezhad et al., 2009). However, some studies have reported that peat layers and other factors offer a more complex relation between hydraulic conductivity and depth (e.g., Beckwith et al., 2003).

1.1.3.6 Peat Subsidence

Peat subsidence is a well-known process that is a function of water table fluctuations (Ojanen et al., 2014; Pronger et al., 2014; Hooijer et al., 2012; Lewis et al., 2011; Zanello et al., 2011; van Asselen, 2010; van Asselen et al., 2009; Petrone et al., 2008; Petrone et al., 2007; Strack and Waddington, 2007; Long et al., 2006; Camporese et al., 2006; Price and Schlotzhauer, 1999; Parent et al., 1982). Before examining compressibility characteristics of peat, it is important to consider the nature and composition of the peat fabric, i.e. geometrical aspects of a particle, associated inter-particle forces and spatial arrangement, shape, and size of the fibres (O'Kelly and Pichan, 2013). The overall peat fabric is an assemblage of decaying plant

cellular structures, entangled by frequent fibres and leaves, which are in a less decayed state. Structural arrangement is dependent on the parent plant, the environmental factors affecting how the peat was formed and its degree of decomposition. Decomposition rates may accelerate as a function of episodic fluctuations of the water table, which causes air entry. The increase in oxygen concentration within the deposit promotes decomposition within the peat column.

Fibrous peat typically has a very high shrinkage capacity, reducing in volume by up to 50% on air-drying (Huat et al. 2011). Shrinkage of the thin- walled tissues and collapse of the cellular structure produces a reduction in the water holding capacity and particle porosity (Wong et al. 2009). Lowering of the groundwater table causes shrinkage and reduction in volume of the peat deposit on account of: i) stress increase on underlying peat layers and hence additional consolidation settlement as a result of the decrease in buoyancy; ii) shrinkage due to capillary forces along with high shrinkage capacity of the fibres on drying; iii) more rapid biological decomposition of the organic matter content under aerobic conditions (Drajad et al. 2003).

The general consensus in the scientific literature is that the compressibility of peat reduces with increasing degree of decomposition (Price et al. 2005; Hobbs 1986). Canadian peats reduced in volume with increasing von Post number, most strikingly for fibric peat (i.e. H1 to H4).

It is well known that soils experiencing intense swelling and shrinkage processes, can result in non-rigid volume conditions that can be divided into four major phases: (a) structural shrinkage with increased rigidity of the soil pore system, (b) ongoing desiccation leading to proportional shrinkage and drainage of smaller pore spaces, (c) further desiccation resulting in intense soil drying, where volume loss is smaller than residual loss, and (d) nearly complete dryness, where soil volume ceases to change (zero shrinkage) (Gebhardt et al., 2012; Reeve et al., 1980). However, less is known about the shrinkage characteristics of organic soils such as peat (Gebhardt et al., 2010). Shrinkage intensity depends on the type of organic matter. Shrinkage generally tends to increase with degree of decomposition (Päivänen, 1982; Schwarzel et al., 2002). In contrast to mineral soils, and clays in particular, the four zones of shrinkage cannot be identified for highly heterogeneous peat soils. Instead, structural and proportional shrinkage have been identified. McLay et al. (1992) explains the

absence of the residual zone as due to the lack of rigidity from structures such as sand and silt particles. However, studies by Kennedy and Price (2005) have found the existence of residual and zero shrinkage zones in peat soils. Leifeld et al. (2012) and Kasimir-Klemedtsson (1997) explain that the nonlinear subsidence seen in drained peatlands can be attributed to three major processes: primary consolidation of low density peat layers with the onset of drainage, followed by shrinkage due to evaporative losses and carbon loss by oxidative decomposition of the aerated peat.

The subsidence of organic peat-containing soils known as histosols has been defined by early work as the lowering of surface elevation after drainage due to causes other than erosion (Jongedyk et al., 1950). It is well known that land subsidence is a major consequence of the oxidation of histosols, which increases significantly when peatland systems are naturally or artificially drained, or when natural flow paths are blocked. Both result in dry-oxidative-promoting conditions in the upper aerated zone of the soil organic fraction (Gambolati et al., 2006; Gambolati et al., 2005; Wosten et al. 1997; Deverel and Rojstaczer 1996). Such processes are conducive to the extensive loss of soil mass, which manifests itself as peat subsidence.

The ability of the peat matrix to retain and conduct water with the presence of a deep water table has important implications for surface moisture availability, peat subsidence and the likelihood of desiccation (Moore et al., 2015). The oxidation of aerated peat soils is a bio-oxidation reaction, which is primarily controlled by temperature and the presence of atmospheric oxygen. The rate of peat soil oxidation is dependent on soil water content, increasing primarily at low soil water content and high ambient air temperature. Because moisture content is sensitive to the amount of precipitation received, dry and hot summer seasons are the most favorable conditions for the occurrence of the oxidation of organic soils. In contrast, winter organic soil oxidation slows down to almost zero. Substantial decrease in water table elevation causing the upper layer of peat to dry is a well-known contributing factor to the oxidation of the peat profile (Kool et al., 2006; Gambolati et al., 2006; Gambolati et al., 2005).

The collapse of peat due to aeration and subsequent oxidation can result in chemical changes to the peat profile. Such chemical changes may affect the re-growth of peat. Chemical effects may include: increase in acidity, due to oxidizing minerals; release of

nitrogen, due to oxidation of the stored carbon; depletion of oxygen after collapse due to water saturation; and the increase in nutrient release as the peat continues to oxidize. However, the results of chemical measurements by previous studies show that peat re-growth, though slow, is resilient to such chemical changes (Leifeld et al., 2012; Kool et al., 2006; Williams et al., 1998).

The main controlled variable for peat protection management is the ground water level (Schindler et al., 2004). However, decreasing ground water levels are not the sole destructive factor affecting peat quality. Schindler et al. (2004) concludes that the maintenance of low ground water levels is critical for the reduction of peat loss and function, and for the protection of fens. Slow rates of decay, characteristic of peatlands, may help limit peat subsidence resulting from decreased water table (Moore et al., 2015).

1.1.3.7 Peat Anisotropy

Anisotropy, defined as having different properties in different directions, is relevant to peat soils because it best describes flow through the heterogeneous porous media. Fibrous peat is considered strongly cross-anisotropic (different values for different plane orientations) (Hendry et al., 2014; Wong *et al.* 2009; Zwanenburg and Barends, 2007), meaning the depositional process introduces an anisotropic soil fabric (like at soil horizons) with transverse isotropy (Sun et al., 2013). Anisotropy of fibrous peat is a function of its high degree of permeability anisotropy (ratio of hydraulic conductivity values for flow in the horizontal to vertical directions), which is caused by the predominantly horizontally orientated and laminated nature of the fibres (Hendry et al., 2014; Huat *et al.* 2011; Huang *et al.* 2009; Mesri and Ajlouni 2007; Yamaguchi *et al.* 1985). This causes the structure of the peat to be stronger with respect to the horizontal direction versus the vertical direction. The cross-anisotropic nature of peat results in excess pore pressures that are proportional to the change in deviatoric stress, which is dependent on the orientation of the peat fibres with respect to principle stresses. Peat fibres have also shown transitional qualities from isotropy to cross-anisotropy with increasing vertical strain and effective confining pressure (Hendry et al., 2014).

Beckwith et al. (2003) examined anisotropy of bog peat, and created the modified cubic method (MCM) for anisotropic measurements. The anisotropic factor in this particular

study was 0.28. Schlotzhaver and Price (1999) found A = 0.27. Lewis (2012) found a higher anisotropic factor of 0.45. Significant fibrous anisotropy, with the fibrous organic matter highly oriented in the horizontal direction have been reported by Yamaguchi et al. (1985), even for surficial fibrous peat deposits.

Surridge et al. (2005) studied a floodplain fen peat in situ up to 6 m deep in Norfolk, UK. Slug tests matched laboratory MCM hydraulic conductivities with $K_{slug} > K$ from the MCM due to scale dependency. In conclusion, shallow hydraulic conductivities were consistently measured due to the presence of shallow roots ($K_h > K_{v)}$, however, laboratory measurements in contrast found $K_v > K_h$. Surridge et al. (2005) found lower magnitude anisotropy in contrast to Beckwith et al. (2003).

1.1.4 Road Effects and Restoration

When managing hydrology, it is vital to characterize the observable and quantifiable natural constraints imposed by climate and landscape (Price et al., 2003). Restoring hydrological function should be the first priority in peatland restoration. Keddy (1999) estimated that hydrology is the single most important environmental factor (50 % relative importance) in controlling plant community structure. Rochefort (2000) defines the goals of bog restoration in North America as re-establishing vegetation dominated by *sphagnum* and the diplotelmic hydrogeological layers (acrotelm and catotelm). The success of achieving these goals would imply an adequate level of productivity returning the site to a peat-accumulating system, re-establishing nutrient cycling, and returning a vegetation structure and microhabitats containing faunal and floral diversity (Rochefort, 2000; Price et al., 2003).

The effect of roads on ecological values has been the focus of recent literature. Research has mostly examined the effects of roads on amphibian and reptile populations (Cosentino et al., 2014; Vargas-Salinas et al., 2014; Mazerolle, 2004; Beebee, 2013; Petranka and Francis, 2013; Colino-Rabanal and Lizana, 2012; Karraker and Gibbs, 2011; Beaudry et al.. 2008; Steen and Gibbs, 2004; Marchand and Litvaitis, 2004; Patrick and Gibbs, 2010; Dorland et al., 2014; DeCatanzaro and Chow-Fraser, 2010), the distribution of birds (Yuan et al., 2014; Mammides et al., 2014; Grilo et al., 2014; and Borda-de-Agua et al., 2014), insect populations (Dymitryszyn, 2014; and Soluk et al., 2011), and plant diversity (Houlahan et al., 2014).

Nevertheless, more research and discussion are needed on the effects of access infrastructure on peat columns and local peatland groundwater systems. There is a paucity of information regarding the immediate and long-term impacts of roads on peatland hydrologic processes. Linear disturbances such as road construction represent one of the major ways landscapes are transformed (Williams et al., 2013). Roads are still necessary in 21st-century oil sand development, despite how destructive they are to northern peatlands. However, current literature focuses on the permafrost and discontinuous permafrost zones, which do not directly pertain to the effects of roads in the Athabasca Oil Sands region. Many concerns remain regarding the most effective planning, construction and maintenance of access infrastructure on peatlands located within Canada's boreal ecozone. Gaps in the literature include how to reduce the environmental impact of access infrastructure on peatland hydrogeology, how to improve the loading capacity of peatland soils, the suitability of foundation materials for roads and, lastly, but of utmost importance, understanding the long-term cumulative impacts of access infrastructure, specifically on the peat column.

The impact of roads can be mitigated and minimized through best management practices. Williams et al. (2013) proposed the following mitigation methods for the construction of roads in zones of discontinuous and continuous permafrost, which may also be applicable to road construction within the boreal forest ecozone. Route planning would aid the avoidance of sensitive areas, while making use of pre-existing disturbance pathways would minimize impact. Also, surface preparation of the disturbance site should be carefully considered to minimize compaction to the soil surface. For example, refrain from a complete removal of trees across the disturbance site and only selectively remove vegetation for narrow disturbances such as roads to increase the likelihood of accelerated regeneration of the disturbance. Phillips (1997) and the B.C. Ministry of Environment (2008) provided generalized guidelines for the construction of roads through wetlands: These guidelines are related to the appropriate design and installation of road networks.

2.0 Site Description

2.1 Athabasca Oil Sands Region

This study was conducted in the Athabasca Oil Sand Region of Alberta, Canada. The climatological characteristics of this boreal region are extremely cold winters and warm summers, with air temperatures ranging from -70 to 30 ^{o}C on an annual basis. The growing season of the boreal ecozone is < 120 days, with low precipitation (200-600 mm/year) (Bonan and Shugart, 1989; Bonan et al., 1992). The boreal ecozone is predicted to be the Canadian ecozone most affected by climate change, as temperatures have increased by 2-4 ^{o}C during the past 40 years. By 2050, it is predicted that most parts of the Canadian boreal will have temperatures 3-4^{o}C warmer than in 1961-1990, while winter temperatures are predicted to warm even more by an average of 4-6 ^{o}C (Schindler and Lee, 2010).

Low winter temperatures coupled with low amounts of precipitation limit the northern extreme of the boreal forest. Climatically, the position of the summer-time arctic front, also known as the 10-13 ^{o}C July isotherm, is correlated with the northern extent of the boreal forest (Bonan and Shugart, 1989; Pielke and Vidale, 1995).

The Western Boreal Forest contains three broad physiographic regions. The eastern Kazan Region is part of the granitic/gneissic Precambrian Shield. The central interior plains and the Western Cordillera are both underlain primarily by Paleozoic and Cretaceous sedimentary and metamorphic rock. Most of the western region's geology experienced intense Pleistocene glaciation. Soils, which dominate in the Western Boreal Plain include Podzols (dominant in the Kazan Region), Brunisols, Gleysols, Histosols (Organics), Cryosols and Regosols (dominant in the Cordilleran region).

The oil sand deposits within the Western Boreal Forest form three deposits (Figure 2-1, page 23). Lower Cretaceous sediments host the largest deposit, the Athabasca Oil Sands group. The second largest group, the Cold Lake deposit, contains heavy oil and consists of a vast number of small reservoirs in the Lloydminster region of Alberta and Saskatchewan. The third and smallest group, the Peace River group, is made up of Paleozoic carbonate rocks, which subcrop beneath the Athabasca Oil Sands group (Brooks et al., 1988). The Athabasca Oil Sands group contains an estimated 206.7 billion m^3 of bitumen (Evans et al., 2002). The Cold Lake deposit has been estimated to contain 31.9 billion m^3 of bitumen, and

the Peace River group is estimated to contain a relatively meager 20.5 billion m^3 of bitumen (Evans et al., 2002).

Geochemical data suggests that the origin of the Cretaceous bitumens was derived from mature, conventional oil, which was derived from presently unknown source facies. This particular oil seems to have suffered massive biodegradation from migrating long distances. Surficial mineral species located at the Alberta Oil Sands area include mica, montmorillonite, kaolinite, chlorite and vermiculite (Spiers et al., 1983).

Canada's oil sands resources contain an estimated total of 259 billion m^3 of bitumen, with recoverable bitumen estimated at 28.3 billion m^3. The majority of this bitumen occurs in the province of Alberta and is among the world's largest reserves of hydrocarbons (Evans et al., 2002). Oil sand production is projected to reach more than 3.3 million barrels/day by 2020 (Hall et al., 2012). Approximately 15 % of Canada's crude oil is produced from Suncor and Syncrude surface mining operations alone (Brooks et al., 1988).

Figure 2-1. Map of Alberta showing oil sand deposits. (Source: http://en.wikipedia.org/wiki/Athabasca_oil_sands).

2.2 Firebag Site

Fieldwork was conducted at Suncor's Firebag Site located north of Fort McMurray, Alberta (UTM coordinates: 57° 13' 29" N; 110° 53' 29" W), at the Pad 106 Access Road (Figures 2-2 and 2-3). The Pad 106 Access Road, connecting to the Pad 106 in-situ steam-assisted gravity drainage (SAGD) well pad, had been built during the summer of 2007. A subsequent above-ground pipeline rendered the road useless, as the pipeline separated the well pad from the road. (See photograph in Appendix 1.) The length of the road measured 228 m, with the width measuring 19.5 m at road well 1-4, 21 m at road well 2-4, 20 m at road well 3-4, and 23 m at road well 4-4. The average depth of the road was 1.5 m $\pm$ 0.1 m (minimum depth = 1.4 m, maximum depth 1.7 m). The western portion of the site included a corridor; a pathway cut for increased efficiency of infrastructure maintenance vehicles to navigate Firebag, especially during the winter season and runs parallel to the road (Figure 2-2).

Fieldwork occurred during the summer months of 2013 from June 1 to August 17. Site instrumentation was set up within and perpendicular to the road. Groundwater wells, peat subsidence monitoring plates, and meteorology equipment were set up perpendicular to the road. Road groundwater wells and road peat subsidence monitoring plates were set up within the road (Figure 2-3).

Road surveying took place simultaneously with the road removal process. Peat depth elevation refers the depth of the peat from the ground surface to the underlying mineral layer relative to sea level. Peat depth was measured at all well sites and also at in between well site locations to improve the resolution of this thesis. Peat depth at groundwater well sites is shown in Table 2-1.

The first ground temperature (Tg1) profile was installed on the east side of the road between wells 2-2 and 3-2, the second (Tg2) located between wells 2-3 and 3-3, the third (Tg3) between 2-5 and 3-5, and lastly, the fourth (Tg4) was located between wells 2-6 and 3-6. These profiles measured both ground temperature and relative humidity.

Road removal lasted from June 18 to July 4, 2013. The following materials and volumes were extracted during the removal of the road: clay – 486 m^3, mud and organics – 987 m^3, and gravel – 181 m^3. The University of Alberta's Civil Engineering department conducted measurements of road material properties. The total moisture weight of the Pad 106 Access Road was approximately 1,504,400 kg, while total weight of the road was

approximately 11,515,400 kg. Moisture content of the road was 25 % (volume percent assuming the density of water is 1 kg/L), while total pressure exerted by the road was approximately 23,599 N/m^2 (see Appendix 2 for calculations). Excavated materials were reused to build parking lots at Suncor's Firebag Site.

At Suncor's Firebag Site, the tree cover includes: *Picea mariana, Populus tremuloides, Larix laricina* and *Betula papyifera*. As with boreal peatlands, sphagnum mosses are the dominant peat-forming species onsite. Some of the most commonly occurring forbs and shrubs onsite include: *Andromeda polifolia, Chamaedaphne calyculata, Eriophorum angustifolium, Eriophorum vaginatum, Kalmia polifolia, Ledum groenlandicum, Oxycoccus microcarpus, Rubus chamaemorus, Smilacina trifolia, Sphagnum spp,* and *Vaccinium myrtilloides.*

Plants found on site but not within the 1 m^2 plots include: *Hieracium umbellatum, Drosera rotundifolia* and *Typha latifolia.* The complete vegetation survey is in Appendix 3. Bryophytes found on site but not within the 1 m^2 plots include: *Amblystegiaceae, Aulacomniaceae, Bryaceae, Brachytheciaceae, Dicranaceae, Ditrichaceae, Hylocomiaceae, Hypnaceae, Mniaceae, Polytrichaceae, Thuidiaceae, Sphagnaceae,* and *Marchantiophyta*. Bryophytes were more abundance in the saturated upstream northeast side of the road (Miller et. al., 2015, unpublished).

Table 2-1: Recorded field measurements of peat depth at each of the groundwater well sites at the Pad 106 Access Road site.

Well ID	Peat Depth (cm)	Mineral Texture
1-1	115.1	Sandy- coarse grained- small cobbles→sand matrix
1-2	165.3	Clay
1-3	195.6	Clayey sand
1-4	102.5	Fine grained clay- dark grey
1-5	168	Sandy clay
1-6	138	Clay- brown/grey- very fine
1-7	99	Med. coarse grained sandy clay- light grey
2-1	139	Pure clay
2-2	101.5	Sandy clay-dark grey/black- noticeably less flooded area
2-3	107.3	Clayey sand- fine grained
2-4	132	Sandy clay- visible med. Coarse grains
2-5	89	Light grey dry sandy clay- no visible grains
2-6	79	Sandy clay- med. Coarse grained
2-7	67	Sandy clay- fine grained
3-1	126.2	Sandy clay- very sandy- med. coarse grained
3-2	83.8	Med. coarse grained sand
3-3	111.1	Clayey sand
3-4	45	Clay (40-45cm)
3-5	45.5	Sand- little clay- med. coarse grained- beige-dry
3-6	39.5	Sandy clay
3-7	42	Sand clay- light brown- fine grained
4-1	150.6	Pure clay- dark grey
4-2	156.6	Pure sand- beige- med. coarse grained- see grains
4-3	151	Pure clay
4-4	91.5	Sandy clay
4-5	83	Clay- little sand
4-6	36	Sand
4-7	35.5	Light beige sand- dry/crumbly- peat dark reddish brown

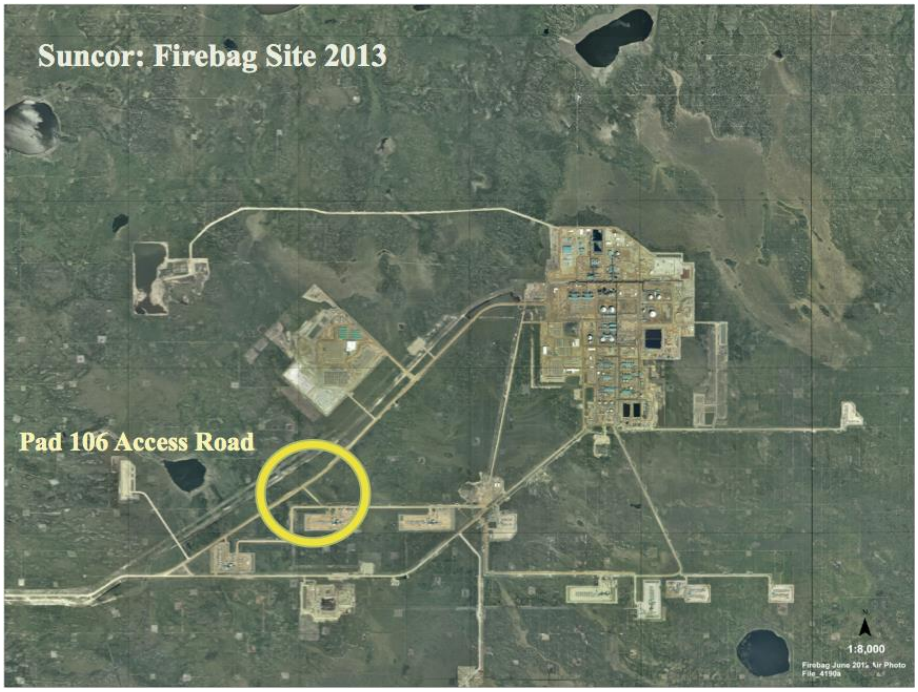

Figure 2-2. Suncor Firebag Site Aerial photograph 2013 with Pad 106 Access Road circled in yellow and photograph taken from the access road. Pad 106 Access Road was a small road that was cut off from Pad 106 by an above-ground pipeline. (Source: Suncor, Corey Vogel, 2013)

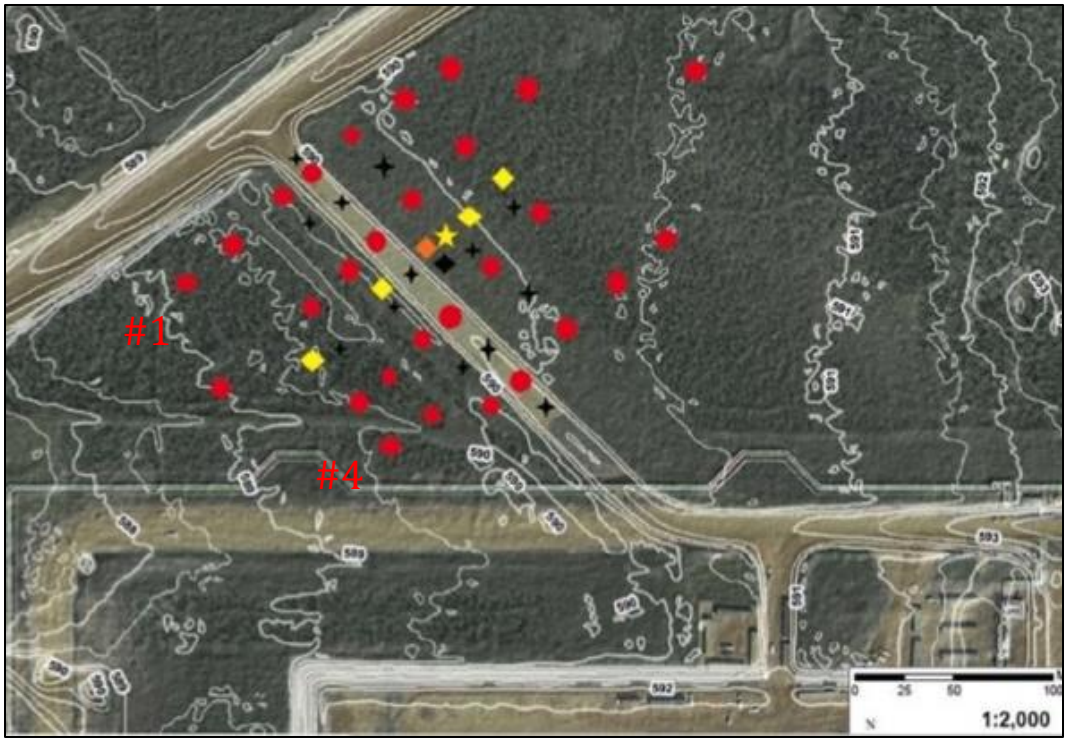

Figure 2-3. Pad 106 Access Road Instrument locations. Transect 1 to transect 4 are indicated by #1 to #4. Transect 4 is located closest to the above-ground pipeline. Subsidence measurements were made at locations indicated by black stars. Red circles represent groundwater wells. Yellow squares represent ground temperature and relative humidity measuring stations. The Meteorological station is represented by the yellow star and the black square represents the tipping bucket for monitoring precipitation. The orange square represents TDR Soil moisture probes. (Source: Terry Osko).

3.0 Methods

3.1 Field Instrumentation

3.1.1 In Situ Hydrometric Variables

A 3 m meteorological tower was set up onsite between transect 1 and transect 2 on the east side of the Pad 106 Access Road, approximately 10 m east from the road center. A CR1000 datalogger archived all weather data at the meteorological tower. Precipitation was measured using a tipping bucket rain gauge (Onset HOBO RG3), which was located approximately 10 m south of the meteorological tower. Meteorological conditions included severe rains and flooding (see next paragraph). The tower measured relative humidity and air temperature (Onset HOBO U23 Pro v2 Temperature/Relative Humidity datalogger – U23-001) at 2 m and 1 m, wind speed (RM Young 05103 anemometer) at 2.5 m, and net radiation (CNR4 radiometer) at 2 m.

Ground temperature was measured (Omega Type T Copper-Constantan thermocouple) at four depths: 10 cm, 30 cm, 50 cm and 100 cm below ground at four locations: Tg1 was located between well site 2-2 and 3-2, Tg2 between 2-3 and 3-3, Tg3 between 2-5 and 3-5, and Tg4 between 2-6 and 3-6. Ground temperature was measured as a function of subsurface relative humidity. Pressure transducers (Onset HOBO U20-001-0x barometric pressure logger) were utilized for the monitoring of changing water levels at specific wells sites and at the meteorological station. Groundwater wells were constructed using PVC pipe (3m in length, 1.5" ID), installed to a depth of 2 m (leaving 1 m stick up), screened throughout their total length. The pressure transducer logger uses a maintenance-free absolute pressure sensor and is ideal for recording water levels in wetlands. The water level accuracy of the pressure transducers is: ±0.05 %, 3.8 cm (0.125ft) water with a maximum error of ±0.1 %, 7.6 cm (0.25 ft) water. Measurements of groundwater were recorded by the pressure transducers every 30 min. Pressure transducers were installed at road wells 1-4, -4, 3-4, 4-4, and wells 1-5 (due to its close proximity to the receiving side of the culvert between Rick George Way and the Pad 106 Access Road), 2-2, 2-3, 2-5, and 2-6.

3.1.2 Field Measurement of Peat Subsidence and Survey of Vegetation Cover

Measurements of peat subsidence were taken at locations between transect 1 and 2, and all along the road between road wells (Figure 2-3). Instrumentation used for measuring peat subsidence was a 15 ft piece of rebar and a transparent Plexiglas plate. Clear Plexiglas plates were required to allow UV penetration for uninterrupted photosynthesis. A Plexiglas plate measured 30 cm by 30 cm with a hole for the rebar drilled in the center. All Plexiglas plates were precisely cut onsite by Chad's Contracting: Industrial Services. Bolts (G5 Coarse Thread Buildex – BX12166; Hex bolts 61-8011-0) were securely fastened in each corner of the Plexiglas, each bolt weighing approximately 18.2 g, and each nut 6.9 g. The 15 ft rebar was firmly hammered into the ground so that just 5 ft remained above the surface.

A vegetation survey was conducted using a 1 m^2 quadrat at each well site. Results of the survey are in Appendix 3.

3.1.3 Collection of Peat Samples for Laboratory Analyses of Peat Physical Parameters

Peat cores were obtained from Suncor's Firebag Site and shipped to the University of Waterloo for laboratory experiments. Fen peat columns were extracted from 28 well sites (four transects perpendicular to the Pad 106 Access Road with seven well sites each). A stainless steel Wardenaar peat corer (Wardenaar, 1987) was utilized for retrieving samples from the acrotelm and subjacent peat layers. This particular corer is a double-blade cutter designed to retrieve undisturbed peat monoliths. Dimensions of the extracted monoliths were 100 cm (l) x 10 cm (w) x 10 cm (h). A Russian corer is not ideal for the retrieval of peat samples, as the Russian corer is not designed to cut the living plant material cleanly and will strongly compress the peat (De Vleeschouwer et al., 2010). However, for this study, the Russian corer was used to extract samples where the peat column exceeded 1 m depth (as the Wardenaar corer could not be used for this depth). This worked well at dry well sites, but extraction proved difficult and cumbersome at greatly saturated well sites, which limited the scope of this research. The desired depth of 1 m could not be attained for all peat cores. Russian cores were extracted at well sites: 1-2, 1-3, 1-6, 2-1, 2-3, 3-1, 4-1, 4-2, and 4-3, where peat depth exceeded 1 m.

3.2 Laboratory Analyses of Peat Physical Parameters

In the laboratory, the peat blocks were kept frozen until they could be processed for experimentation. The freezing of the peat is not expected to have affected the peat as freezing occurs in the field each year at this site, but not as deep as 1 m. Peat core lab observations can be found in Appendix 4. Three laboratory tests were conducted: (1) UMS – KSAT for measurements of saturated hydraulic conductivity, (2) UMS – HYPROP for measurements of soil moisture retention, and (3) physical hydraulic parameter tests for the retrieval of porosity, specific yield, bulk density and volumetric soil moisture. Because hydraulic functions may differ dramatically as a function of antecedent moisture conditions, 24-hour sample saturation prior to analysis was done Hardie et al. (2013). A benefit of using the KSAT system, and the HYPROP system is that both use the same stainless steel core containers (250 cm^3), so one sample can be made and run for each system, instead of having to extract two different samples for each system. Measurements of horizontal and vertical saturated hydraulic conductivity were conducted using the KSAT system at 10 cm depth and 60 cm depth. The desired direction was achieved by cutting and subsequently orienting the sample perpendicular to the initial orientation in the instrument. Measurements of soil moisture retention were done at 60 cm depth for all well sites, except road sites and a 'mid-transect' deemed transect 3, which was measured at 10 cm and 60 cm using the HYPROP system, core length permitting.

The extent of decomposition is a key property of organic soils, but the degree of decomposition is difficult to quantify. Decomposition is a relative quantity, approximated by chemical or physical characteristics, which change as the decomposition advances. The Von Post Scale of Humification (vP) is a commonly used measure of the state of peat decomposition, based upon the colour of the water, structure of the residue and amount of peat that passes through the fingers when a fresh saturated sample cutting is squeezed (Price et al., 2005). The vP scale ranges from H1 to H10 with H1 exhibiting the smallest degree of decomposition. As the cores were processed for other measurements, vP values were determined approximately every 10 cm (Appendix 5).

Specific yield and retention are important parameters to assess, despite the focus of this thesis on the saturated zone. The temporary Access Road creates a unique hydrologic setting, such as flooding of the unsaturated zone and drying of the saturated zone. The water

table of such an environment is not likely to behave as a typical fen peatland, with small natural abrupt changes in the unsaturated zone. Therefore it is important all parameters are assessed pertaining to both the saturated and unsaturated zone, due to shifting and unexpected hydrologic conditions. Nonetheless, with imminent climatic change, the hydrologic behaviour and water table are bound to fluctuate, and may potentially yield unsaturated porous media.

3.2.1 UMS HYPROP System

The UMS HYPROP System was used to evaluate soil moisture retention curves as a function of the following parameters: Tensions (ψ), hydraulic gradient (i_m), flux density (q), sample height (h), sample mass (m), and water content loss per volume. The UMS HYPROP System uses the evaporation method according to the Schindler evaluation of evaporation experiments (Schindler 1980, Schindler et al. 2010). The Schindler method has many advantages, including an easy experimental set-up and its applicability to different-sized samples and textures, including peat soils. However, the HYPROP system tends to be problematic when evaluating organic soils because of contact issues of the tensiometer with the soil matrix, which is more problematic in peat soils. It is also difficult to evaluate shrinking soils, which is a well-known phenomenon for peat.

Here we consider it as a method to obtain starting values and parameter boundaries. This simplified evaluation is mathematically summarised in Eq. 3.1-3.2 for the soil water retention curve only. With respect to the soil water retention curve, the underlying principle of this approximation is to establish the water content-matric potential relationship by an approximation of $\theta(t)$ by $\theta_{0.5L}(t)$, the water content at sample mid height and analogously $\theta(t)$ by $\theta_{0.5L}(t)$ in Eq 3.1 and Eq 3.2, respectively.

$$\bar{\theta}(t) = \frac{M_{wet}(t) - M_{dry}}{0.75\pi d^2 L} \approx \theta_{0.5L}(t) \tag{3.1}$$

with $M_{wet}(t)$ [g] representing the measured wet sample volume (after subtraction of the weight of the measurement equipment) and M_{dry}, the oven dry weight of the solid fraction,

both in [g]. $\theta_{0.5L}(t)$ is the water content at medium height and approximated through the assumption of linear water content distribution with depth by $\bar{\theta}(t)$ which is the sample mean weight, both in [cm^3 cm^{-3}], and d [cm] the samples diameter and L the sample height [cm].

$$\bar{h}(t) = \frac{-abs(\sqrt{h_{0.75L}(t)h_{0.25L}(t)})}{2} \approx h_{0.5L}(t) \tag{3.2}$$

Eq. 3.2 as the geometric mean is valid for $h \leq 0$, with $h_{0.25L}$, $h_{0.5L}$, and $h_{0.75L}$ are the matric potentials at the corresponding heights, all in [cm] and was proven to be a better approximation than the arithmetic mean.

Time of the air entry in the tensiometers is assumed to occur at 8800 hPa. The parameter estimation fitted to the retention and conductivity data similar to Peters and Durner (2008) under the assumption of a independently and normally distributed model (Van Genuchten, 1980) errors minimising $\Phi(\boldsymbol{p_l})$ with;

$$\Phi(\boldsymbol{p_l}) = w_\theta \sum_{j=1}^{q} \langle \theta_j - \hat{\theta}_j\,(\boldsymbol{p_l})\,\rangle^2 \tag{3.3}$$

where the model weights are determined by $w_\theta = 1/(\theta_{max} - \theta_{min})$ and $w_K = 1/(log_{10}(K_{max}) - log_{10}(K_{min}))$, where θ_{max}, θ_{min}, K_{max}, and K_{min} are the maximum and minimum values of the respective data set. The lengths of the retention curve dataset are denoted by q and conductivity dataset by r. From this, a set of bounds for α_i could be derived, which were applied to the inverse simulations of the model parameter estimations.

Tensions (ψ) are measured at two heights: an upper and a lower (5.4 cm and 2.9 cm), while the sample masses (m) are measured at time intervals, during a 24-hour period. The hydraulic gradient (i_m) is calculated from the tension values and the tensiometer distance. The flux density (q) is derived from the soil water mass difference per surface area (A) and time unit (Δt). Single points of the water retention curve are calculated on the basis of the water loss per volume of the core sample at time (t) and the mean tension in the sample at that time. The hydraulic conductivity (K) (Equation 3.4) is calculated by,

$$K(\psi) = \frac{\Delta V}{2A \cdot \Delta t \cdot i_m} \tag{3.4}$$

where ψ is the mean tension, averaged over the upper and lower tensiometer and the time interval, A is the cross-sectional area of the sample, and ΔV is the evaporated water volume, obtained by $\Delta V = \Delta m/\rho_w$ with the mass loss Δm in the time interval Δt, ρ_w is the density of water and i_m is the mean hydraulic gradient in the interval (Equation 3.5), given by,

$$i_m = \frac{1}{2}\left(\frac{\psi_{t1,upper} - \psi_{t1,lower}}{\Delta_z} + \frac{\psi_{t2,upper} - \psi_{t2,lower}}{\Delta_z}\right) - 1 \tag{3.5}$$

where $\psi_{t,upper,lower}$ indicate the upper and lower tensiometer values at times t1 and t2, and Δ_z is the vertical distance of the tensiometer positions.

The relationship between moisture and pressure is non-linear (e.g. mathematical retention models, such as the van Genuchten model, are non-linear in its parameters as two parameters are a factor). The interpolation between two points on the measured retention curve is only possible by having many points or by curve fitting retention models to the data.

3.2.1.1 UMS HYPROP Experimental Design and Set-up

For both the HYPROP evaporation experiment and the KSAT saturated hydraulic conductivity experiment, intact soil cores are taken in stainless steel cylinders with a sharpened leading edge to minimize soil disturbance during insertion. Cores are trimmed. Holes are prepared for the tensiometers using a stainless steel mini hand-held auger and template (Figure 3-1). Cores were slowly saturated in the laboratory in a pan of water. Water is poured into the pan until the water is level with the edge of the soil core (water must not spill over the edge of the soil core's edge) while the surface remains open to evaporation. Schwarzel et al. (2006) strongly recommends that the measuring of soil moisture retention for peat soils take place in the laboratory due to its secure nature and cost effectiveness.

Tensiometers consist of three basic interconnected elements: 1) a semi-permeable porous cup, 2) a water reservoir, and 3) a measurement gauge or pressure transducer. Pressure equilibrium between the water in the tensiometer and the surrounding soil is

achieved through water movement across the porous tensiometer cup. The manufacturer, UMS, calibrates the tensiometers to an accuracy of 0.1 % for 100 kPa.

If soil water tension exceeds the air-entry pressure, the cup drains and subsequently becomes air-permeable. Air enters into the tensiometer, and its internal tension drops off. The ceramic cup material of tensiometers is, therefore, always configured to ensure that its air-entry pressure is larger than the highest measureable soil water tension. Vapour pressure is normally the classic experimental limit for the water inside the cup; however, the air-entry value for most tensiometer cup material is > 100 kPa.

The surface roughness of water-filled tensiometers is minimized to reduce the contact surface for air adhesion. The ceramic cup size and surface area is small (diameter 5 mm, height 6 mm). Wall thickness is 1.5 mm, while the inner water- filled space has a diameter of 2 mm. Bubbling pressure of the ceramic tip is between 800 and 1500 kPa. The upper and lower tensiometers have lengths of 5.4 and 2.9 cm, respectively.

Upper tensiometer shaft volume is 0.33 cm^3, and lower tensiometer shaft volume is 0.15 cm^3. Tensiometer response time is fast, on the order of 5-10 s, despite the high bubbling pressure of the ceramic. The piezo-resistive pressure transducers have a measurement range of -300 to 300 kPa. The burst pressure is 500 kPa. The transducers are also temperature compensated in the range of 0-50 ^oC. The air entry pressures for both tensiometers are 8.8 bar.

Peat soil experiments are time consuming because most of the water must evaporate before pore water tension increases appreciably. To minimize the time needed to run a HYPROP evaporation experiment, a fan was installed approximately 50 cm away from the drying peat cores. Roughly six to 10 days are required to perform a HYPROP experiment when the evaporation rate varies between 2 and 3 mm d^{-1}.

Intact soil cores were taken in stainless steel cylinders, 8 cm diameter, 5 cm height and 250 ml volume, with a sharpened leading edge to minimize soil disturbance during insertion. Cores were then trimmed and holes drilled with a mini hand-held soil auger and special template for tensiometers. Degassed tensiometers (connected to a computer and measured at 10 minute intervals) were installed in the upward direction to reduce the amount of water flowing into the soil after tensiometer failure. Both tensiometers and HYPROP bases (pressure transducers) were degassed in the same way (Figure 3-2).

Cores were slowly saturated in the laboratory in a bin of water. To minimize air entrapment, the water table was increased to a final height of ~ 0.2 mm below the sample surface. Samples were saturated for 24-48 hours. When tensiometer measurements commenced, the tension difference was adjusted to a hydraulic equilibrium, i.e., to 0.25 kPa. The soil surface was subsequently exposed to evaporation and tension and sample mass were recorded. Tension is is the difference in pressure occurring between atmospheric pressure and the water pressure inside each tensiometer, and is expressed as a positive quantity in kPa.

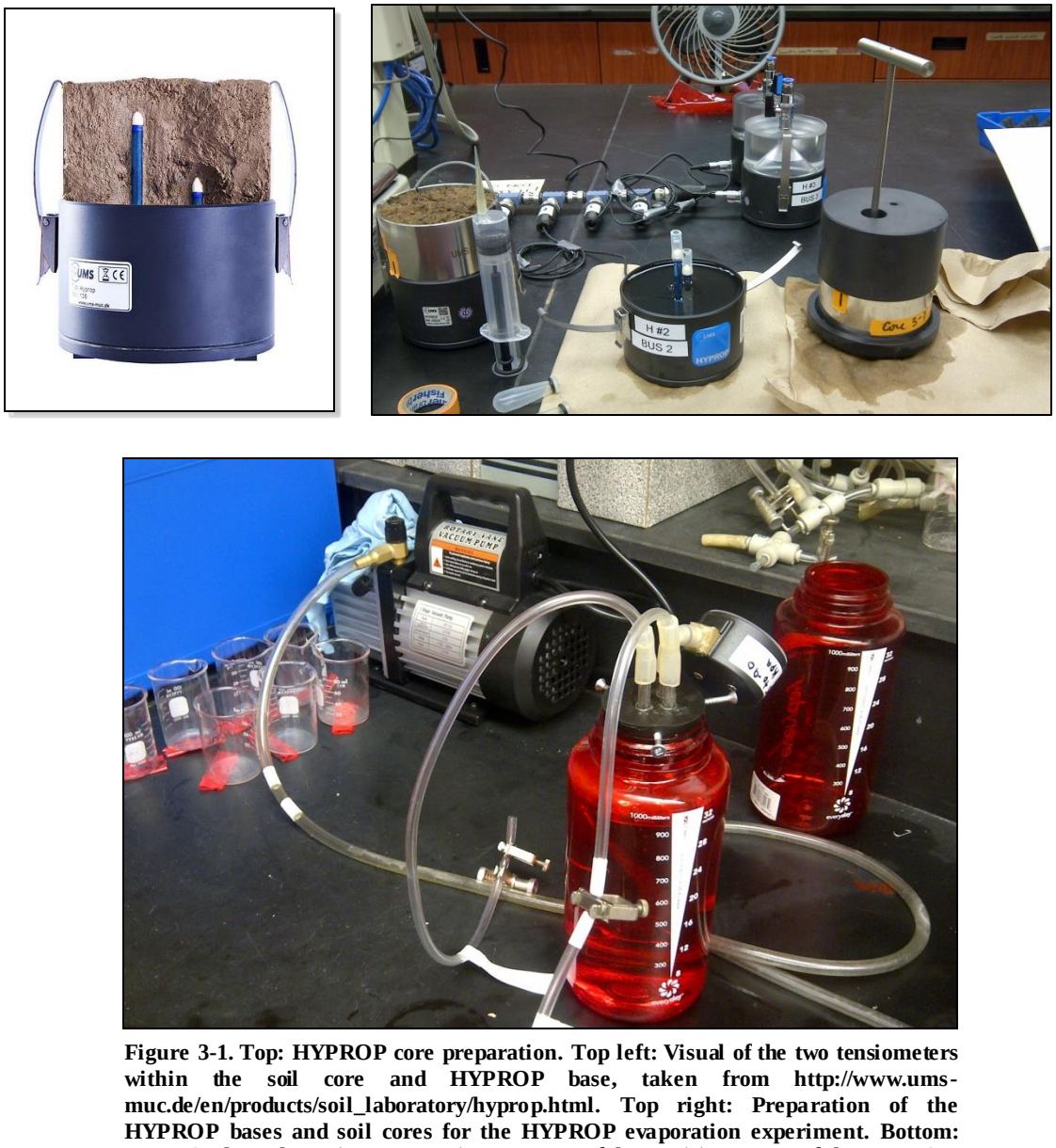

Figure 3-1. Top: HYPROP core preparation. Top left: Visual of the two tensiometers within the soil core and HYPROP base, taken from http://www.ums-muc.de/en/products/soil_laboratory/hyprop.html. Top right: Preparation of the HYPROP bases and soil cores for the HYPROP evaporation experiment. Bottom: HYPROP base degassing preparation. Because of the sensitive nature of the HYPROP base pressure sensor, a secondary 'buffer bottle' (at right, without lid) was also attached to the main chamber bottle seen in the front with the pressure gauge on top. See also Figure 3-2.

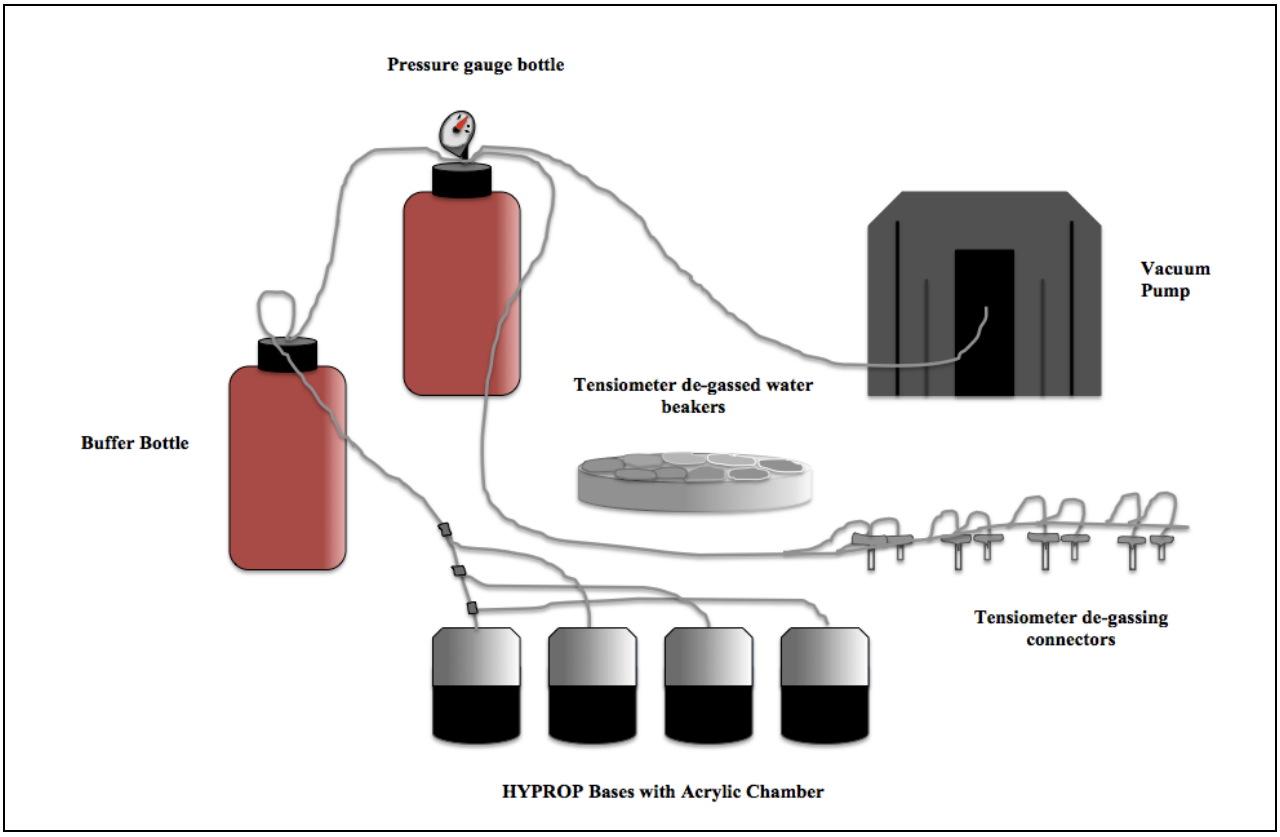

Figure 3-2. Above: HYPROP degassing system set-up schematic. Below: HYPROP experiment initial set-up.

Figure 3-2 shows the initial start-up of the HYPROP evaporation experiment. At the beginning, the pressure head profile is linear as the evaporation rate is given by the atmospheric demand of the laboratory air. The first phase of the experiment entails the evaporation rate remaining almost constant because of the decrease in soil moisture retention due to water loss, which is sufficiently compensated by the increase of the hydraulic gradient (Peters and Durner, 2008). The second phase of the evaporation experiment yields a gradual decrease in the evaporation rate.

At the end of the HYPROP evaporation experiment, the residual amount of storage water is derived from water loss on oven-drying (80 ^{o}C for peat to avoid organic matter from burning off).

Three distinct stages exist for a classic HYPROP evaporation laboratory experiment: In the first stage, the measured tension reflects the matric potential of the surrounding soil. The upper limit is usually ~80 kPa for most tensiometers (Young and Sisson, 2002). For optimal performance, the water inside the tensiometers is free of dissolved gases. Should dissolved gas be present, any small gas bubble that forms will expand continually during drying, which will yield a slightly delayed tensiometric measurement. It is important to check that the tensiometers are functioning properly before installation to avoid this problem.

'Vapour pressure' is deemed the second stage. Water inside the tensiometer will begin to boil if the absolute soil water pressure decreases below the vapour pressure of the liquid's vapour pressure. Pressure inside the tensiometer equilibrates to the vapour pressure, which is nearly close to a vacuum. Water in contact with the porous cup will flow through the cup into the surrounding soil, while the vapour bubble inside the cup continually expands. Consequently, soil in the intermediate vicinity of the cup will be less dry and exhibit lower tension. Tensiometer readings are no longer representative of the soil water matric potential in this stage. The initiation of stage two, however, can be retarded if boiling retardation occurs.

'Air entry' is the third and final stage. It occurs when the tension in the surrounding soil exceeds the air-entry pressure of the ceramic material. The largest continuous pore of the ceramic tip of the tensiometer drains, and air enters from the soil into the tensiometer. At this moment, the measured tension collapses towards zero, which is easily visible in the tensiometer reading.

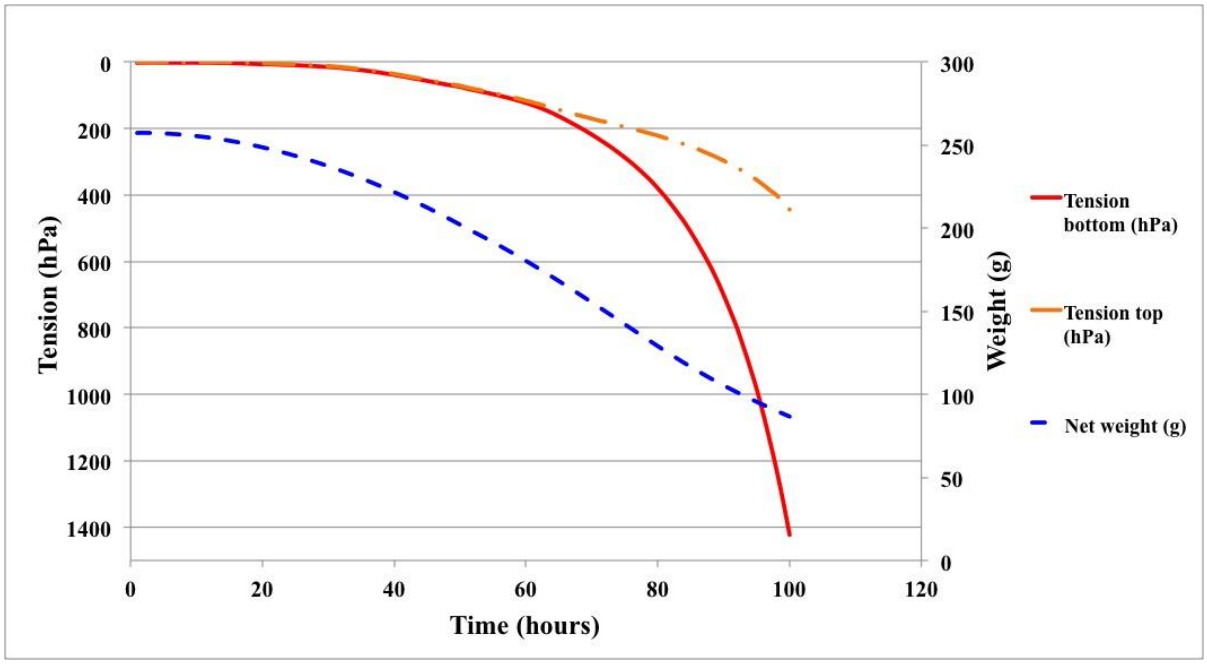

Figure 3-3. Example of raw HYPROP measurement results. Curves show tensions and weight change over time, i.e. evaporation rate over time. The example seen here is peat core sample 1-7; 60 cm.

Figure 3-3 displays the temporal evolution of tension and weight change of a typical HYPROP sample. A typical measurement will initially show continuous loss of net weight at an almost constant rate, which is function of the evaporation rate in the laboratory environment. Temperature fluctuations occurring in the laboratory can cause small changes in the slope of the net weight.

'Stage-1' evaporation refers to the measurement period of constant weight loss. This phase is controlled entirely by atmospheric conditions. Next, the net weight slope becomes less steep as the evaporation rate drops. 'Stage-2' evaporation refers to the second phase where the rate of water loss is controlled by the resistance of the drying soil near the soil surface. Stage-2 begins at the time the upper tensiometer reaches its air entry value, which is located at approximately 70 hours in Figure 3-3. The air entry point can be found where there is a sudden drop in pressure in the upper and lower tensiometers (UMS Manual 2015; Schindler et al., 2010; Peters and Durner, 2008).

3.2.2 Laboratory Measurements of Saturated Hydraulic Conductivity (KSAT)

For the measurement of saturated hydraulic conductivity, a relatively simple instrument was utilized. The KSAT system (Figure 3-4) determines the saturated hydraulic conductivity of 250 cm^3 intact soil cores using a constant-head or falling head experiment. Measurements are based on the Darcy equation (Equation 3.6). Cores were cut horizontal and vertical relative to the site position of the peat core for the determination of horizontal hydraulic conductivity (K_h) and vertical hydraulic conductivity (K_v). Cores were placed into the KSAT in the same way they were cut, and thus allowed the determination of both K_h and K_v.

The theory underlying the measurement principle of KSAT is that a fully saturated soil core percolates water perpendicular to its cross-section and, subsequently, the flow rate and the driving hydraulic gradient are measured. Hydraulic conductivity (K) is calculated from the soil sample length (L) of 5 cm, volumetric water flux (V), and divided by the hydraulic head difference (ΔH), between 0 and 15 cm, determined by the pressure transducer, soil sample area (A), and time (t) along the direction of flow (Equation 3.6),

$$q = \frac{V}{A \cdot t} = -K_s \frac{\Delta H}{L} \quad \rightarrow \quad K_s = -\frac{LV}{\Delta H \cdot A \cdot t} \tag{3.6}$$

The preparation of KSAT soil samples is identical to that of HYPROP sample preparation (see 3.2.1 for further details). Samples were saturated for a minimum of 24 hours from below. Water was not poured onto the sample as this could potentially have created air pockets. At the end of a KSAT measurement, two distinct measurements of saturated hydraulic conductivity are determined: 'Ks soil' and 'Ks total.' 'Ks soil' is the measurement of the saturated hydraulic conductivity of the soil sample only. Likewise, 'Ks total' is the measurement of total hydraulic conductivity including the hydraulic conductivity of the system (stainless steel ring with porous plate + crown) and the hydraulic conductivity of the soil sample. The peat was directionally sampled for both vertical and horizontal hydraulic conductivity.

The KSAT of the peat cores was tested using falling head measurements, where the peat core was connected to a burette with water at 20 cm, 15 cm, 10 cm, and 5 cm (geometric average of the data at these pressure heads was calculated at the end). Water was passed from

the burette into the peat core. As the water column height decreased, water flowed through a pressure sensor below the soil core, connected to a computer software package, which determined the rate of flow through the porous media.

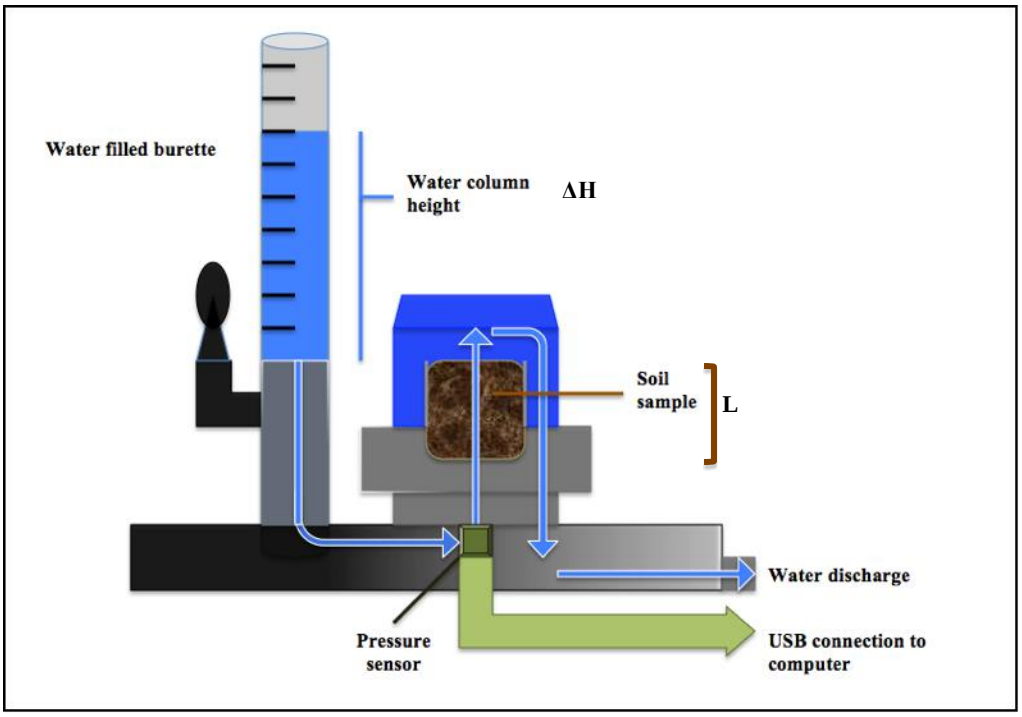

Figure 3-4. KSAT schematic depicting how the KSAT system operates. Image adapted from KSAT Operation Manual, http://www.ums-muc.de/en/products/soil_laboratory/ksat.html.

3.2.3 Measurement and Testing of Physical Parameters

Samples for the measurement of physical parameters (Figure 3-5) such as porosity (measure of the volume of void (interstitial) space relative to the total sample volume), specific yield (also known as drainable porosity; volume of water porous material will yield under gravity drainage) and bulk density (mass of the particles of a material's particles divided by the total volume those same particles occupy, highly dependent on degree of compaction) were extracted from thawed peat cores at 10 cm intervals of depth for all well sites. Each peat core also had samples taken for isotope analysis at 10 cm and 60 cm, though this depth guidance varied depending on the length of each core.

Once the cores thawed, desired interval lengths in increments of 10 cm were recorded on the peat core shipping boxes. The peat cores were then sliced into the desired sections,

removed from the shipping box, and placed on plastic film wrap. The metal core rings (250 ml) for the HYPROP and KSAT, label included, were weighed and the weights recorded before acquiring the samples from the peat cores. A rubber mallet was used to gently apply pressure to the metal 250 ml stainless sub-core, which gradually sliced into and extracted the sub-core sample at the desired depth within the peat core (Figure 3-6). The Von Post degree of humification was determined simultaneously as cores were extracted.

ANOVA SPSS (t-tests) statistical tests were done for the comparison of data sets across the site (east, west and road) for water table, physical hydraulic properties, saturated hydraulic conductivity, volumetric soil moisture, depth dependent trends of physical hydraulic properties and ground temperature. Results were deemed to be significant where $p < 0.05$. Post hoc tests (Tukey) were used to confirm where differences occurred between groups when significant differences occurred within group means.

Figure 3-5. Physical parameter peat cores 2-2.

Figure 3-6. Peat core extraction for HYPROP and KSAT experiments. Metal core ring (250 ml) for HYPROP and KSAT used to extract a sub-core from the larger peat core for determining horizontal conductivity.

For the measurement of peat physical parameters, standard techniques were used. Changes in the moisture content of peat cores of known volume were used to determine these parameters. Briefly, the volume of each core was determined. Cores were saturated (from below) and weighed (wet-weight) to determine porosity. Cores were subsequently drained for a period of 24 hours (to determine specific yield, and the top of the sub-cores were covered with plastic film wrap as they drained to prevent evaporation of the cores. Gravity-drained samples were weighed after a 24-hour period. Finally, cores were dried at 80 ^{o}C for a minimum of 24 hours to obtain the dry weight. Formulas for various calculations of physical hydraulic properties can be seen in Table 3-1.

Table 3-1. Formulas for various calculations of physical hydraulic properties.

Physical Hydraulic Property	Formula from Measured Values
Porosity (ϕ)	$\boldsymbol{\phi} = \frac{(\boldsymbol{wet\ weight\ (g)}) - (\boldsymbol{dry\ weight(g)})}{\boldsymbol{Volume(ml)}} \frac{\mathbf{1}}{\boldsymbol{\rho_{H_20}}}$
Specific Yield (Sy)	$\mathbf{Sy} = \frac{(\boldsymbol{wet\ weight(g)}) - (\boldsymbol{gravity\ drained\ weight(g)})}{\boldsymbol{Volume(ml)}} \frac{\mathbf{1}}{\boldsymbol{\rho_{H_20}}}$
Bulk Density (ρ_b)	$\mathbf{\rho b} = \frac{(\boldsymbol{dry\ weight(g)}) - (\boldsymbol{PVC\ tube\ \&\ label\ weight(g)})}{\boldsymbol{Volume(ml)}}$

Volumetric soil moisture (%) was calculated based on gravimetric data collected in the laboratory. Volumetric soil moisture is an excellent indicator of the ability of a material's ability to transmit and retain water. The moisture content of a soil can be expressed as volumetric water content, which is defined as the volume of water relative to the total volume of soil (Equation 3.6),

$$Volumetric\ soil\ moisture = \left(\left(\frac{(total\ sample\ weight\ (g)) - (dry\ weight\ (g))}{Volume\ (ml)}\right) \times\ 100\right) \frac{\mathbf{1}}{\boldsymbol{\rho_{H_20}}} \quad (3.6)$$

3.2.4 Manipulation of Water Level Measurements

Measurements of water levels in wells were taken and recorded throughout the 2013 field season on June 4, June 17, July 4, July 30, August 8 and August 17. These allow for determining the head. The equation for calculating water depth, illustrated by Figure 3-7, is,

$$x = (D - S) \tag{3.7}$$

where x is water table height with respect to the ground surface, D is the from the measured water level, and S is the value of stick-up.

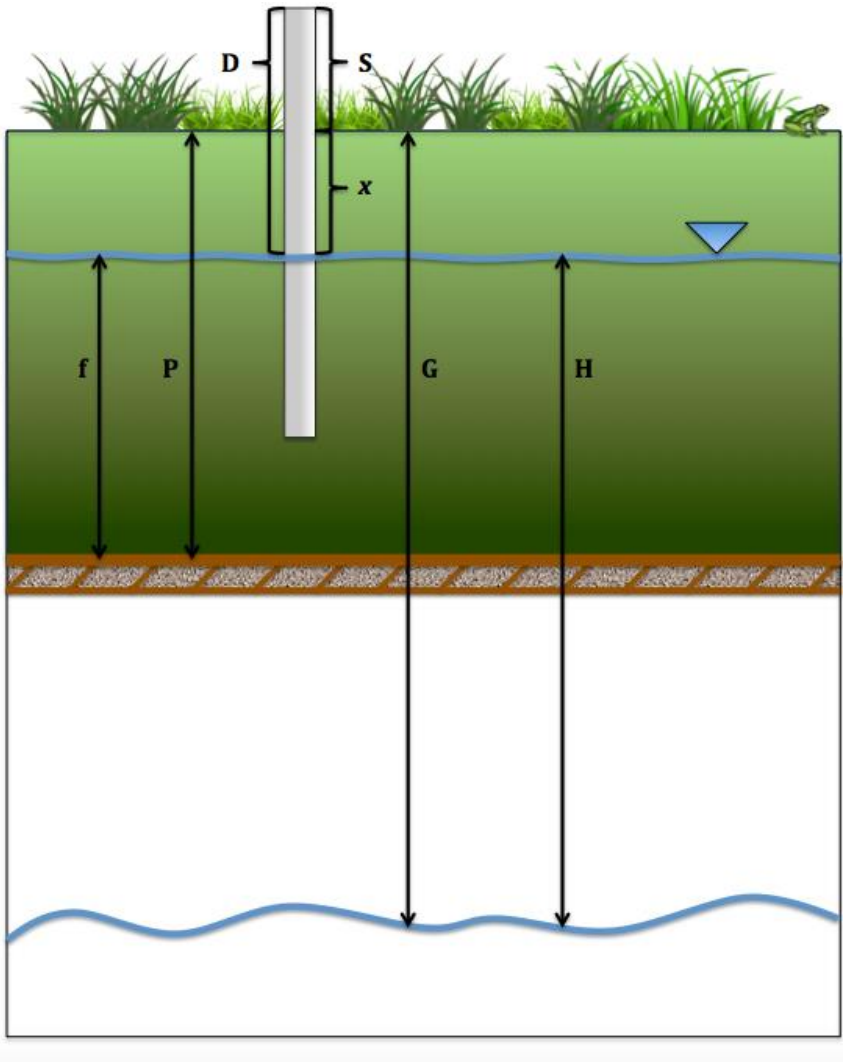

D- depth to water table from stick-up
S- stick-up
P- peat depth
f- height of saturated flow face
G- ground elevation (m.a.s.l.)
H- head of water (m.a.s.l.)
***x*- depth from ground surface to water table**

Figure 3-7. Various hydrogeological equation variables (field parameters). Measurements of water table elevation were calculated bimonthly throughout the 2013 field season.

3.2.5 Calculation of Volumetric Flow

Figure 3-8 illustrates how volumetric flow was calculated. Flow faces (blue) were established on the east (left) and western (right) sides of the road (grey, centered). The east side contains all the *n*-1, *n*-2 and *n*-3 wells; the east blue flow face contains all the *n*-2 wells. The western side contains all the *n*-5, *n*-6 and *n*-7 wells; the western blue flow face contains all the *n*-6 wells. The road contains only the *n*-4 wells. The blue arrows, moving east to west, indicate approximate flow direction. (Variable *n* refers to the specific well in each of the four transects.)

Before flow across each flow face could be established, pre-calculations were conducted and needed the following variables: x, water table with respect to ground surface (m); M, depth to mineral layer (m.a.s.l.); f, height of the saturated flow face (m); P, peat depth (m); H, head elevation (m.a.s.l.); D, depth to water table from stick-up (m), and; and S, stick-up (Table 3-2). The visualization of such calculations can be found in Figure 3-7. Head elevation with respect to sea level (m.a.s.l), H, was measured on site using the Suncor Base Station.

Table 3-2. Formulas for the pre-calculation of flow.

Flow Parameter	Formula for the pre-calculation of Flow
(x) Water table depth with respect to ground surface	$= (\boldsymbol{D} - \boldsymbol{S})$
(M) Mineral Depth	$= \boldsymbol{G} - \boldsymbol{P}$
(f) Saturated Flow Face Height	$= (\boldsymbol{G} + \boldsymbol{x}) - \boldsymbol{M}$

After completing pre-calculations, flow for the Pad 106 Access Road side could be calculated for the east, road and western flow faces after establishing the average head for wells upstream and downstream to the blue flow face of interest (Figure 3-8). For example, the wells located on the east side, parallel to the blue flow face are all the *n*-1 and *n*-3 wells. Average distance for well transects before and parallel to the saturated flow faces in question, as well as the distance across the saturated flow face itself, were determined using GIS software.

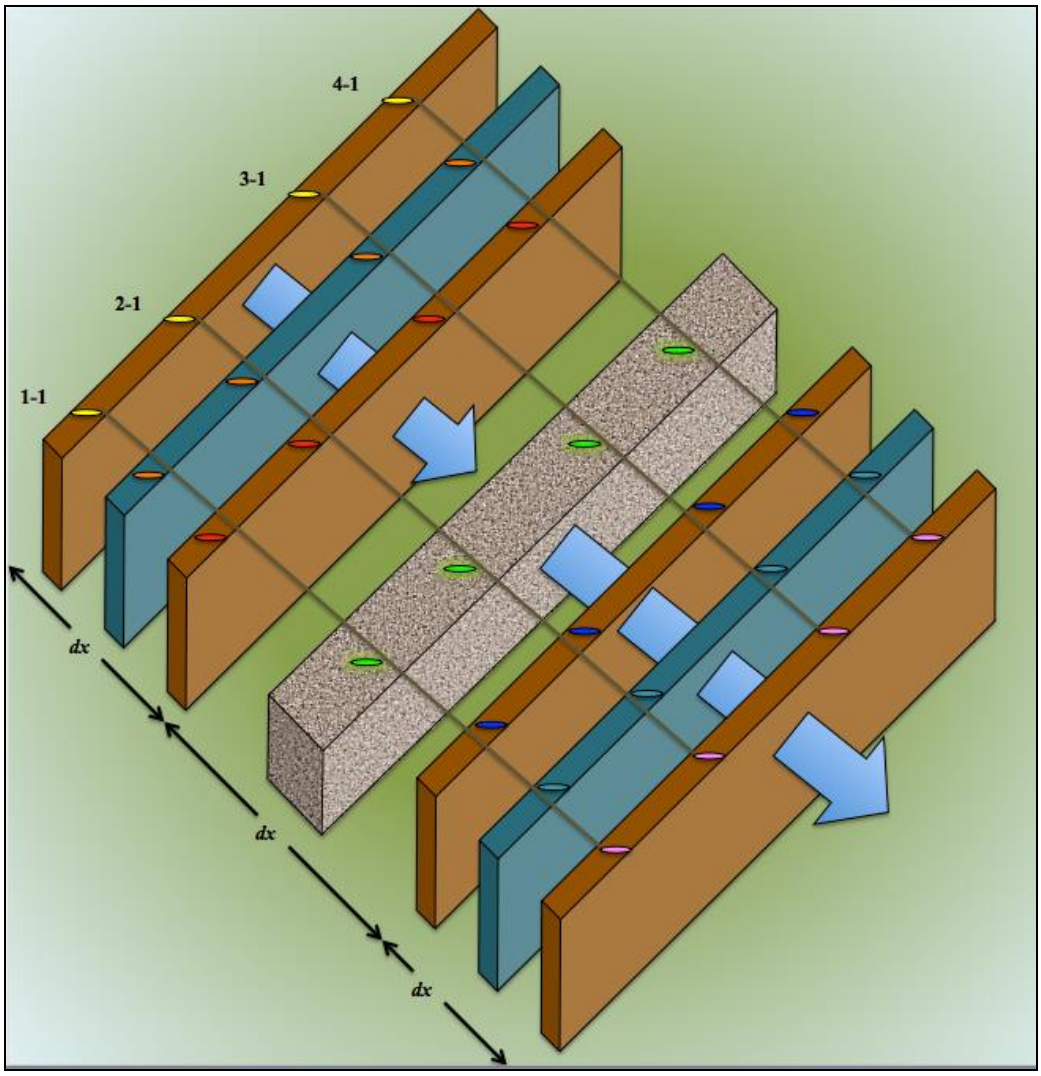

Figure 3-8. Volumetric flow face schematic. The blue flow face seen on the upper left hand side illustrates the eastern side of the road, and the lower right hand side blue flow face depicts the flow calculated for the western side of the road.

Before volumetric flow can be calculated, the calculations of: (a) flow face area, (b) hydraulic gradient, and (c) Darcy's flux must be completed. Flow face area, A, is a function of the length, L, and height, f, of the saturated flow face (Equation 3.8),

$$A = L\ f \tag{3.8}$$

Secondly, a vector gradient between two measurements of hydraulic head over the length of the flow path must be determined. This is referred to as i, the hydraulic gradient,

$$i = \frac{h\,(1) - h(2)}{\Delta l} \tag{3.9}$$

where h(1) refers to the head east (upgradient) of the flow face, h(2) refers to the head west (downgradient) of the flow face, and Δl is the distance (Equation 3.10).

Darcy's flux, q, can then be calculated as,

$$q = K_{\mu}\ i_{\mu} \tag{3.10}$$

where K_{μ} is the average hydraulic conductivity (m/s), and i_{μ} is the average hydraulic gradient (Equation 3.9).

Volumetric flow (m^3/day) may now be determined by,

$$Q = K_{\mu}\ i_{\mu}\ A \tag{3.11}$$

where A is the saturated flow face area (Equation 3.11). This is also known as 'Dupuit flow,' which has important assumptions such as homogeneity, isotropy, features of an unconfined system and flow occurring strictly parallel to the water table. Volumetric flow (m^3/day) (Figure 3-9), for the east and western sides of the road before and after road removal, is determined relative to flow through the road. Volumetric flow occured approximately perpendicular to the road. Road removal lasted June 18 to July 4.

3.2.6 Calculation of Anisotropy

Anisotropy (A) used in this contesxt is when the vertical (K_v) and horizontal hydraulic conductivites (K_h) differ by a factor > 5, or < 0.2,

$$A = \frac{K_v}{K_h} \tag{3.11}$$

A factor of 5 was choosen because it allows for uncertainty in the determination of hydraulic conductivity values. Anisotropic ratios greater than 5 indicate anisotropy with greater vertical hydraulic conductivity, while anisotropic ratios less than 0.2 indicate anisotropy with greater horizontal hydraulic conductivity.

Anisotropy can also be determined graphically by plotting K_h versus K_v; if the points appear on the 1:1 line the medium is isotropic, and if they deviate from the 1:1 line the medium is anisotropic. In the fields of earth science and groundwater management, anisotropy often pertains to geologic formations as well as the hydraulic conductivity of aquifers from a number of natural mechanisms.

3.2.7 Calculation of Transmissivity

Transmissivity, T (m^2/s) (Equation 3.12), is a concept that describes the measurable capacity of a saturated aquifer to transmit water approximately horizontally (K_h) with a contant thickness, b (Dingman, 1994). Transmissivity can be defined as,

$$T = b\ K_h \tag{3.12}$$

Transmissivity is also related to volumetric flow (Equation 3.13). The below equation set demonstrates how transmissivity is a good indicator of flow, along with hydraulic gradient (if volumetric flow cannot be calculated). Volumetric flow (Q) is,

$$Q = K\frac{\Delta h}{\Delta L}\ A = K\ \frac{\Delta h}{\Delta L}\ \ b\ \ L \tag{3.13}$$

where b is the height of the saturated flow face (thickness), L is the length of the saturated flow face. This can be simplified to,

$$Q = K\ i\ b\ L \tag{3.14}$$

where i is the hydraulic gradient and K is hydraulic conductivity. Transmissivity ($T = bK_h$) may be substituted in (Equation 3.15),

$$Q = T\ i\ L \tag{3.15}$$

3.2.8 Calulation of Consolidation Percent Difference

Percent difference (Equation 3.16), defined as the difference between a determined and theoretical value relative to the theoretical value, was calculated using calculated averages of porosity and bulk density. Porosity and bulk density are used as they are indicative of the compaction or consolidation of the peat. Averages of bulk density and porosity were calculated separately for the road and for the *n*-1 well locations *n*-2 well locations, *n*-3 well locations etc. Pristine locations are the outer most n-1 and n-7 well locations. The following formula was used to calculate percent difference relative to pristine locations,

$$\%\ diff. = \frac{(n-1 \text{ wells, or } n-2 \text{ wells, or } n-3 \text{ wells, etc.}) - (n-1\ and\ n-7\ average)}{(n-1\ and\ n-7\ average)} \tag{3.16}$$

3.2.9 Calulation of Peat Subsidence

Peat subsidence (Equation 3.17) was calculated relative to the initial measurement for a continuous portrayal of cumulative subsidence over time,

$$\Delta h_{peat} = h_i - h_o \tag{3.17}$$

where h_i is height at time *i*, and h_0 is height at time zero. July 3 (day 0) measurements were used as h_0, and July 4 (day 1), July 30 (day 27), August 8 (day 35) and August 18 (day 45) measurements were used as h_i. A constant pressure was applied by the plexiglass plate

(average: 63.47 Pa, standard deviation: 0.0925, max: 63.64 Pa, min, 63.38 Pa) equally to all measurements. Road removal was June 18 – July 4.

4.0 Results

During the summer of 2013, the site-specific meteorological conditions at Suncor's Firebag Site Pad 106 Access Road were cool, dry and sunny to cloudy with light rain and fog. However, extreme rains occurred June 8 and June 9, 2013 (Figure 4-1). (The operation of the meteorological tower was briefly interrupted while the site flooded June 8 and 9.) Fort McMurray precipitation data (Appendix 6) illustrates the scope of the extreme rainfall and subsequent flooding occurring in that nearby area of Alberta on June 8 and 9. Precipitation occurring in Fort McMurray (Appendix 6) and precipitation at the Pad 106 Access Road site at Firebag are nearly the same in magnitude and duration. Historical climate data for Fort McMurray can be found in Appendix 6.

The east side of the road flooded (Figure 4-1), while the west side of the road remained relatively dry because the Pad 106 Access Road prevented floodwater from entering the west side. An industrial water pump was set up to help divert floodwater to the west side of the road to aid the acceleration of the delayed road removal process. Though the severe flooding of June 8 and 9 substantially delayed the road removal process, the flooding clearly demonstrated the significant effect of roads on hydrology, in which roads act as barriers to regional water flow.

Figure 4-1. Road site flooding photographs June 2013. Left: June 8 and 9 flooding. South view of Pad 106 Access Road. Right: June 11: pumping station installed, water diverted to the drier northwestern side of the road, and flood water migrated down a ditch along Rick George Way to small ponds.

4.1 Meteorology at Firebag Fen

Figure 4-2 displays precipitation, windspeed and net radiation measured from June 3 to October 17. Mean seasonal windspeed, net radiation and precipitation were event magnuitude 1.77 $\pm$ 1.1 m/s, 67.6 $\pm$ 147 W/m^2 and 1.31 $\pm$ 5.7 mm, respectively. Ground temperature locations 1 and 2 are situated on the east side of the road, while locations 3 and 4 are situated on the west side. Figure 4-3 shows the ground temperature, relative humidity and air temperature as a function of distance from the road between transects 2 and 3. Relative humidity and air temperature (Figure 4-3) for all four locations showed variability between sites but consistency over time. Relative humidity varies significantly when the temperature changes, which corresponds to relative humidity being a function of available moisture and air temperature. Relative humidity fluctuated in values ranging from approximately 40-100 %. Mean relative humidity at locations 1, 2, 3, and 4 for June, July and August were 74.4 $\pm$ 3.1 %, 74.3 $\pm$ 2.6 %, 77.0 $\pm$ 2.0 % and 75.6 $\pm$ 3.0 %, respectively. Mean air temperature at locations 1, 2, 3, and 4 for June, July and August were 15.7 $\pm$ 0.67 °C, 15.8 $\pm$ 0.62 °C, 15.7 $\pm$ 0.77 °C, and 15.5 $\pm$ 0.67 °C, respectively.

Average ground temperatures at depths of 10 cm, 30 cm, 50 cm and 100 cm are 15.1 °C, 13.9 °C, 13.3 °C and 12.1 °C, respectively. Temperature fluctuated at the surface and became less variable with increasing depths at 50 cm (location 1: 13.5 $\pm$ 0.75 °C; location 2: 13.7 $\pm$ 0.73 °C; location 4: 12.6 $\pm$ 0.6 °C) and 100 cm (location 1: 12.3 $\pm$ 0.61 °C; location 2: 12.2 $\pm$ 0.49 °C; location 4: 11.7 $\pm$ 0.5 °C), which is why statistical testing was done only for depths of 10 and 30 cm. Unusual data was produced by location 3 at 50 cm and 100 cm, probably due to sensor error, and were omitted from Figure 4-3. Statistical testing (ANOVAs) showed that depth specific ground temperatures did not differ ($p > 0.05$) at 10 and 30 cm for the east (mean = 13.7; std. dev = 1.0) and west sides (mean = 13.7; std. dev = 1.72).

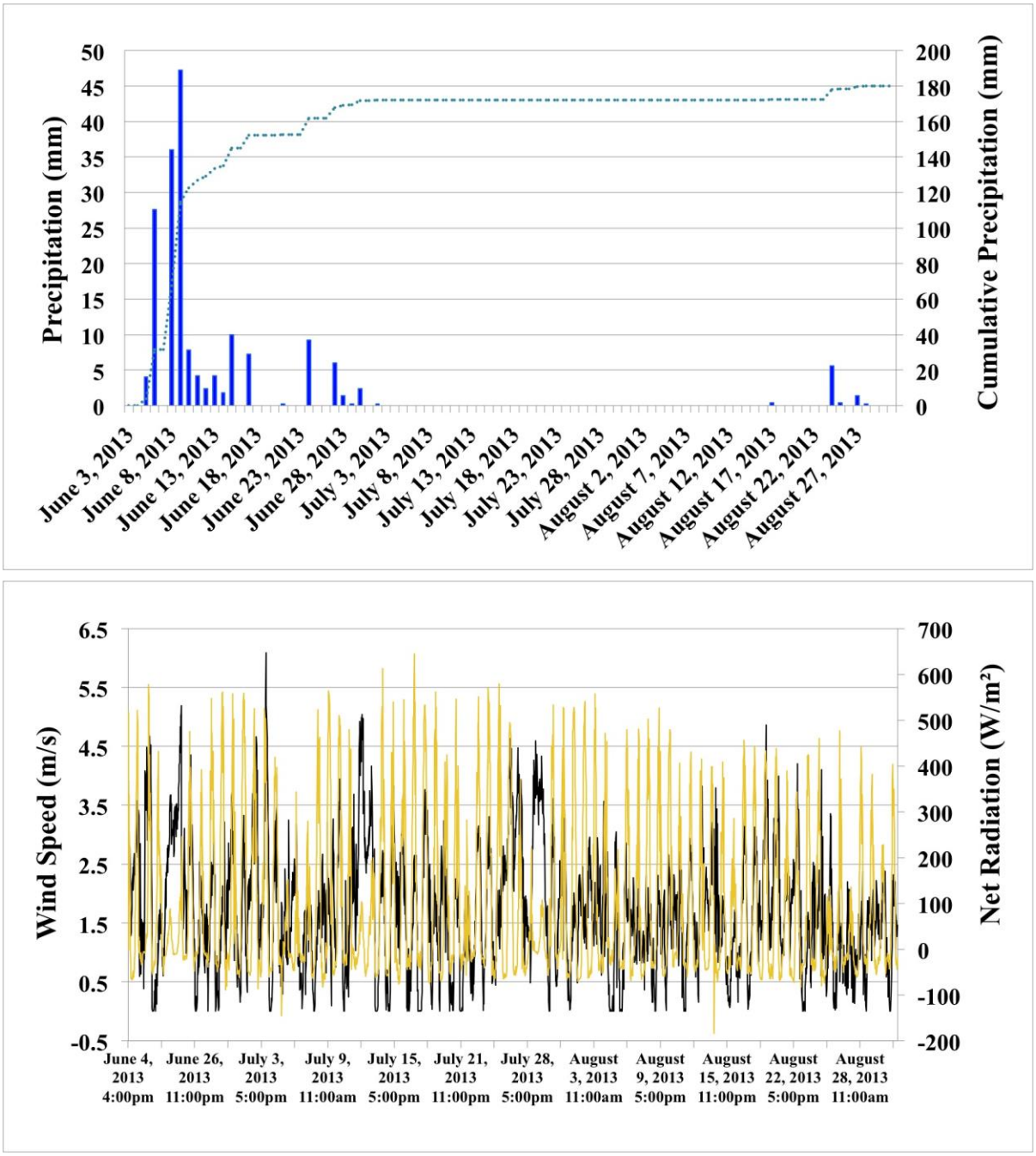

Figure 4-2. Meteorological parameters at Firebag fen: wind speed and net radiation, and cumulative (horizontal blue line, secondary axis) and daily precipitation.

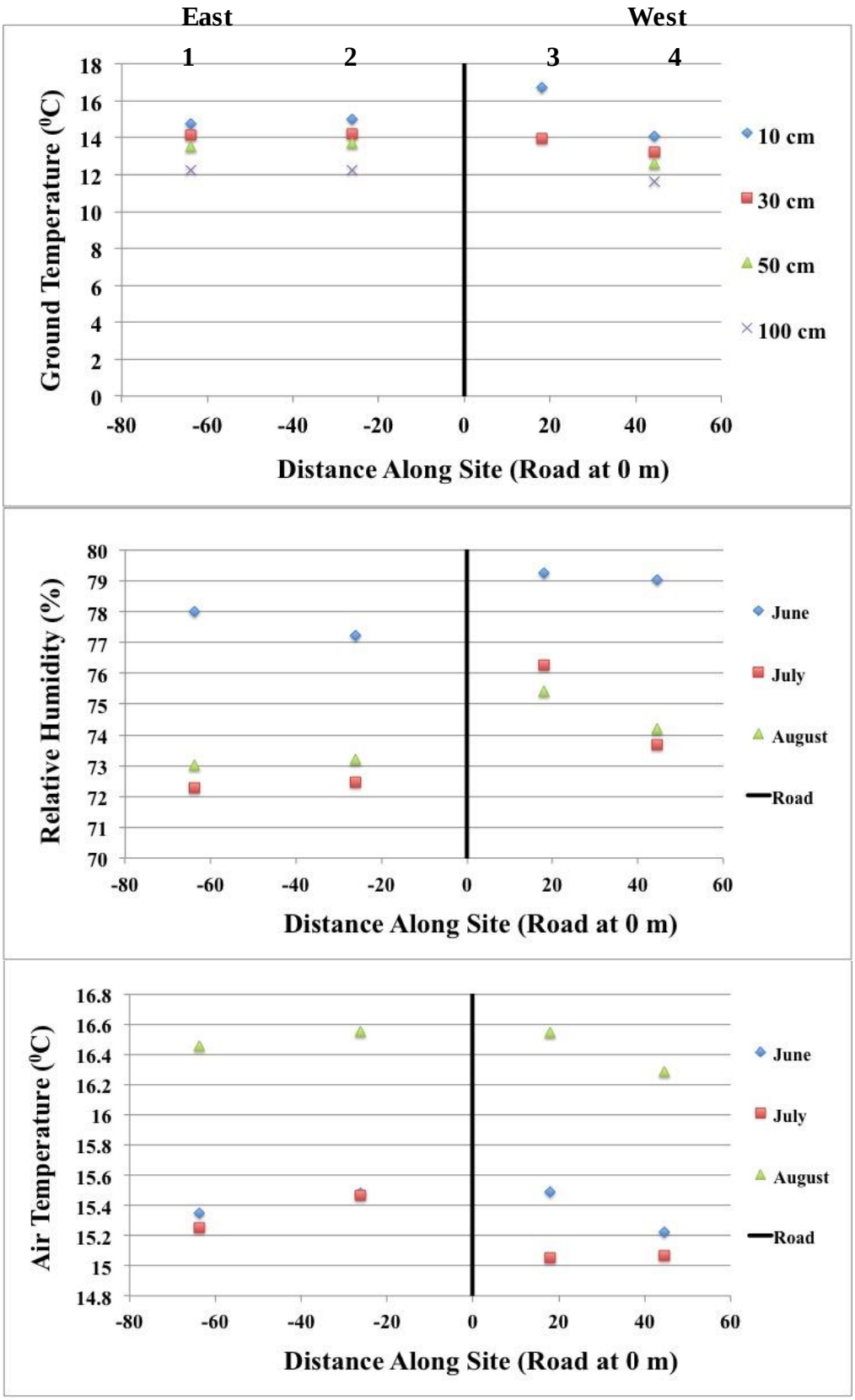

Figure 4-3. Ground temperature in hummocks and hollows at depths of 10, 30, 50 and 100 cm, air temperature, and relative humidity as a function of distance from the road averaged for the entire 2013 field season. Sensor locations are located above for each of the four measuring points. Locations 1 and 2 are situated on the east side, while locations 3 and 4 are located on the west side.

4.2 Spatial Variability in Peat Physical Properties

Mean and standard deviations of porosity, specific yield and bulk density for transects 1, 2, 3 and 4, the west and east side of the Pad 106 Access Road, the road wells, the eastern wells, and 'natural' wells can be found in Table 4-1. In this context, 'natural' is a relative term, defined as the outermost (or pristine) well sites on both the east (*n*-1) and western (*n*-7) sides of the Pad 106 Access Road. The average physical parameters for transects 1, 2, 3 and 4 gradually change along the road, with porosity decreasing and bulk density increasing from transect 1 to 4.

Table 4-1. Physical parameter (porosity, bulk density, and specific yield) mean (μ) and standard deviation (σ) for each transect, the eastern and western sides, road and natural locations.

Transect or Relative Region	Porosity (ϕ)		Bulk Density (ρ_b)		Specific Yield (Sy)	
	μ	σ	μ	σ	μ	σ
1	0.87	0.04	0.15	0.06	0.13	0.05
2	0.85	0.03	0.17	0.07	0.11	0.05
3	0.83	0.06	0.20	0.13	0.09	0.04
4	0.81	0.16	0.22	0.25	0.12	0.07
West (Dry)	0.81	0.12	0.25	0.19	0.12	0.05
Road	0.82	0.05	0.20	0.02	0.14	0.03
East (Wet)	0.88	0.03	0.12	0.05	0.10	0.06
Natural (*n*-1, *n*-7)	0.86	0.04	0.11	0.05	0.12	0.07

4.2.1 Differences in Peat Properties between the Road and Adjacent Peatlands

Average porosity with distance from the road (road indicated by line at 0 m) in Figure 4-4a, shows higher values to the east, which suggests the peat is more dense on the western side. This is the side with the vehicle maintenance corridor, which has likely decreased the void space.

The road (0 m) and the sites located along the maintenance vehicle winter corridor on the western side of the road (*n*-5 and *n*-6 wells, ~8 to 35 m away from the road) clearly indicate the largest range in porosity (Figure 4-4a). The large range in porosity (0.75-0.93) within the road and wells sites located along the corridor indicates a decrease in porosity from natural values likely from the disturbance of the peat column under pressure by large vehicles. Some porosity values are higher than normal for peat, and may be accounted for by altered biostructures and decay. Significant differences in porosity were observed between the east and west sides of the road ($p = .002$; d.f. = 162), and the east side and the road ($p = .002$; d.f. = 113), but not between the west side and the road ($p > 0.05$; d.f. = 87).

Average spatial bulk density (Figure 4-4b) shows an increasing trend across the site from the east to the west. The spatial trends for average specific yield are greater on the eastern side of the road compared to the western side. (In contrast, mean bulk density was greater on the western side (Figure 4-4b).) Statistical tests on differences in specific yield showed that significant differenes exist for specific yield between the east side of the site and peat beneath the road ($p = .014$; d.f. = 113). However, there were no significant differenes for specific yield for the east versus the west side of the site ($p = .170$; d.f. = 162), and specific yield of the west side of the site versus the road ($p = .351$; d.f. = 87). The increase in specific yield within the western section reflects the apparent decrease in porosity also seen in the west. Bulk density remained consistent within the eastern saturated portion of the site. Bulk density of the road in comparison to the outer, seemingly more natural, transects did not vary in range. A significant difference ($p < 0.05$) in bulk density was observed among the east side, road, and west side. Post-hoc analyses revealed that bulk density differed between the east and west sides, ($p < .001$; d.f. = 162), and between the east side and the road ($p < .001$; d.f. = 113), but bulk density did not differ between the west side and the road ($p < 0.05$; d.f. = 87).

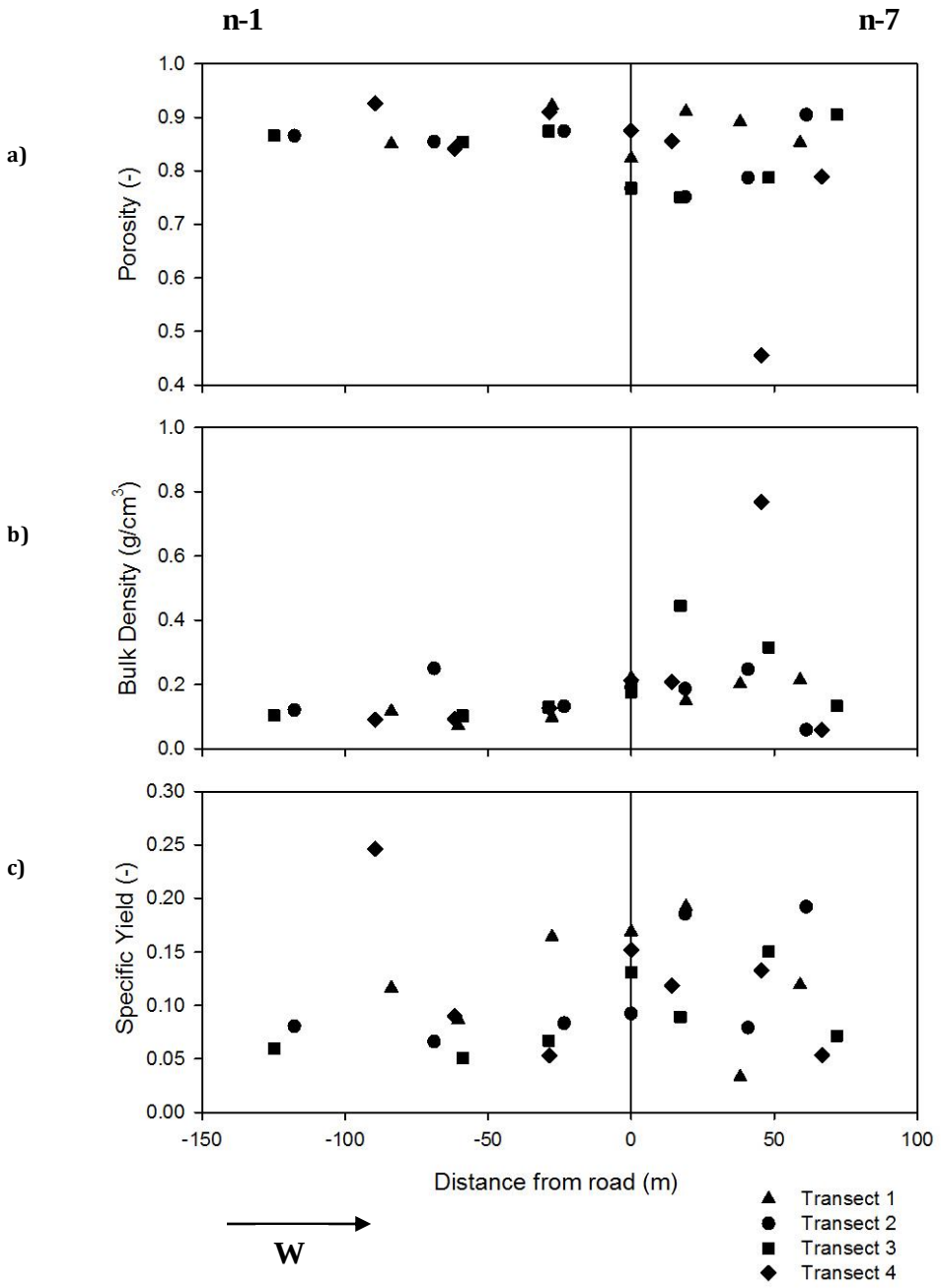

Figure 4-4. a) Average porosity, b) average bulk density and c) average specific yield with distance from road.

4.2.2 Vertical Differences in Peat Properties

Physical parameters were examined statistically at depths of 20 cm and 60 cm for porosity, bulk density and specific yield, and compared individually for the east, west and road areas. No significant differences were found for the three groups ($p > 0.05$). Cross-site comparisons were not made.

4.2.2.1 Changes in Porosity with Depth

Road porosity and natural porosities are shown in Figure 4-5a. The natural wells include: 1-1, 2-1, 3-1, 4-1 on the eastern side and 1-7, 2-7, 3-7, 4-7 on the western side. In comparison to the road, natural locations show a slight increase in porosity. It was hypothesized that natural areas would exhibit higher values of porosity, indicating lack of disturbance and compression. However, the differences between the natural and the road are not significant; both sites show values at 0.8, typical porosity of peat). Statistical tests for porosity at 20 cm and 60 cm for the east ($p = .694$; d.f. = 22), the west ($p = .119$; d.f. = 16), and the road ($p = .478$; d.f. = 4) did not show significant differences.

4.2.2.2 Changes in Bulk Density with Depth

Figure 4-5b shows road bulk densities compared to the natural bulk densities of outlying well sites. Road bulk densities show a smaller range, yet surprisingly fall within the natural range. The road peat was clearly more compact upon core extraction. The smaller road bulk density range further illustrates this compact state. Bulk densities of the road and the natural locations show a tendency to increase with depth, which coincides with the initial hypotheses that bulk density would increase with depth for both the afflicted (road) peat column and the pristine peat column. The average and standard deviations for road bulk density were 0.20 ± 0.02 g/cm^3. As for the natural outermost locations, the average and standard deviations were 0.111 ± 0.049 g/cm^3. Statistical tests for bulk density at 20 cm and 60 cm for the east ($p = .277$; d.f. = 22), the west ($p = .902$; d.f. = 16), and the road ($p = .064$; d.f. = 4) did not show significant differences.

4.2.2.3 Changes in Specific Yield with Depth

Figure 4-5c shows the specific yield of the road plotted in contrast to the specific yield of natural locations. Specific yield, or drainable porosity, shows the same range and trends for both the road and the outermost well sites. Nevertheless, 'natural' transect 4 shows a disparate trend, and a higher specific yield, which may be due to the presence of overburden and compression due to the construction of the above ground pipeline running along transect 4. Transect 4 runs closely alongside the above ground pipeline, an adjacent road and the SAGD in-situ pad, all of which are operational. It may be that the addition of sand and gravels along this transect were artificially introduced with construction. The average and standard deviations for road specific yield were 0.136 and 0.032, respectively. As for the 'natural' outermost locations, the average and standard deviation were 0.117 and 0.068, respectively. Statistical tests for specific yield at 20 cm and 60 cm for the east ($p = .963$; d.f. = 22), the west ($p = .376$; d.f. = 16), and the road ($p = .648$; d.f. = 4) also did not show significant differences.

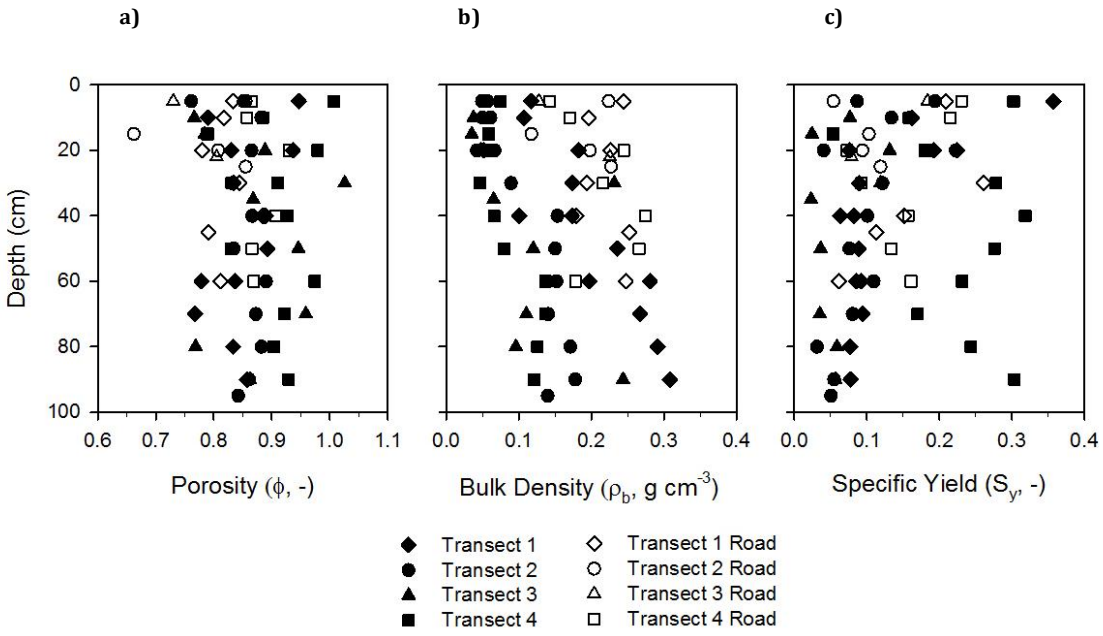

Figure 4-5. Natural vs. road physical hydraulic parameters: a) porosity, b) bulk density, and c) specific yield. Natural parameters represented by soild symbols, road represented by hollow symbols.

4.2.3 Consolidation

Consolidation throughout the Pad 106 Access Road site is shown in Figure 4-6. The ranges of -120 m to 0 m and 0 m to 80 m represent the eastern and the western sides of the road, respectively. The road is represented at 0 m. All sampling points were included by averaging the *n*-1, *n*-2,… *n*-7 wells of the four transects separately. The line at 0 consolidation is for visual aid.

Consolidation was measured by using percent differences of bulk density and porosity. Figure 4-6 shows that bulk density and porosity are inversely related. Figure 4-6, in general, shows that the larger percent differences of porosity and bulk density correspond to each other. Bulk density mostly increased from east to west. Porosity decreased significantly at the road and close to the winter maintenance vehicle corridor. The winter maintence corridor may have been in place for a longer period of time versus the road, which could account for the higher consolidation seen on the western side of the road. Large numerical changes in bulk density corresponded to the same changes in porosity. The linear regression for percent difference bulk density and porosity is: $y = -0.044x$, $R^2 = 0.5694$. This shows a strong correlation that as bulk density increases, porosity decreases.

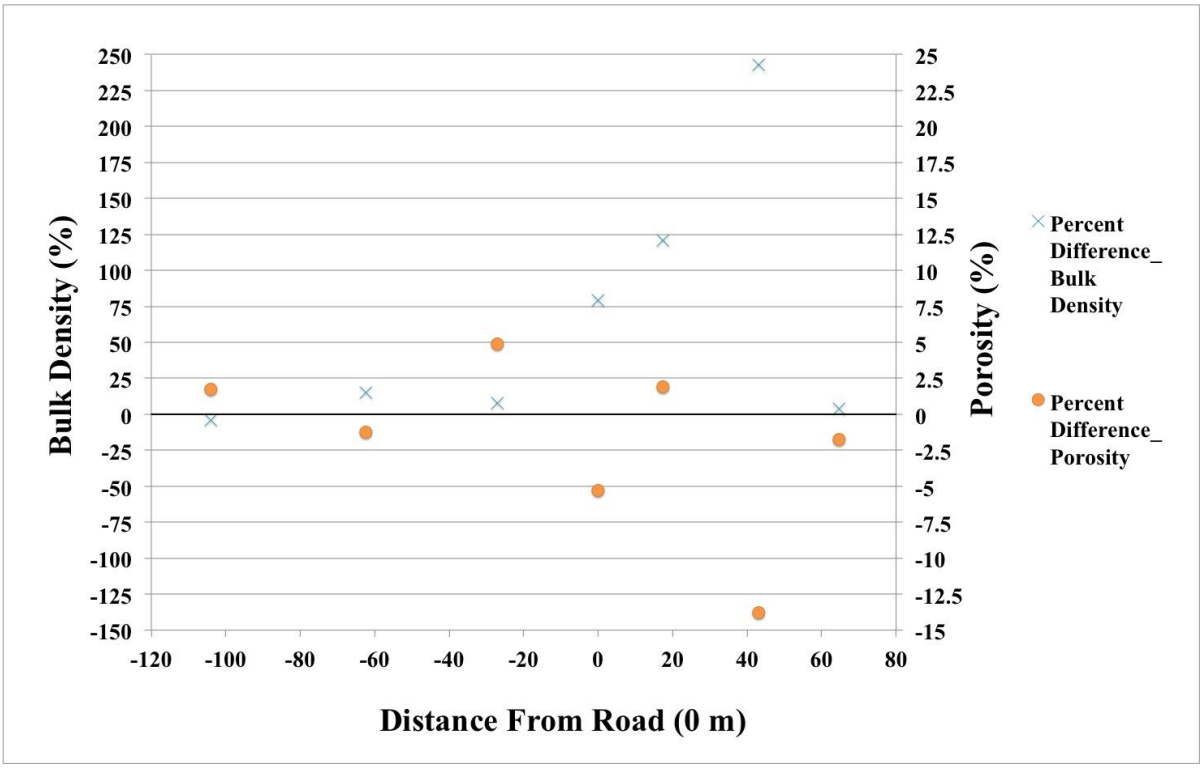

Figure 4-6. Top: Consolidation as a function of bulk density and porosity. The road peat is at 0 m, natural peat locations are at approximately -105 m and 63 m.

4.3 Variability in Peat Hydrologic Parameters and Variables

4.3.1 Volumetric Soil Moisture

Figure 4-7 depicts volumetric water content for peat at the well sites located on the eastern and western sides of the road, and for the road sampled after road removal. Volumetric water content for the Pad 106 Access Road (50.3 $\pm$ 9.8 %) is the least moist, in comparison to the adjacent wells located on the eastern (66 $\pm$ 11 %) and western (56 $\pm$ 18 %) sides. The high variability of volumetric soil moisture observed on the western side of the road may be a function of the prevention of flow from the road, resulting in lowered moisture levels; however, a certain degree of saturation may have been maintained by some channeling of water underneath the road.

Statistical tests for volumetric soil moisture for all increments of 10 cm depth showed significant differences between east versus west, east versus road, and west versus road. All p values were less than .01 in post hoc tests. However, when comparing volumetric soil moisture only at specific depths of 20 cm and 60 cm, significant differenes were discovered between the east versus the west ($p < .02$; d.f. = 112), and the east versus the road ($p < .02$; d.f. = 161), but not the road versus the west ($p = .02$; d.f. = 87) as shown by post hoc tests.

4.3.2 Soil Moisture Retention

Figures 4-8 and Figure show soil moisture retention curves of transect 1 and 2 and transect 3 and 4, respectively, for the Pad 106 Access Road site. The calculation of retention data from the measured tensions and weight changes follow the simplified evaporation method (Schindler, 1980; Schindler et al., 2010b; Peters and Durner, 2008). For calculations, only the tensions and weights in the time window between start and stop time are considered. Negative pressure head increases from left to right along the x-axis. Sample 2-5 was excluded due to the first trial failing, and subsequently not being able to run the core a second time due to advanced dessication.

Soil moisture retention curves for all transects show a starting point at ~85 % water content at 0.1-0.6 pF, and are reduced to about half by 2.6 pF. However, not all samples followed the same curve, for example, 1-3 at 60 cm, 1-2 at 60 cm and 1-4 at 10 cm deep stray from this trend. Curve 1-4, 60 cm, was able to retain water for longer, which may be

attributed to the compact nature of the peat beneath the road, resulting in smaller pores holding water for longer periods till higher negative pressure heads arise. However, this trend was not observed in the other road locations.

Road retention curves tend to hover around the starting point of 80 % for water content range, and end with negative pressure very close to the other samples (2.85 pF). However, the resulting water content end points for the road vary (15-50 %) across the transects.

Transect 1 retention curves for the saturated eastern area beside the road fall below retention curves for the non-flooded northwest area. However, a culvert and pumping station were established at transect 1 throughout the field season, resulting in the wet conditions within the downstream receiving well sites (1-5, 1-6 and 1-7) due to the extra input of water. Elevation also increases across the Pad 106 Access Road site, from transect 1 to transect 4, which also contributes to the wet conditions witnessed at transect 1. Soil moisture retention curves for the west area are more similar to each other than the curves for the east.

4.3.3 Saturated Hydraulic Conductivity

Figure 4-10 shows saturated hydraulic conductivity as box plots for the east ($1.3 \times 10^{-3} \pm 2.0 \times 10^{-3}$ m/s), and the west ($0.7 \times 10^{-3} \pm 1.5 \times 10^{-3}$ m/s) side of the road and the road ($6.7 \times 10^{-4} \pm 4.1 \times 10^{-4}$ m/s). Median saturated hydraulic conductivity values were on the order of 10^{-3} – 10^{-2} m/s. Box plots present four regions: the 4th quartile (upper whisker), 3rd quartile (upper box), 2nd quartile (lower box), and 1st quartile (lower whisker). The quartiles are limited by the upper range, 75th percentile, median, 25th percentile, and lower range. The data is presented on a logarithmic scale to better illustrate the range of magnitudes for hydraulic conductivity.

In general, the saturated hydraulic conductivity did not significantly differ between the east and west sides ($p > 0.05$; d.f. = 22), the east versus the road ($p < 0.05$; d.f. = 14), and also the west versus the road ($p = .870$; d.f. = 14). The median saturated hydraulic conductivity also did not vary between the road and adjacent peatlands.

Figure 4-11 shows anisotropy for the Pad 106 Access Road site peat. The anisotropic factor for the east, west and road are 4.0, 1.86 and 1.9 respectively. The data clearly does not adhere to the 1:1 line, which would be an indication of anisotropy. All road well sites except

for 2-4 are above the 1:1 line, which means vertical hydraulic conductivity was greater than horizontal conductivity.

Peat soils can be described as exhibiting random heterogeneous qualities, which may have attributed to the random anisotropic nature of the peat columns for the Pad 106 Access Road site. Values of vertical and horizontal hydraulic conductivity, accompanied by their anisotropic ratios, can be found in Appendix 7. Values of saturated hydraulic conductivity determined by the KSAT lab setup were depth-averaged, as well as geometrically averaged. The geometric averages for saturated hydraulic conductivity can be found in Table 4-2. A geometric average is best used for measurements of saturated hydraulic conductivity because of high variations in magnitude. Due to core length limitations, geometric averages could not be obtained for transects 2 and 3 saturated hydraulic conductivity at 60 cm.

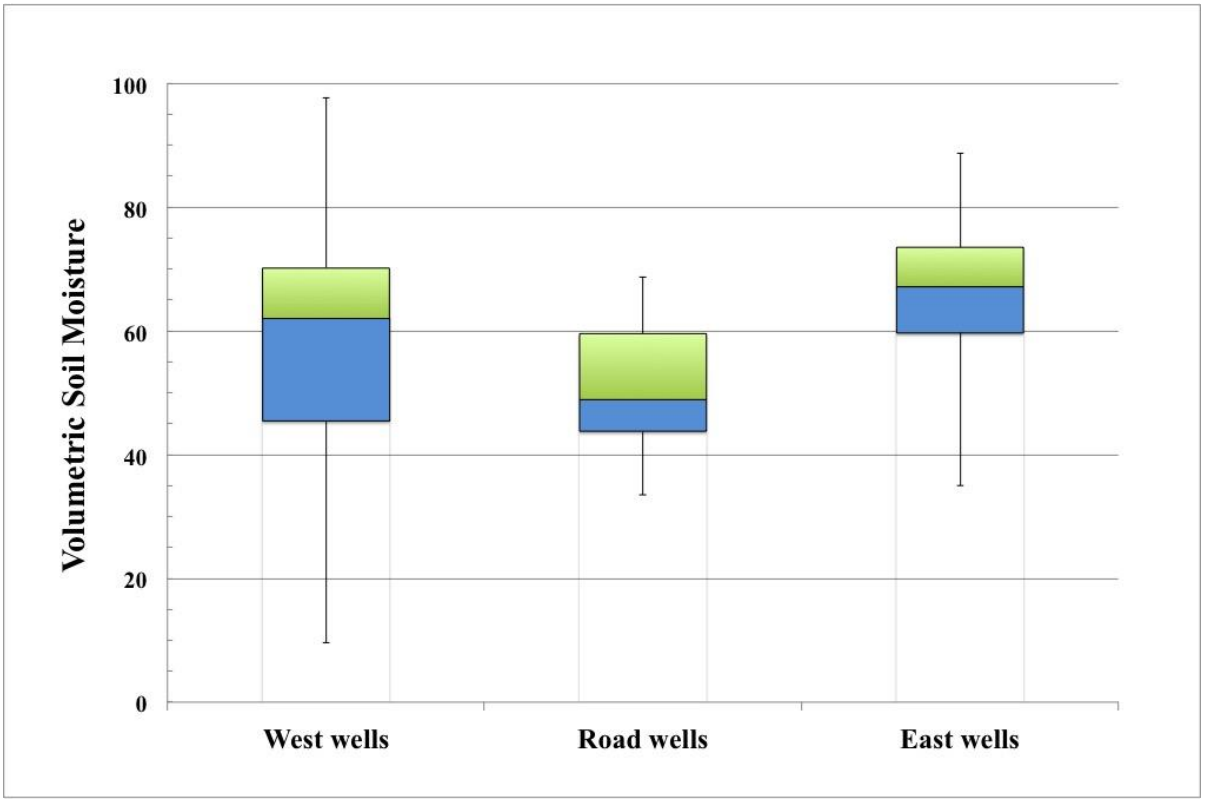

Figure 4-7. Volumetric soil moisture (%) for the western and eastern sides and the road. The five horizontal lines represent, from bottom to top: the minimum, the 25th percentile, the median, 75th percentile, and the maximum. There are four regions expressed in each box plot, from bottom to top: the bottom whisker is the minimum to 25th percentile, the blue box is the 25th percentile to the median, the green box is the median to the 75th percentile, and the top whisker is the 75th percentile to the maximum.

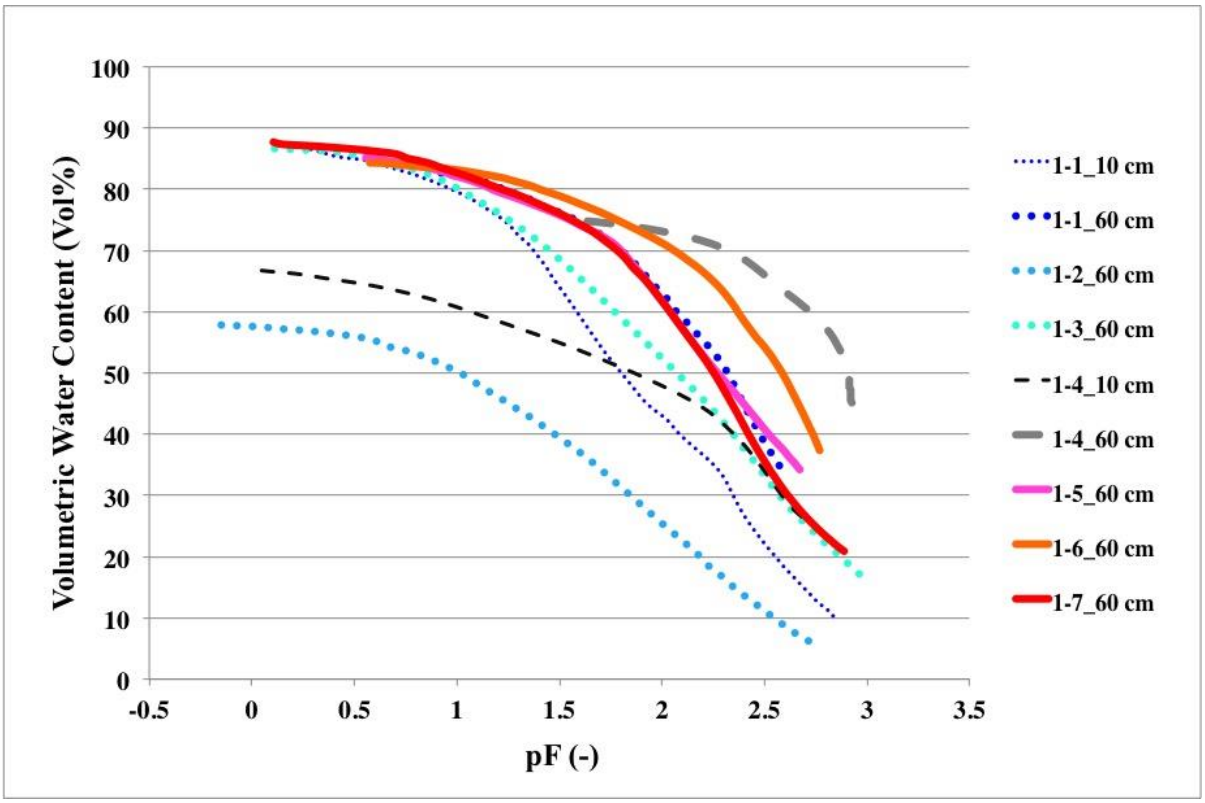

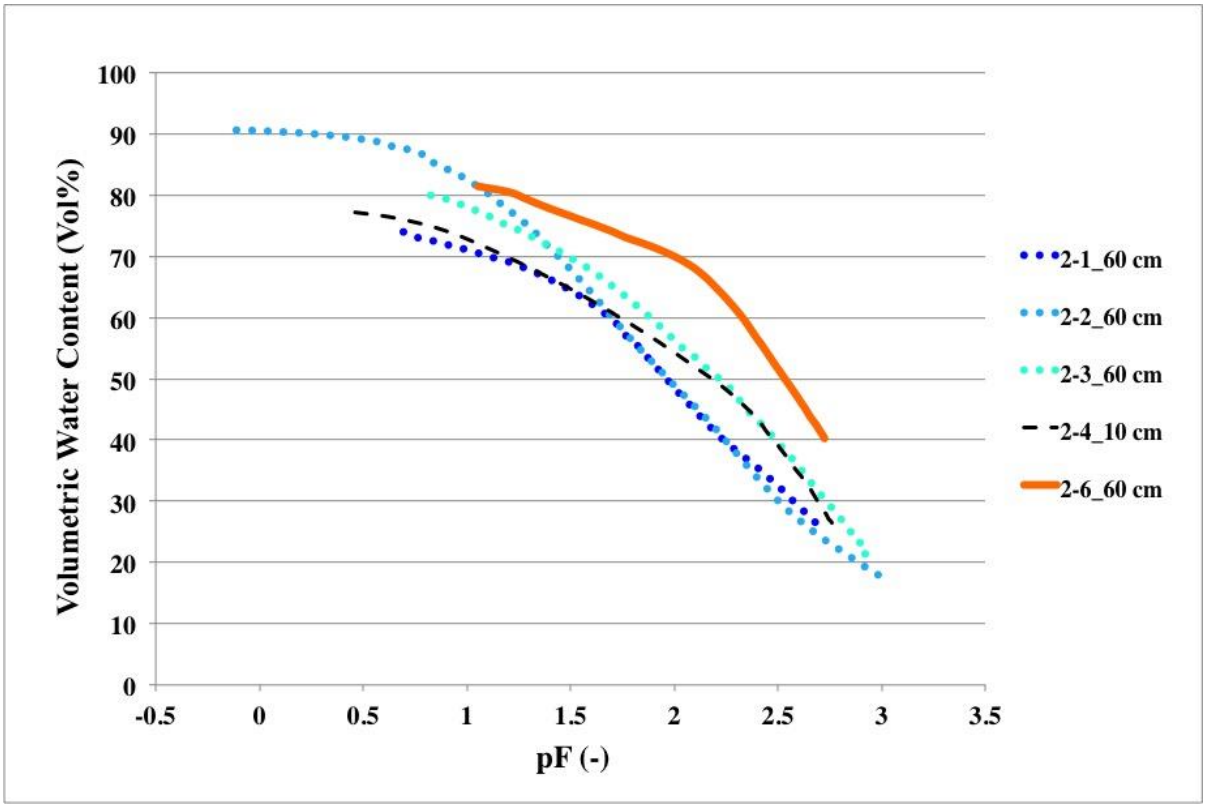

Figure 4-8. Soil moisture retention curves for transects 1 and 2. Soil moisture curves were obtained at depths 10 cm and 60 cm, core length permitting. All transects except for transect 3 had moisture curves computed at only 60 cm. Ideally, transect 3 and the Pad 106 Access Road had retention curves calibrated at 10 cm and 60 cm, core length permitting. Transect 3 was ambiguously chosen for comparison purposes with the Pad 106 Access Road.)

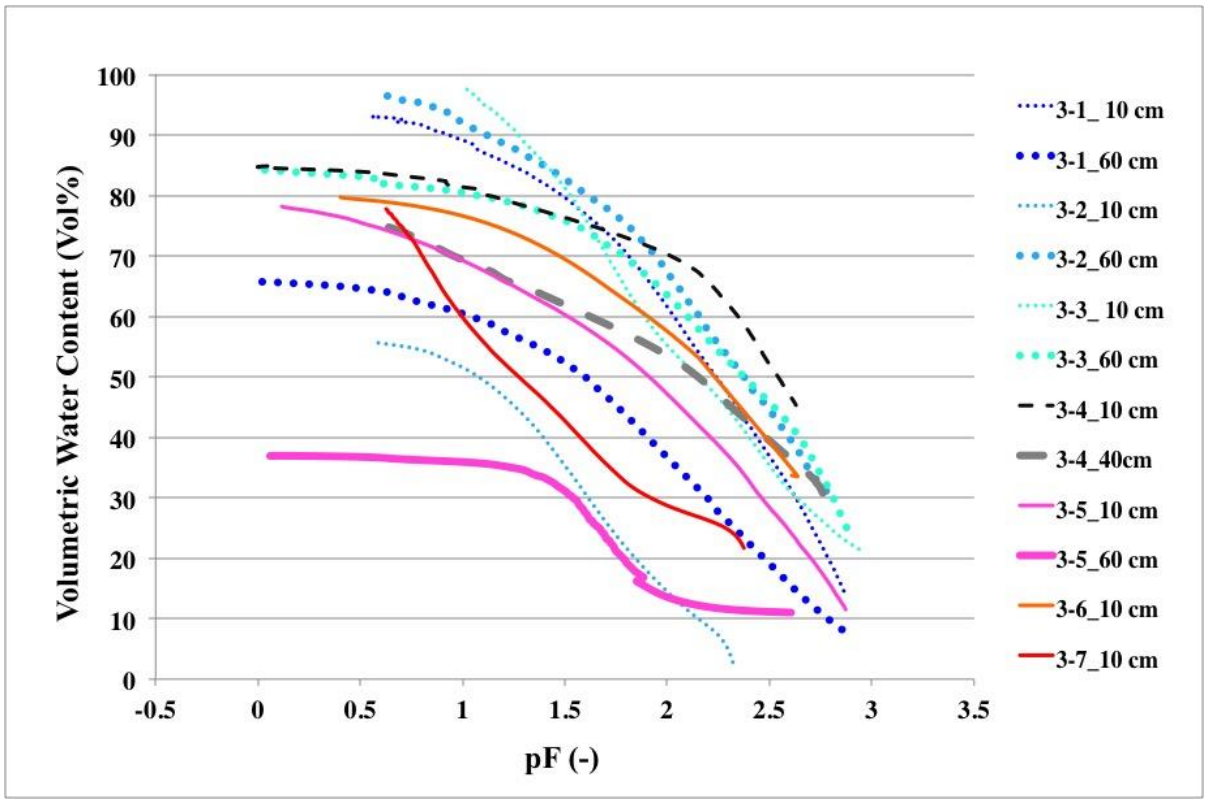

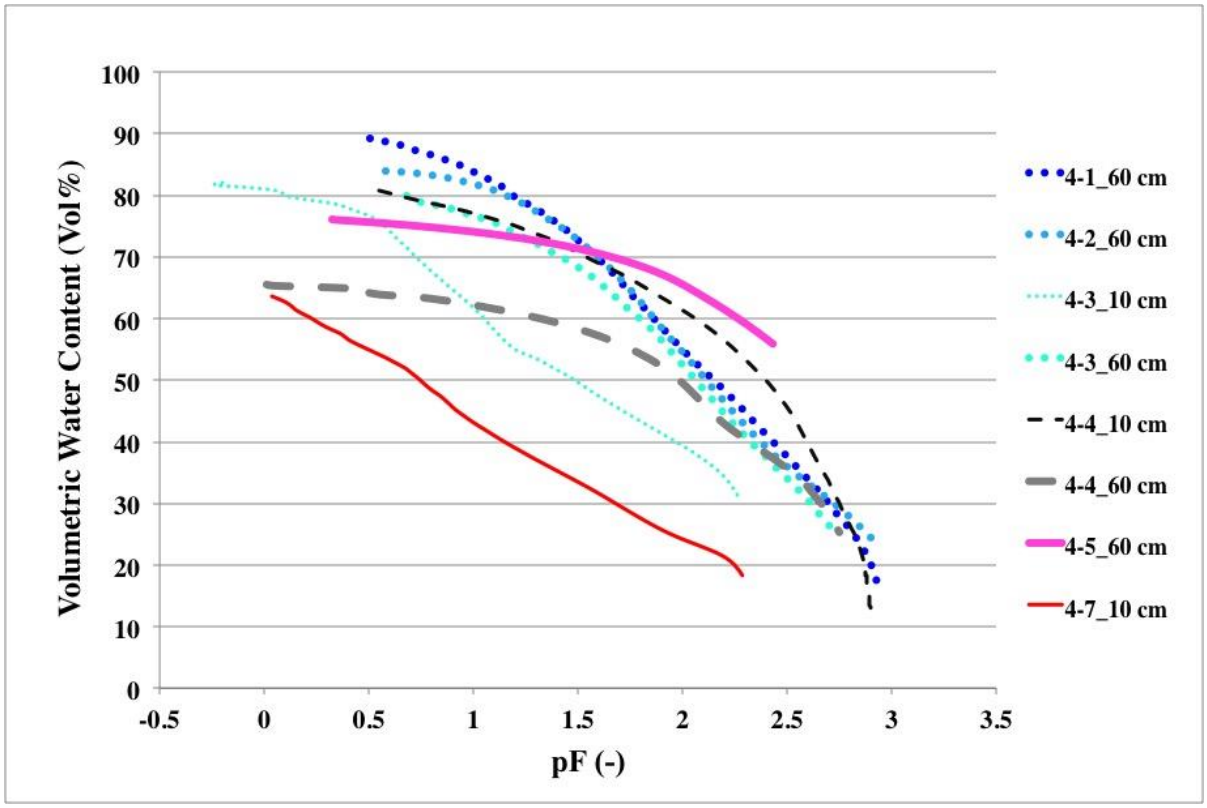

Figure 4-9. Soil moisture retention curves for transects 3 and 4. Soil moisture curves were obtained at depths 10 cm and 60 cm, core length permitting. All transects except for transect 3 had moisture curves computed at only 60 cm. Ideally, transect 3 and the Pad 106 Access Road had retention curves calibrated at 10 cm and 60 cm, core length permitting. Transect 3 was ambiguously chosen for comparison purposes with the Pad 106 Access Road.

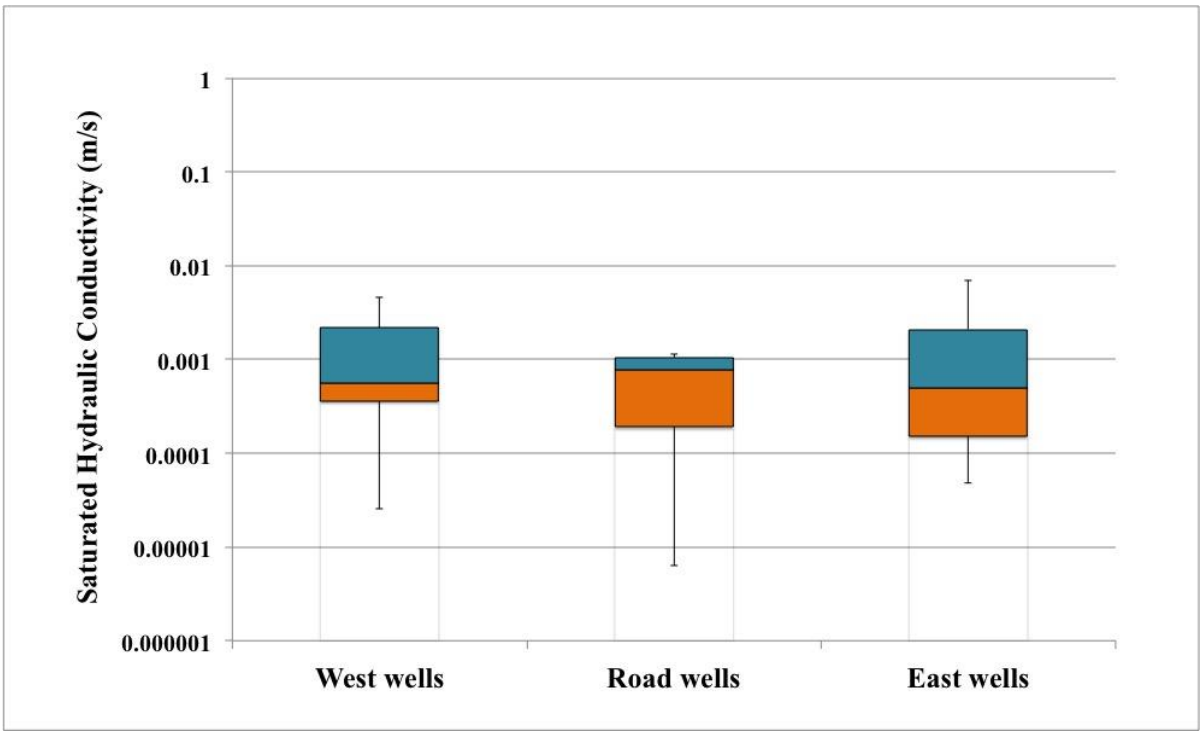

Figure 4-10. Average saturated hydraulic conductivity for the western and eastern sides and the road. The five horizontal lines represent, from bottom to top: the minimum, the 25th percentile, the median, 75th percentile, and the maximum. There are four regions expressed in each box plot, from bottom to top: the bottom whisker is the minimum to 25th percentile, the orange box is the 25th percentile to the median, the blue box is the median to the 75th percentile, and the top whisker is the 75th percentile to the maximum.

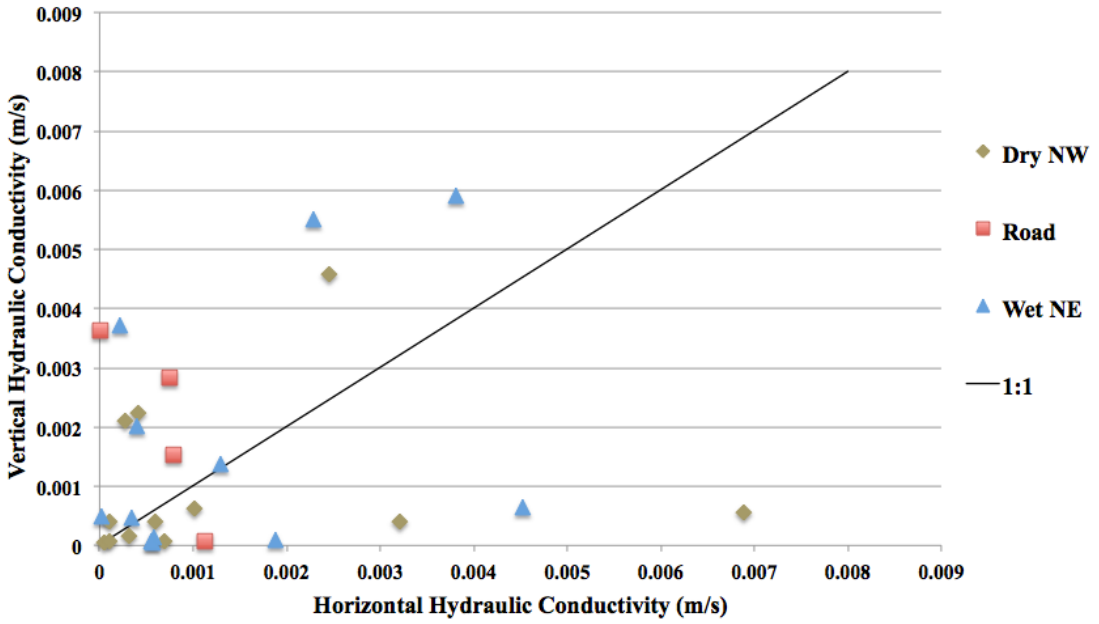

Figure 4-11. Anisotropy for hydraulic conductivity: vertical hydraulic conductivity vs. horizontal hydraulic conductivity.

Table 4-2. Geometric means of saturated hydraulic conductivity (K) at 0.1 m and 0.6 m depth for the natural and road areas of the Firebag fen.

Transect	Natural		Road	
	$K_{0.1}$	$K_{0.6}$	$K_{0.1}$	$K_{0.6}$
1	1.43×10^{-3}	1.47×10^{-4}	3.52×10^{-3}	3.37×10^{-7}
2	3.20×10^{-3}	3.98×10^{-4}	1.13×10^{-3}	n/a
3	5.16×10^{-4}	1.76×10^{-4}	6.31×10^{-6}	n/a
4	1.10×10^{-3}	2.13×10^{-4}	8.58×10^{-4}	7.27×10^{-4}
Geometric mean	1.3×10^{-3}	2.2×10^{-4}	3.8×10^{-4}	1.6×10^{-5}

4.4 Effects of Road on Fen Hydrology

4.4.1 Groundwater Conditions and Volumetric Flow

Average water table heights ranged from 564.45 - 566.40 m.a.s.l along the road (Figure 4-12). Figure 4-10 shows that heads decrease by 0.68 m from the eastern area (566.01 m.a.s.l. mean) to the western area (565.33 m.a.s.l. mean). Heads also tend to decrease from Transect 4 (565.86 m.a.s.l. mean) to Transect 1 (565.54 m.a.s.l mean), but as a much smaller gradient. Thus, the true flow direction is diagonal to the road. Furthermore, groundwater flow does occur in the downstream direction (east to west) across the road (Table 4-3).

From Figure 4-12, the linear regressions ($y = mx + b$) of head vs. distance along the road for transects 1, 2, 3, and 4 are: $y = -0.0057x + 565.48$, $R^2 = 0.981$; $y = -0.0059x + 565.51$, $R^2 = 0.937$; $y = -0.0066x + 565.60$, $R^2 = 0.946$; and $y = -0.0057x + 565.82$, $R^2 = 0.975$, respectively. The slope indicates the hydraulic gradient parallel to the road. The slopes do not vary along transects parallel to the road.

Figure 4-13 shows average water table height before (a) and after (b) road removal. Before road removal, head on the east side is higher than the head on the west side, and it varies with topography. Figure 4-13 shows a decrease in head with decreasing ground elevation. After road removal, the water table is more gentle in slope across the site. The water pooling on the road corresponds to the water table above the road surface and was seen near Transect 4 near the above ground pipeline (120 m to 160 m along the road).

Statistical tests showed that there were significant differences in water table across the site. A comparison of the east versus the west ($p < .001$; d.f. = 142), the east versus the road ($p < .001$; d.f. = 94), and the west versus the road ($p < .001$; d.f. = 94) showed a significant difference across the site for the east, west and the road for the entire summer 2013 period.

Table 4-3. Average hydraulic conductivities and volumetric fluxes east and west of the road, before and after road removal.

	Before road removal			After road removal		
	East	Road	West	East	Road	West
Hydraulic Conductivity, K (m/s)	2.49×10^{-3}	5.72×10^{-4}	1.24×10^{-3}	2.49×10^{-3}	5.72×10^{-4}	1.24×10^{-3}
Volumetric Flux, Q (m^3/day)	219.3	97.1	113.1	192.9	100.2	36.3

The pattern of water table elevations, which indicate the direction of flow at the Pad 106 Access Road site can be seen in Figure 4-14. All contours were based on measurements of ground elevation and head elevation. Black circles represent groundwater well locations; white circles indicate road well locations. The road is shown at 0 m along the x-axis, the eastern side is depicted by the -125 m to 0 m range and the western side, by the 0 m to 50 m range on the x-axis.

The flow pattern shifted in the western direction as the road was removed; however, the footprint of the road can still be seen, as it affected hydraulic conductivity. The immediate effect indicates that total head closely followed the topography of the site (Figure 4-14). Head as shown in the upper left hand side diagram, very slightly increases towards the pipeline beside transect 4 (uppermost horizontal transect).

The results of Figure 4-14 show a very slight and gradual shift in head observed after road removal. More change in head occurred from June 4 to June 17 before road removal, than after road removal, which may be attributed to the severe influx of water from the June 8 and June 9 precipitation and flooding of the site.

Following road removal head approaches steady state conditions due to minimal change temporally between sampling dates. The flow direction is slightly off parallel from the road.

Figure 4-15 displays continuous water table elevation measurements from pressure transducers for wells 1-4, 1-5, 2-2, 2-3, 2-4, 2-5, 2-6, 3-4 and 4-4 during the summer of 2013

at the Suncor Firebag Site. It should be noted that road removal did not commence until June 18, and, therefore, each road well pressure transducer could not be installed until its particular area of road was fully removed. Accordingly, the data for the road wells do not begin until some time after June 18, as can be seen in Figure 4-15. There is strong positive correlation between the pressure transducer groundwater data and the manually derived groundwater data (well 1-4: $y = 0.935x$, $R^2 = 0.532$), however, not for all wells (well 2-3: $y = -0.147x$, $R^2 = 0.029$).

Volumetric flow for the road site is shown in Figure 4-16. The volumetric flow of the east and the west sides of the road correlate after removal but not before (Figure 4-16). Values of the ratio between volumetric flow of the east side and volumetric flow for the west side before road removal are 0.97 and 5.8 and after road removal have a range of 4.1 to 6.4 for 4 sampling events, thus showing that volumetric flow before road removal is less correlated between east and west. Volumetric flow is rapid towards the road as indicated by the high volumetric flux crossing *n*-2 flow face (193 m^3/day), but, as the flow approaches and crosses the road, the volumetric flow decreased (100 m^3/day) due to low hydraulic conductivity, thus indicating water was either lost or put into storage.

4.4.2 Transmissivity

Transmissivity across the Pad 106 Access Road site is shown in Figure 4-17. The road is indicated by 0 m, and the east and west portions of the site are represented from -150 m to 0 m and 0 m to 100 m perpendicular to the road, respectively. The transmissivity (m^2/s) for transect 1 is $2.2 \times 10^{-3} \pm 4.1 \times 10^{-3}$, for transect 2 is $1.6 \times 10^{-3} \pm 1.5 \times 10^{-3}$, transect 3 is $3.8 \times 10^{-4} \pm 3.7 \times 10^{-4}$, and transect 4 is $8.4 \times 10^{-4} \pm 4.9 \times 10^{-4}$. All four transects show less than an order of magnitude in range. Most variation in T is due to K, as *b* is consistent.

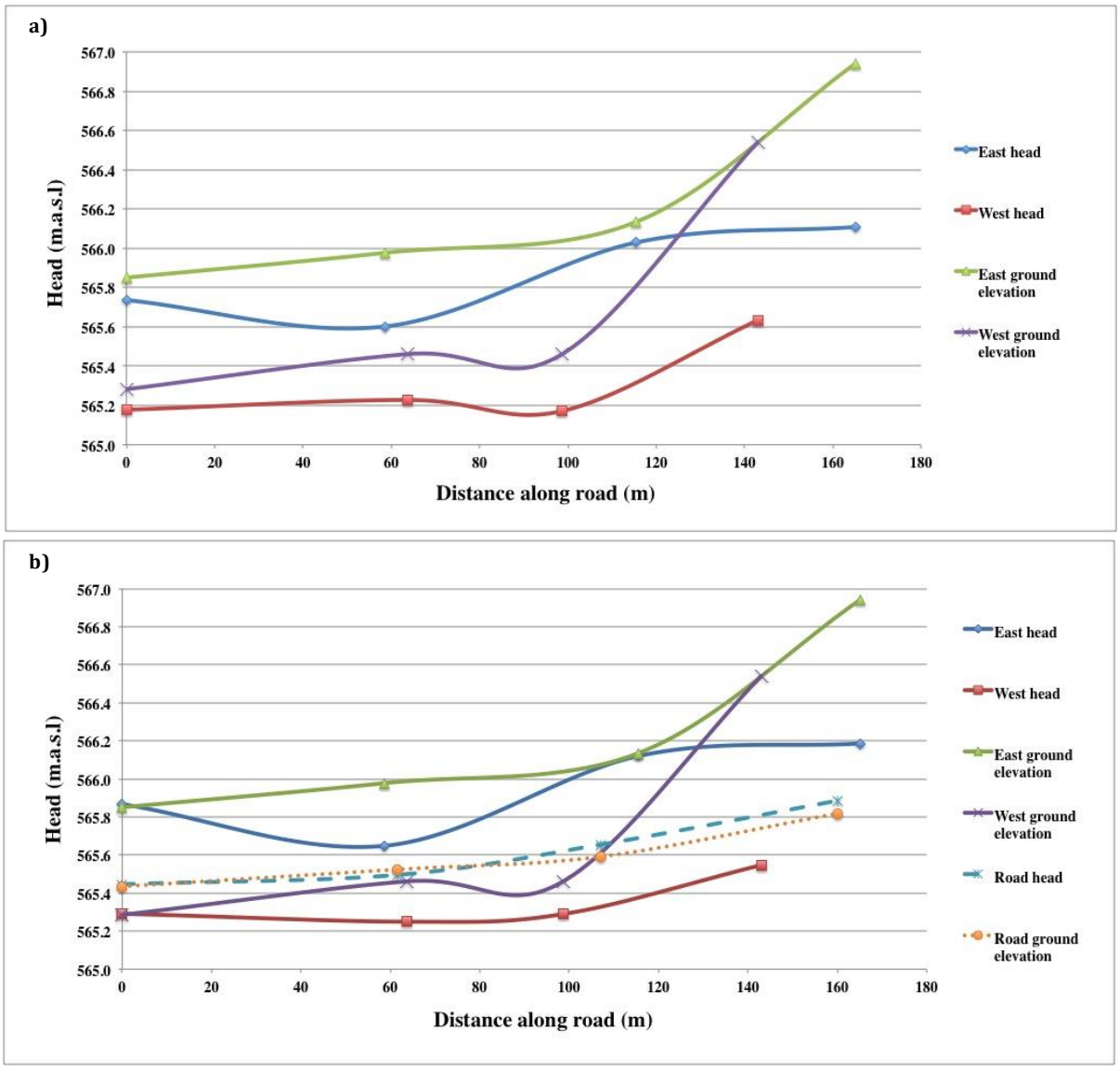

Figure 4-12. Average water table heights as a function of the distance from the road area at the Firebag fen. , The road is represented as 0 m along the x-axis, while -150 m to 0 m and 0 m to 100 m represent the respective eastern and western sides, respectively.

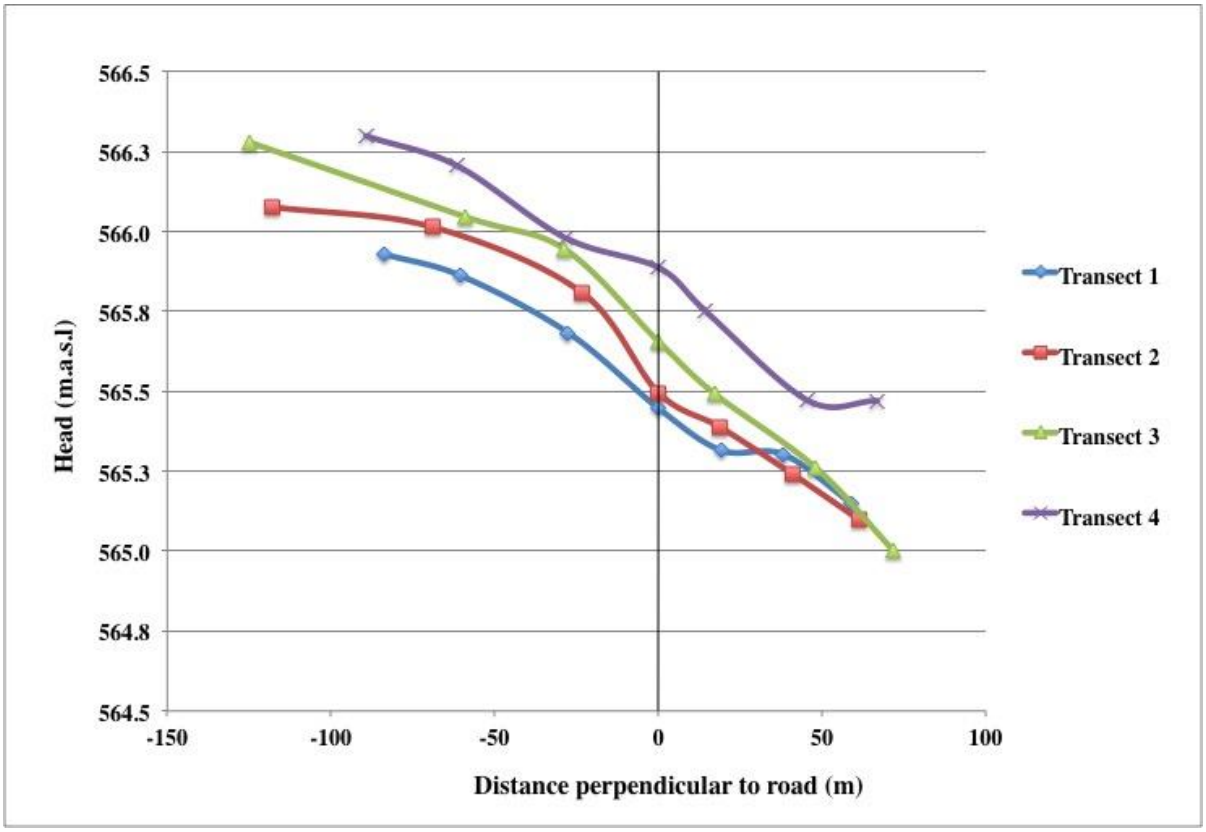

Figure 4-13. Average water table heights for a) before road removal, and b) after removal.

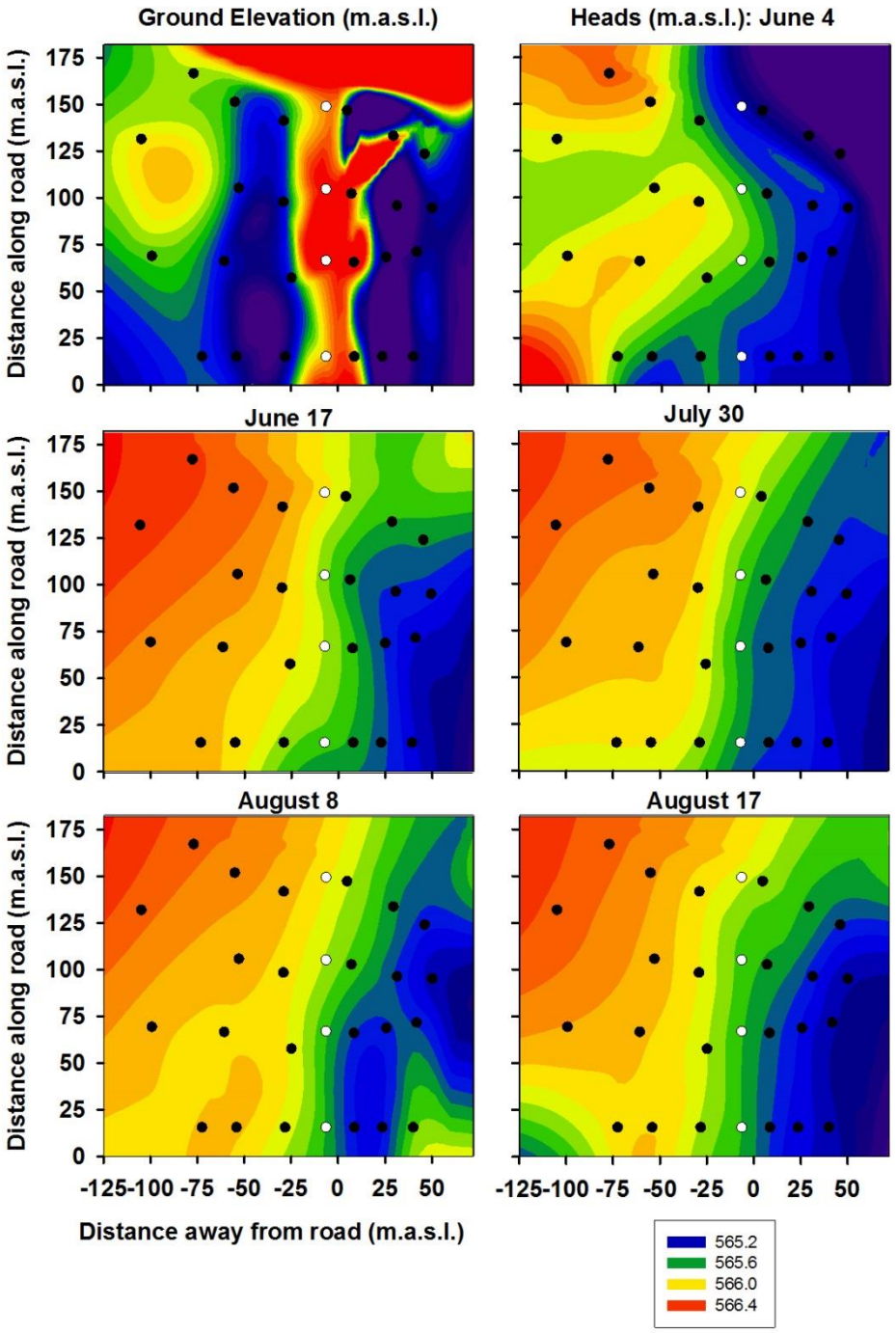

Figure 4-14. Flow contours. Water table conditions were created from an aerial view. Black dots indicate wells; white dots indicate road wells; bottom left-hand corner of each diagram represents the east corner of the Pad 106 Access Road site; and the bottom left-hand well is well 1-1. Top left: ground elevation. Top right: water level June 4 before road removal. Middle left: June 17 water before road removal. Middle right: July 30 water level after road removal. Bottom left: August 8 water level. Bottom right: August 17 water level.

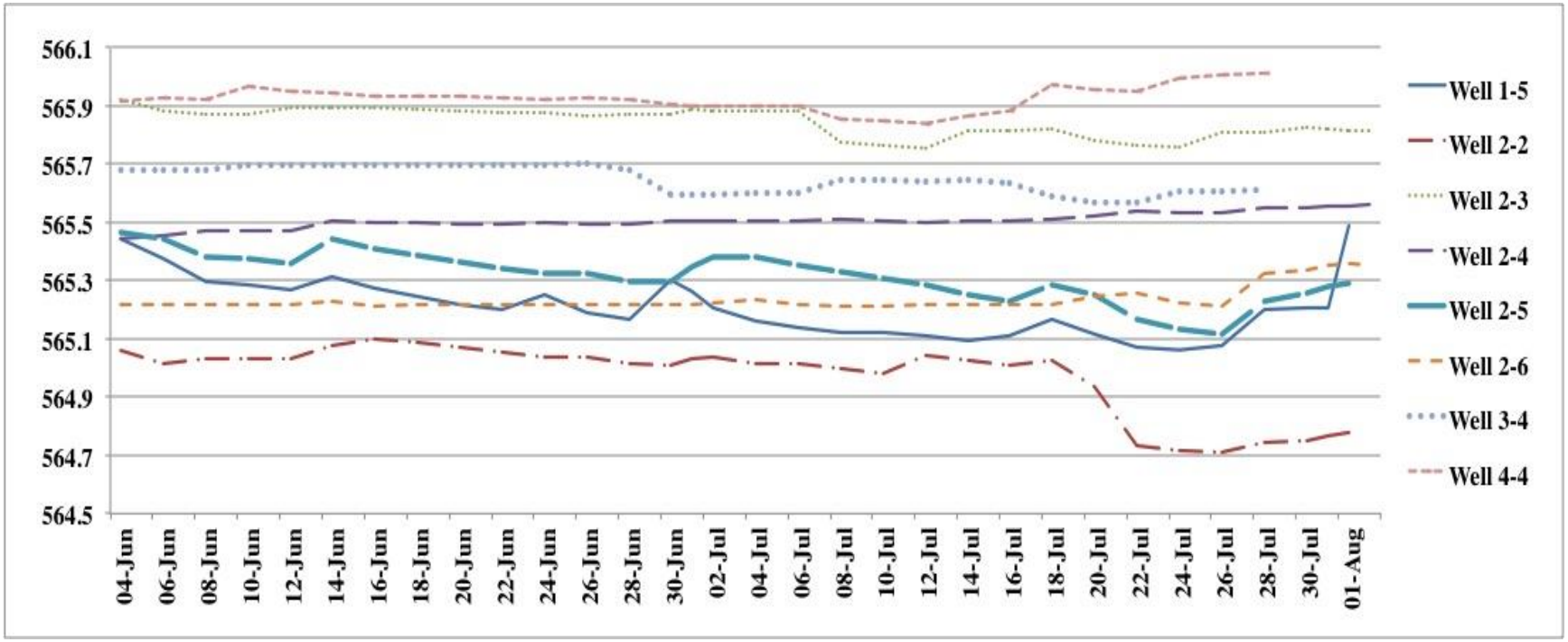

Figure 4-15. Continuous daily head elevation averages June 4-August 31, 2013, the end of the summer field season.

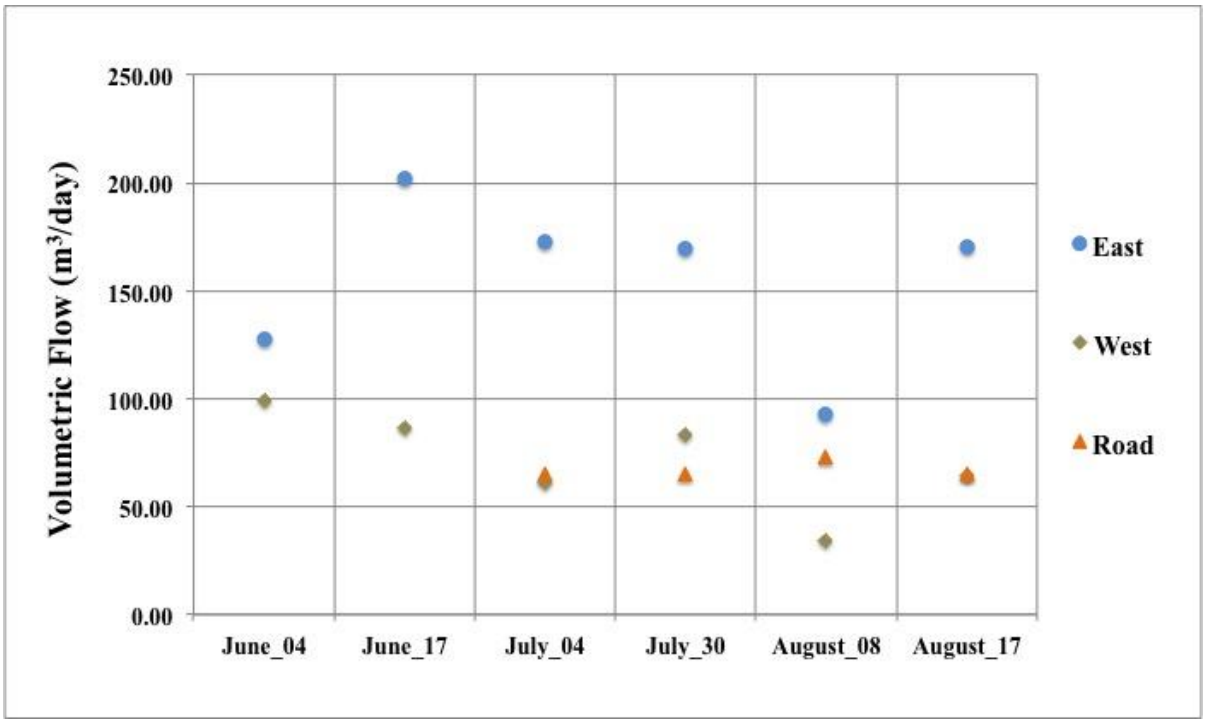

Figure 4-16. Volumetric flow for east and west sides and the road.

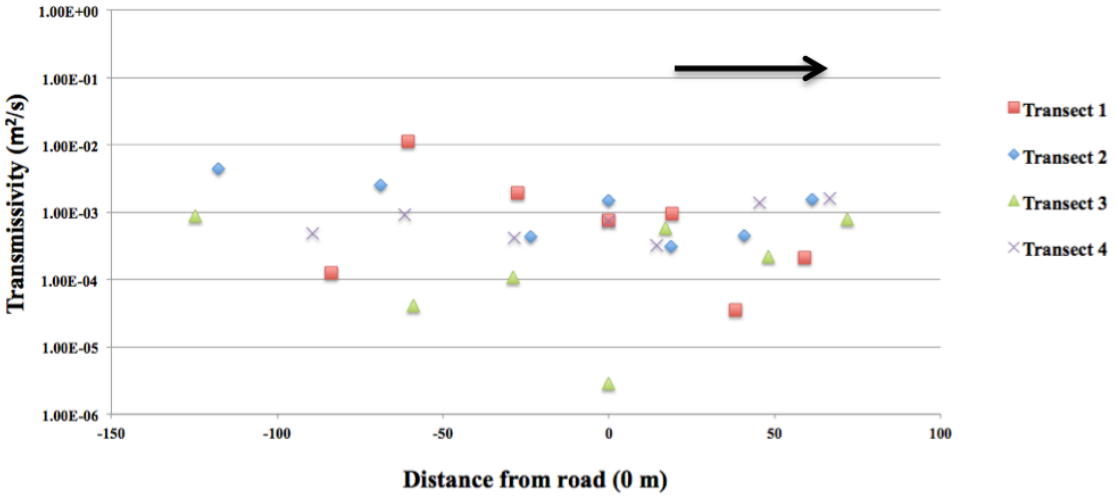

Figure 4-17. Average peat transmissivity as a function of distance from the road area. Black arrow indicates direction of flow.

4.5 Recovery of the Peat Profile

Because peat subsidence is a function of water table fluctuations, the initial hypothesis for the immediate response of the compressed peat column beneath the Pad 106 Access Road was that this peat would absorb the water unleashed by the road barrier once it was removed, and would subsequently rebound much like a decompressing sponge (Petrone and Osko, 2013). Nevertheless, the question remains as to how long this process would take, if it takes place at all.

Figure 4-18 illustrates the results for peat subsidence measured during the summer of 2013 for the Pad 106 Access Road site. The top graph in Figure 4-18 shows cumulative peat subsidence values for the peat monitoring plates set-up perpendicular to the road, located between transect 1 and transect 2. The top graph in Figure 4-18 shows peat cumulative subsidence values directly measured for the Pad 106 Access Road. The bottom graph in Figure 4-18 depicts cumulative peat subsidence perpendicular to the road and contains 'negative days' corresponding to time before road removal. Peat monitoring plates could not be installed within the road prior to removal; hence, the bottom graph in Figure 4-18 for the road does not include negative days, as no measurements of peat subsidence could be taken for the road while it was still in place.

Peatland cumulative height displacements perpendicular to the road in Figure 4-18 (bottom graph) show a decrease on the relatively dry western side of the Pad 106 Access Road. Nevertheless, the long-term effects are seen by the noticeable decrease in peat subsidence. In contrast, measurements of peat subsidence for the road itself show oscillating movement. The peat column takes time to change, and subsidence is not significant until day 21. Subsidence maximizes at day 35, with extremes seen at the road edges. The peat shows signs of rebounding, due to the decreasing trend of subsidence seen on day 45, to the initial state on day 0, after reaching a peak on day 35 (Figure 4-18, top graph). The percents of subsidence at 45 days relative to the maximum subsidence that occurred at 35 days were calculated. The values are 95 %, 24 %, 75 % 48 % and 88 % for measurement locations 1, 2, 3, 4, and 5, respectively. The difference between 100 % and the preceding values correspond to recovered peat subsidence relative to the maximum subsidence at 35 days.

a)

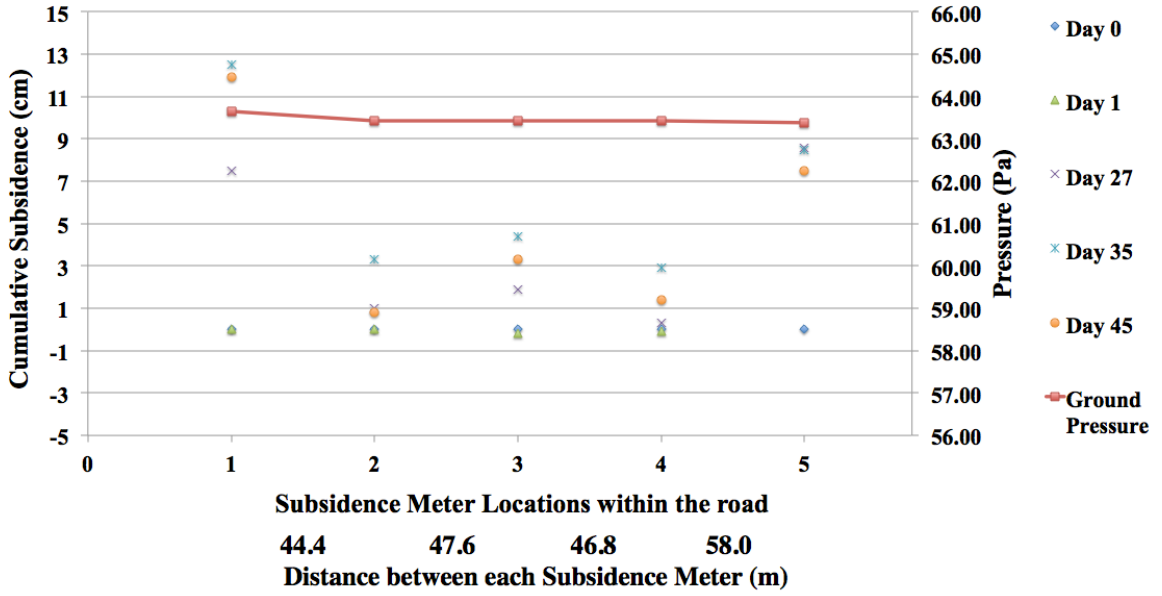

b)

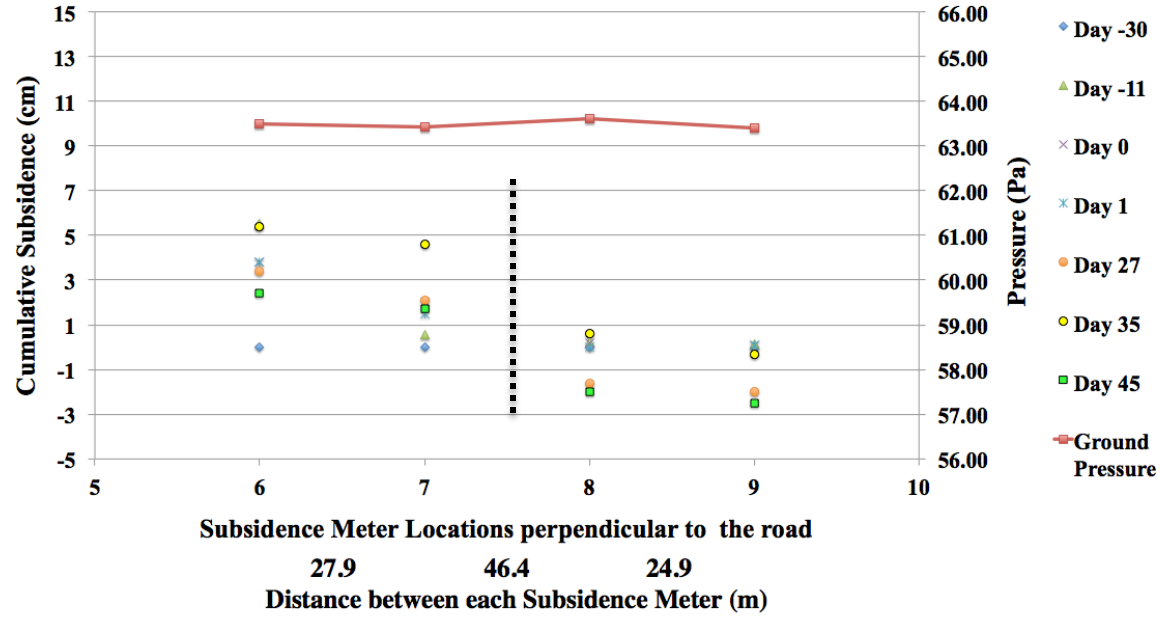

Figure 4-18. Cumulative peat subsidence perpendicular (a) and parallel (b) to the road area. Subsidence meter locations (a) 1-5 within road, and (b) 6-9 perpendicular to road are indicated by top row of numerals along the x-axis. Distance between each subsidence meter indicated by second row of numerals (a) 44.4-58.0 m and (b) 27.9-24.9 m. Ground Pressure (red line) is the pressure resultant from the weight and area of the plexiglass plate on top of the peat column and is given to illustrate the minimal effect of the plate relative to natural peat subsidence processes. The road is indicated by the black dotted line, between subsidence meter 7 and 8 in (b). Subsidence meters 6 and 7 are located on the east side and subsidence meters 8 and 9 are located on the west side of the road.

4.6 Discussion

Laboratory measurements, rather than field, of hydraulic conductivity were conducted for this thesis. There are several advantages and limitations of labortatory measurements versus field measurements. Advantages of laboratory measurements include controlling variables (such as laboratory temperature and ambient pressure) along with ease of measuring K_v versus K_h. Limitations of laboratory measurements are time delays in shipping and storing samples for extended periods of time (up to 6 months), which can cause changes in moisture content and possible compaction of samples. Another possible error in laboratory measurements is scale dependency of hydraulic conductivity (Bradbury and Muldoon, 1990; Neuman, 1990).

There is a scale dependency of hydraulic conductivity, based on the measurement type, from small-scale permeameter tests to single borehole slug tests, and then to large-scale pumping and tracer tests (Neuman, 1990). The small scale testing of K measurements tend to underestimate K because the entire site region is not tested, and therefore high K layers are not detected (Nilsson et al., 2001; Schulze-Makuch et al., 1999; Bradbury and Muldoon, 1990; Neuman, 1990). Although this error exists, laboratory experiments are accurate point measurements (Hopmans et al., 2002) and are appropriate for the initial analysis of the Pad 106 Access Road site.

The saturated hydraulic conductivities are calculated based on Darcy's equation and thus needs a gradient. The gradients used in laboratory experiments were determined from the head difference and sample thickness and is approximately 1 - 3. Field gradients however are on the order of 0.01. This is a difference by a factor ≥ 100. The assumption is that lower gradient values of the field would be applicable with these hydraulic conductivity values determined with larger gradients, although the physical poroperities of the sanple will affect this.

Flow face calculations used for the determination of volumetric flow at the Firebag fen contain important assumptions associated with Dupuit flow. These assumptions are flow parallel to the water table in an unconfined aquifer and the aquifer is both homogeneous and isotropic. These conditions are not met, and contribute to error and inaccuracy for volumetric flow. Limitations of Dupuit's analysis include failure to consider vertical flow components,

and also lack of providing an accurate seepage face near a position of outflow. These unmet assumptions and limitations must be taken into consideration for the results of volumetric flow at the Firebag fen.

The immediate, post-road removal, hydrologic response of the peatland, along with the physical hydraulic parameters of the peat column, resulted in subtle change as a function of the slow rate of response of the site. The post-road removal topography of the peatland showed signs of shifting back into hydrologic equilibrium, with flow moving across the former road (Section 4.4.1). It was evident at this site that the road impeded flow. The road impeding flow is likely caused by the compaction of the acrotelmic peat the road was placed on and subsequently decreased the hydraulic conductivity.

Following road removal, changes in water table were small across the entire site for the summer 2013 field season. It is evident that the site hydrology followed ground surface topography, as shown by hydraulic gradients and head elevation. Very little change in total head occurred following road removal during the 2013 field season. Therefore, the road site, especially on the western side, may require intervention over the long-term if the peat fails to decompress naturally as water continues to flow in the west direction.

Physical hydraulic properties showed very little change from the road to the outermost, relatively 'natural' well sites. Porosity showed very little difference from natural values; however, bulk density and specific yield showed slightly more change with distance from the road. Decreased values of bulk density with distance from the road on the western side may be evidence of the maintenance vehicle corridor. Bulk density was greater on the western side (Figure 4-6; Table 4-1), which may be attributed to larger pore space existing within the substrate.

Thompson and Waddington (2013) found that humification was inversely related to water retention. This finding contradicts results from the Pad 106 Access Road site. Here, although the peat column showed increased decomposition with depth, there was no inverse relationship for soil moisture retention and increased decomposition. In contrast to Thompson and Waddington (2013), soil moisture away from the road showed high variation with depth rather than increase with depth (McCarter and Price, 2012).

Moore et al. (2015) and Chason and Siegel (1986) demonstrated that bulk density from fen peatlands in Minnesota, though occupying different hydroclimatic settings than

Firebag, showed positive correlation with depth. Almendinger and Leete (1998) reported that bulk density (0.18 g/cm^3 – 0.39 g/cm^3) was also found to increase with depth in calcareous fen peatland environments. This is likely due to compression forces of the overlying peat column, and agree with the bulk density findings for the Pad 106 Access Road site. However, the true values may have been overestimated (potentially equally in both cases) because of peat compression during coring. However, it should be considered that these sites vary greatly in geology and hydroclimatology from Pad 106 and that the peat itself may be exhibit differences in composition. Weiss et al. (1998) found that bulk density is a good predictor of water retention, however, no such correlation was found for bulk density and soil moisture retention for Pad 106.

Schindler et al. (2004) and Rydin (1985b) found that physical hydraulic properties were altered significantly as a function of drainage. As consolidation processes began, porosity and bulk density were found to be inversely related. Findings for the Pad 106 Access Road site are in agreement, based on high values of bulk density and low values of porosity on the dry side of the road relative to the wet side. Overall, this suggests that the dry conditions led to collapse and oxidation, which is also supported by the peat subsidence monitoring perpendicular to the road, which showed peat subsidence increases on the dry side.

Peatland desiccation and water table drawdown inevitably leads to peat subsidence, increased bulk density, decreased specific yield and soil moisture retention (Moore et al., 2015; Waddington et al., 2010; Casselman, 2009). This is in agreement with findings for the dry portion of the Pad 106 Access Road area and for the road itself. Lowered water tables on the visibly drier western portion of the road may have resulted in the oxidation of the organically rich soils, which significantly impacts the ability of the peat materials to transmit and absorb water.

Results from Moore et al. (2015) showed that short-term drying causes subsidence of the peat surface. Parent et al. (1982) concluded that within 5 - 10 years following a steady decrease in water table elevation, subsidence in the peatland takes place by consolidation of the peat mass as formerly anoxic peat layers begin to oxidize. Therefore, it is expected that the Pad 106 Access Road peat experienced subsidence due to overburden compression because the road was in place for six years (2007-2013). Peat is widely recognized as being

highly compressible, more so than soft clays (virgin compression index of peat approximately 5 to 20 times larger than that of soft clays) (Shafiee et al., 2015). The compression of soils can be divided into primary compression, which occurs duing the increase in effective vertical stress, and secondary compression, which follows during constant effective vertical stress. Fibrous peat displays extreme compressibility during both primary and secondary compression (Mesri and Ajlouni, 2007).

Belk and Phillips (1993) and Parent et al. (1982) showed that subsidence represents a hydrologically significant loss of soil moisture capacity, which contradicts the findings from the Pad 106 Access Road site. Here, measurements show that soil moisture retention for the dry side, where expansion occurred, retained water just as effectively as for the wet side. Belk and Phillips (1993) and Parent et al. (1982) further indicated that the loss of peat due to subsidence and the associated water storage capacity were the only permanent hydrologic effects associated with the artificial drainage. This may be an implication of the long-term effects for the Pad 106 Access Road site.

Results from Belk and Phillips (1993) also showed no significant differences in water table elevations and soil moisture retention between natural and disturbed sites due to artificial drainage. This is in agreement with results from Pad 106, which showed little change in head over time, which followed the site topography.

The flow on the west side may be lower than the road due to shallower gradients and a smaller flow face. Regardless of what is occurring on the western flow face, what is of importance here is that flow rates are clearly reduced by the road along the flow path.

The water table in peatlands is typically located in lower saturated hydraulic conductivity, and even more so at relatively drier sites. The decrease in saturated hydraulic conductivity with depth has been observed in numerous peatlands (Moore et al., 2015; Letts et al., 2000). Saturated hydraulic conductivity decreased with depth at the Pad 106 Access Road site, for both natural locations and the road. However, some samples had decreased hydraulic conductivity, while other hydraulic conductivites remained within the same order of magnitude.

Belk and Phillips (1993) found that mean water table elevations were higher at natural sites than at artificially drained sites. The dry side of the road at Pad 106 displayed a lower water table elevation in agreement with their finding. However, the decreasing

hydraulic head across the road, including the sharp drop off in head at the road, is also a contributing factor. Therefore, the decreased head on the dry side of the road is a factor of both natural gradients and artificial gradients. This pattern is true for all transects.

Varosio (2000) reported that peat, because of its high porosity relative to the porosity of mineral porous media and thus the high hydraulic conductivity, often has fast groundwater flow. High water level variation, combined with the presence of soft porous peat, enhances the transmission of groundwater. Transmissivity for the Pad 106 Access Road site had a geometric mean of 4.9×10^{-4} m^2/s, ranging from 2.8×10^{-6} m^2/s to 1.1×10^{-2} m^2/s. Varosio (2000) found transmissivity values for peat to be in the range of 1.0×10^{-2} m^2/s to 3.0×10^{-2} m^2/s for peat depths of approximately 2 m, which is similar to the peat depths studied here. Results from van der Schaaf (2004) found that degraded peat exhibited low transmissivity values of 1.2×10^{-5} m^2/s to 2.3×10^{-5} m^2/s. In contrast to what was initially expected, transmissivity results for Pad 106 ($K = 5.7 \times 10^{-4}$ m/s, $T = 2.2 \times 10^{-4}$ m^2/s) were found to be closer to findings of natural ($K = 1.4 \times 10^{-3}$ m/s, $T = 5.7 \times 10^{-4}$ m^2/s) transmissivity, despite there being an approximate order of magnitude difference, further supporting the conclusion that the effects of the road were less than initially expected (Shafiee et al., 2015; Tashiro et al., 2015; O'Kelly and Orr, 2014; Zhang and O'Kelly, 2014; Mesri and Ajlouni, 2007).

A significant transition in saturated hydraulic conductivity occurs throughout the peat profile, as saturated hydraulic conductivity tends to decrease with peat depth. The sharp decrease in saturated hydraulic conductivity means that the transmissivity for the acrotelm is strongly dependent on water table elevation. Large values of saturated hydraulic conductivity occur near the surface opposed to small values at depth. The Pad 106 Access Road site exhibits this trend in saturated hydraulic conductivity. The difference may be up to several orders of magnitude (van der Schaaf, 1999; Balyasova, 1979), as also seen in the Pad 106 results for saturated hydraulic conductivity.

Nevertheless, management implications can be drawn from this research. First, while blocked and subsequently deteriorated systems are generally associated with high levels of soil moisture, water tables and ponding during wet periods, that does not necessarily mean these are consistent. Though ponding was present at the road, significant differences and therefore, inconsistencies were present in volumetric soil moisture and water table at the Pad 106 Access Road.

4.6.1 Future Research

In the future it may be beneficial to run oedometer compressibility tests to determine how compacted the peat column was beneath the road compared to outer sites to precisely determine how the depths of compressed peat columns relate to the depths of un-compressed peat columns. Running oedometer tests on both disturbed road peat and natural peat may help improve our understanding of how extensive the compressibility impact of temporary access infrastructure is on the peat column in the short term and long term.

This study examined the saturated zone. Samples, field data, and laboratory analyses exist pertaining to the unsaturated zone. Future studies at this particular site would greatly benefit from exaiming the unsaturated zone, such as the time for surface contamination to reach thte water table and water storage capacity.

Distributions of microform *Sphagnum* might be tested as a mechanism to help reduce the dry conditions created by roads, as recommended by Moore et al. (2015). They suggest that the initial short-term hydrological impacts of a lowered water table on peat physical hydraulic properties (bulk density, specific yield, and soil moisture retention) may be counteracted because of the competitive advantage of hummock *Sphagnum* under dry conditions.

More understanding of the long-term cumulative impacts of access infrastructure, specifically on the peat column, is needed for the implementation of best-in-class management practices for the construction, use and decommission of roads in boreal peatlands. Further research at other sites in Canada's boreal ecozone, as well as the continued monitoring of the Pad 106 Access Road site over the next decade, will give more technical knowledge of the long-term effects of roads and the ability of the hydrologic system's ability to recover. The immediate characterization of the Pad 106 site, though important, is not enough to determine whether or not the disturbed peatland will shift back into hydrologic equilibrium without intervention.

5.0 Conclusions

The goal of this research was to characterize the immediate effects of the Pad 106 Access Road at Suncor's Firebag Site following the removal of the road during the summer field season of 2013. The specific objectives addressed in this thesis are: (1) a comparison of disturbed and undisturbed peat physical parameters (porosity, buk density and specific yield), which showed significant differences exisiting between the east versus the west side of the road and the east side of the road and the road; and (2) statistical comparisons of water table pre- and post road removal, which showed significant differences across the site (east versus west, road versus east and road versus west). In contrast, significant differenes were not found for saturated hydraulic conductivity. However, significant differences in the hydrologic status of the pre- and post-road removal water table may imply that, hydrologic functions have been interrupted for long periods, however, the hydrologic regime was altered non-permanetly (gradient, peat expansion, recovery of vegetation communities) and recent studies at the Pad 106 Access Road site conducted after this study indicate that the peat once buried beneath the road is decompressing and not causing a hindrance to flow, which previously was a concern of long-term impact. In conclusion, hydrologic restoration can be accomplished at the Pad 106 Acces Road site by passively allowing nature to "take its course." Since no detailed parameterization for the effects of roads on peatland hydrogeological properties were found in the published literature, the values provided here give a certain first insight into the role that access infrastructure plays both while in use and after decommission in disrupting fen peatland hydrology.

References

Abbaspour KC, Johnson CA, van Genuchten MT. 2004. Estimating uncertain flow and transport parameters using a sequential uncertainty fitting procedure. Vadose Zone J. **3**: 1340-1352.

Ahuja LR, Johnsen KE, Heathman GC. 1995. Macropore transport of a surface-applied bromide tracer: Model evaluation and refinement. Soil Sci. Soc. Am. J. **59**: 1234-1241.

Alberta Culture and Tourism. n.d. Oil sands discovery centre facts. Accessed online March 27, 2015, at http://history.alberta.ca/oilsands/resources/docs/facts_sheets09.pdf

Almendinger JE, Leete JH. 1998. Regional and local hydrogeology of calcareous fens in the Minnesota River Basin, U.S.A. Wetlands **18**: 184-202.

Bachmann J. 1996. Wettability related to the degree of humification of soil organic matter and its impact on infiltration and soil water retention curves. J. Rural Eng. Dev. **37**: 190-196.

Bakker G, van der Ploeg MJ, Hoogendam CW, Gooren HA, Huiskes C, Koopal LK, Kruidhof H. 2007. New polymer tensiometers: measuring matric pressures down to the wilting point. Vadose Zone J. **6**: 196-202.

Baldocchi D, Kelliher FM, Black TA, Jarvis P. 2000. Climate and vegetation controls on boreal zone energy exchange. Glob. Change Bio. **6**: 69-83.

Balyasova YL. 1979. Methods for estimating the reliability of experimentally determined major hydrologic characteristics of bogs. Soviet Hydrol. **18**: 117-123.

Bayley SE, Prather CM. 2003. Do wetland lakes exhibit alternative stable states? Submersed aquatic vegetation and chlorophyll in western boreal shallow lakes. Limnol. Oceanogr. **48**: 2335-2345.

B.C. Ministry of the Environment. 2008. Wetland ways: management guidelines for wetland protection and conservation in British Columbia.

Beaudry F, deMaynadier PG, Hunter ML. 2008. Identifying road mortality threat at multiple spatial scales for semi-aquatic turtles. Biol. Conserv. **141**(10): 2550-2563.

Becher HH. 1971. A Method for Measuring the Unsaturated water conductivity. Z. Pflanzenernähr. Bodenkd. **128**: 1-12.

Beckwith CW, Baird AJ, Heathwaite Al. 2003. Anisotrophy and depth- related heterogeneity of hydraulic conductivity in a bog peat: Laboratory measurements. Hydrol. Process. **17**: 89-101.

Beebee TJC. 2013 Effects of road mortality and mitigation measures on amphibian populations. Conserv. Biol. **27**(4): 657-668.

Belk DR, Phillips JD. 1993. Hydrologic Recovery of Artificially-Drained Wetlands In Coastal North Carolina. Coastal Zone: Proceedings of the Symposium on Coastal and Ocean Management, 3254-3268.

Biebighauser TR. 2007. Wetland drainage, restoration and repair. University Press of Kentucky, Lexington, Kentucky.

Bittelli M, Flury M. 2008. Errors in water retention curves determined with pressure plates. Soil Sci. Soc. Am. J. **73**: 1453-1460.

Boels D, Boels JB, van Gils HM, Veerman GJ, Wit KE. 1978. Theory and system of automatic determination of soil moisture characteristics and unsaturated hydraulic conductivities. Soil Sci. **126**: 191-199.

Boelter DH. 1965. Hydraulic conductivity of peats. Soil Sci. **100**: 227-231.

Boelter DH. 1968. Important Physical Properties of Peat Materials. Proceedings of the Third International Peat Congress, Quebec, Canada. 150-154.

Boelter DH. 1969. Physical Properties of peats as related to degree of decomposition. Soil Sci. Soc. Am. **33**: 606-609.

Boelter DH. 1976. Methods for analyzing the hydrological characteristics of organic soils in marsh-ridden areas. Hydrology of Marsh-Ridden Areas. Proceedings of IASH Symposium, Minsk. 1972. IASH, UNESCO, Paris,, 161-169.

Boelter DH, Verry ES. 1977. Peatland and water in the northern lake states. General Technical Report NC-31. U.S. Dept. of Agriculture, Forest Service, North Central Forest Experiment Station, St Paul, MN.

Bohne K, Salzmann W. 2002. Inverse simulation of non-steady state evaporation using nonequilibrium water retention data: a case study. Geoderma **110**: 49-62.

Bonan GB, Pollard D, Thompson SL. 1992. Forest response to climatic change: effects of parameter estimation and choice of weather patterns on the reliability of predictions. Climatic Change **20**: 87-111.

Bonan GB, Shugart HH. 1989. Environmental factors and ecological processes in boreal forests. Annu. Rev. Eco. and Syst. **20**: 1-28.

Borda-de-Agua L, Grilo C, Pereira HM. 2014. Modeling the impact of road mortality on barn owl (*Tyto alba*) populations using age-structured models. Ecol. Model. **276**: 29-37.

Bouma J, Belmans C, Dekker LW, Jeurissen WM. 1983. Assessing the suitability of soils with macropores for subsurface liquid waste disposal. J. Environ. Qual. **12**: 305-311.

Bradbury KR, Muldoon MA. 1990. Hydraulic Conductivity Determinations in Unlithified Glacial and Fluvial Materials. Ground water and Vadose Zone Monit. **1053**: 138-151.

Bradley C. 1996. Transient Modelling of water table variation in a floodplain wetland, Narborough Bog, Leicestershire. J. Hydrol. **185**: 87-114.

Bradshaw A. 2000. The use of natural processes in reclamation-advantages and difficulties. Landscape and Urban Planning **51**: 89-100.

Brooks PW, Fowler MG, MacQueen RW. 1988. Biological marker and conventional organic geochemistry of oil sands/heavy oils, Western Canada Basin. Organic Geochemistry **12**: 519-538.

Bryant D, Nielsen D, Tangley L. 1997. The last frontier forests: ecosystems and economies on the edge. World Resources Institute, Washington, D.C.

Campbell JD. 1974. A simple method for determining unsaturated conductivity from moisture retention data. Soil Sci. **117**: 311-314.

Camporese M, Ferraris S, Putti M, Salandin P, Teatini P. 2006. Hydrological modeling in swelling/shrinking peat soils. Water Resour. Res. **42**: 1-15.

Carman, PC. 2003. Fluid flow through Granular Beds. Trans. Inst. Chem. Eng. **15**: 150-166.

Carrier WD. 2003. Goodbye, Hazen; Hello, Kozeny-Carman. J. Geotech. Geoenviron. **129**: 1054-1056.

Carter MR, (ed.). 1993. Soil Sampling and Methods of Analysis. Lewis Publishers: London, 814 pages.

Casselman T. 2009. Seney National Wildlife Refuge Comprehensive Conservation Plan. United States Fish and Wildlife Service.

Chason DB, Siegel DI. 1986. Hydraulic conductivity and related physical properties of peat, Lost River peatland, northern Minnesota. Soil Sci. **142**: 91-99.

Chee WL, Vitt DH. 1989. The vegetation surface water chemistry and peat chemistry of moderate-rich fens in central Alberta, Canada. Wetlands **9**: 227-261.

Chow TL, Rees HW, Ghanem I, Cormier R. 1992. Compactibility of cultivated Sphagnum peat material and its influence on hydrologic characteristics. Soil Sci. **153**: 300-306.

Clewell AF, Aronson J. 2007. Ecological restoration: principles, values and structure of an emerging profession. Island Press, Washington, D.C.

Clymo RS. 1973. The Growth of Sphagnum: some effects of environment. J. Ecol. **61**: 849-869.

Clymo RS, Hayward PM. 1989. The Ecology of Sphagnum. In: Heal OW, Perkins DF, Brown WM. (eds.), Bryophyte Ecology, Chapman and Hall, London, 229–288.

Coffin AW. 2007. From roadkill to road ecology: A review of the ecological effects of roads. J. Transp. Geogr. 15: 396-406.

Colino-Rabanal VJ, Lizana M. 2012. Herpetofauna and roads: A review. Basic and Applied Herpetology **26**: 5-31.

Colley BE. 1950. Construction of highways over peat and muck areas. Am. Highways. **29**: 3-6.

Cosentino BJ, Marsh DM, Jones KS, Apodaca JJ, Bates C, Beach J,…Willey A. 2014. Citizen science reveals widespread negative effects of roads on amphibian distributions. Biol. Cons. 180: 31-38.

Cresswell HP, Green TW, McKenzie NJ. 2008. The adequacy of pressure plate apparatus for determining soil water retention. Soil Sci. Soc. Am. J. **55**: 41-49.

Da Silva FF, Wallach R, Chen Y. 1993. Hydraulic properties of Sphagnum peat moss and tuff (scoria) and their potential effects on water availability. Plant Soil. **154**: 119-126.

Dane JH, Hruska S. 1983. In-situ determination of soil hydraulic properties during drainage. Soil Sci. Soc. Am. J. **47**: 619-624.

DeCatanzaro R, Cvetkovic M, Chow-Fraser P. 2009. Relative importance of road density and physical watershed features in determining coastal marsh water quality in Georgian Bay. Environ. Manage. **44:** 456–467.

DeCatanzaro R, Chow-Fraser P. 2010. Relationship of road density and marsh condition to turtle assemblage characteristics in the Laurentian Great Lakes. J. Great Lakes Res. **36**(2): 357-365.

de Rooij GH, Kasteel RTA, Papritz A, Fluhler H. 2004. Joint distributions of the unsaturated soil hydraulic parameters and their effect on other variates. Vadose Zone J. **3**: 947-955.

de Rooij GH, van der Ploeg MJ, Gooren HA, Bakker G, Hoogendam CW, Huiskes C, Kruidhof H, Koopal LK. 2009. Measuring very negative water potentials with polymer tensiometers: Principles, performance and applications. Biologia **64**: 438-442.

Deverel SJ, Rojstaczer S. 1996. Subsidence of agricultural land in the Sacramento – San Joaquin Delta, California: role of aqueous and gaseous carbon fluxes. Water Resour. Res. **32**: 2359-2367.

Devito KJ, Creed IF, Fraser CJD. 2005. Controls on runoff from a partially harvested aspen-forested headwater catchment, Boreal Plain, Canada. Hydrol. Process. **19**: 3–25.

Devito KJ, Creed IF, Gan T, Mendoza C, Petrone RM, Silins U, Smerdon B. 2005. Defining effective watersheds: topography should be considered last. HP Today. **19**: 1705–1714.

De Vleeschouwer F, Chambers FM, Swindles GT. 2010. Coring and sub-sampling of peatlands for palaeoenvironmental research. Mires and Peat. **1**: 1-10.

Dingman SL. 1994. Physical Hydrology. Prentice Hall, Englewood, NJ, 575 pages.

Dise NB, Gorham E, Verry ES. 1993. Environmental factors controlling methane emissions from peatlands in northern extension on raised bogs in the southern coastal area of Finland. Fennia. **170**: 25-94.

Dorland A, Rytwinski T, Fahrig L. 2014. Do roads reduce painted turtle (*Chrysemys picta*) populations? PLOS ONE **9**(5): e98414. doi:10.1371/journal.pone.0098414.

Drajad M, Soekodarmodjo S, Hidayat MS, Nitisapto M. 2003. Subsidence of peat soils in the tidal swamplands of Barambai, South Kalimantan. Jurnal Ilmu Tanah dan Lingkungan. **4**: 32–40.

Drexler JZ, Bedford BL. 2002. Pathway of nutrient loading and impacts on plant diversity in a New York peatland. Wetlands **22**: 263-281.

Durigon A, Gooren HA, de Jong van Lier Q, Metselaar K. 2011. Measuring hydraulic conductivity to wilting point using polymer tensiometers in an evaporation experiment. Vadose Zone J. **10**: 741-746.

Durner W. 1994. Hydraulic conductivity estimation for soils with heterogeneous pore structure. Water Resour. Res. **30**: 211-223.

Dymitryszyn I. 2014. The effect of the construction and renovation of a highway bypass in Central Poland on the carabid beetle fauna (*Coleoptera: carabidae*). Eur. J. of Entomol. **111**(5): 655-662.

Eching SO, Hopmans JW. 1993. Optimization of hydraulic functions from transient outflow and soil water pressure data. Soil Sci. Soc. Am. J. **57**: 1157-1175.

Elrick DE, Reynolds WD. 1992. Infiltration from constant- head well permeameters and infiltrometers. Soil Sci. Soc. Am. J. **30**: 1-24.

Eugster W, Rouse WR, Pielke Sr RA, McFadden JP, Baldocchi DD, Kittel TGF, Chapin FS, Liston GE, Vidale PL, Vaganov E, Chambers S. 2000. Land-atmosphere energy exchange in Arctic tundra and boreal forest: available data and feedbacks to climate. Glob. Change Biol. **6**: 84-115.

Evans MS, Billeck BB, Lockhart LL, Bechtold JP, Yunker MB, Stern G. 2002. PAH sediment studies in Lake Athabasca and the Athabasca River ecosystem related to the Fort McMurray oil sands operations: sources and trends. Oil and Hydrocarbons Spills III, 365-374.

Farouki OT. 1981. Thermal properties of soils. CRREL Monograph. **1**: 134.

Faubert P, Rochefort L. 2002. Response of peatland bryophytes to burial by wind- dispersed peat. The Bryologist **105**: 96-104.

Findlay CS, Houlahan J. 1997. Anthropogenic correlates of species richness in southeastern Ontario. Wetlands Conservation Biology **11**(4): 1000-1009.

Findlay CS, Bourdages J. 2000. Response time of wetland biodiversity to road construction on adjacent lands. Biol. Conserv. **14**: 86-94.

Forman RTT, Alexander LE. 1998. Roads and their major ecological effects. Annu. Rev. Ecol. Syst. 29: 207-231.

Freeze RA, Cherry JA. 1979. Groundwater. Prentice Hall, Englewood Cliffs, NJ, 604 pages.

Frolking S, Talbot J, Jones MC, Treat CC, Kauffman JB, Tuittila ES, Roulet N. 2011. Peatlands in the Earth's 21st century climate system. Environ. Rev. **19**: 371-396.

Fujimaki H, Mitsuhiro L. 2003. Re-evaluation of the multistep outflow method for determining unsaturated hydraulic conductivity. Vadose Zone J. **2**: 409-415.

Gambolati G, Putti M, Teatini P, Camporese M, Ferraris S, Gasparetto GS, Nicoletti V, Silvestri S, Rizzetto F, Tosi L. 2005. Peat land oxidation enhances subsidence in the Venice watershed. Eos **86**: 217-224.

Gambolati G, Putti M, Teatini P, Gasparetto GS. 2006. Subsidence due to peat oxidation and impact on drainage infrastructures in a farmland catchment south of the Venice Lagoon. Environ. Geol. **49**: 814-820.

Gardner WH. 1986. Methods of Soil Analysis: Physical and Mineralogical Methods. Soil Sci. Soc. Am. J. 493-544.

Gardner WR, Miklich FJ. 1962. Unsaturated conductivity and diffusivity measurements by a constant flux method. Soil Sci. **93**: 271-274.

Gebhardt S, Fleige H, Horn R. 2010. Shrinkage processes of a drained riparian peatland with subsidence morphology. Soil and Sediment. **10**: 484-493.

Gebhardt S, Fleige H, Horn R. 2012. Anisotropic shrinkage of mineral and organic soils and its impact on soil hydraulic properties. Soil Till. Res. **125**: 96-104.

Gee GW, Campbell MD, Campbell GS, Campbell JH. 1992. Rapid measurement of low soil water potentials using a water activity meter. Soil Sci. **56**: 1068-1070.

Gervais F, Barker J. 2005. Fate and Transport of naphthenic acids in groundwater. Bringing groundwater quality to the watershed scale (Proc. GQ 2004, 4th International Groundwater Quality Conference). International Association of Hydrological Sciences, Rennes, Frances. **297**: 305-310.

Goetz JD, Price JS. 2015. Ecohydrological controls on water distribution and productivity of moss communities in western boreal peatlands, Canada. Ecohydrology. DOI: 10.1002/eco.1620.

Gorham E. 1991. Northern peatlands: Role in carbon cycle and probable responses to climatic warming. Ecol. Appl. **1**: 182-195.

Gorham E. 1994. The Future of Research in Canadian Peatlands: A Brief Survey with Particular Reference to Global Change. Wetlands. **14**: 206-215.

Green RE, Ahuja LR, Chong SK. 1986. Hydraulic conductivity, diffusivity, and sorptivity of unsaturated soils: Field methods. . Klute (ed.) Methods of soil analysis. Part 1. 2nd ed. Agron. Monogr, Madison, WI, 771-798.

Grilo C, Reto D, Filipe J, Ascensão F, Revilla E. 2014. Understanding the mechanisms behind road effects: Linking occurrence with road mortality in owls. Animal Conservation **17**(6): 555-564.

Halbertsma JM, Veerman GJ. 1994. A new calculation procedure and simple set-up for the evaporation method to determine soil hydraulic functions. Rep. **88**. DLO WiInand Staring Centre, Wageningen, the Netherlands.

Hajek T, Beckett RP. 2008. Effect of water content components on desiccation and recovery of sphagnum mosses. An. Bot. **101**: 165-173.

Hall RI, Wolfe BB, Wiklund JA, Edwards TW, Farwell AJ, Dixon GD. 2012. Has Alberta oil sands development altered delivery of polycyclic aromatic compounds to the Peace-Athabasca delta? PLOS ONE **7**: 1-16.

Hardie MA, Lisson S, Doyle RB, Cotching WE. 2013. Evaluation of rapid approaches for determining the soil water retention function and saturated hydraulic conductivity in a hydrologically complex soil. Soil Till. Res. **130**: 99-98.

Hayward PM, Clymo RS. 1982. Profiles of water content and pore size in Sphagnum and peat, and their relation to peat bog ecology. Biol. Sci. **215**: 299-325.

Hayward PM, Clymo RS. 1983. The Growth of Sphagnum: Experiments on, and simulation of, some effects of light flux and water-table depth. J. Ecol. **71**: 845-863.

Hazen, A. 1911. Discussion of "Dams on sand formations." T. Am. Soc. Civil. Eng. **73**: 199-203.

Heinselman ML. 1963. Forest sites, big processes and peatland types in the Glacial Lake Agassiz region, northern Minnesota. Ecol. Monogr. **33**: 324-327.

Hendry MT, Barbour SL, Martin DC. 2014. Evaluating the Effect of Fiber Reinforcement on the Anisotropic Undrained Stiffness and Strength of Peat. J. Geotech. Geoenviron. Eng. DOI: 10.1061/(ASCE)GT.1943-5606.0001154.

Hill BM, Siegel DI. 1991. Groundwater flow and the metal content of peat. J. Hydrol. **123**: 211-224.

Hillel D. 1998. Environmental Soil Physics. Academic Press, NYC, 771 pages.

Hoag RS, Price JS. 1995. A field scale, natural gradient solute transport experiment in peat at a Newfoundland blanket bog. J. Hydrol. **172**: 171-184.

Hoag RS, Price JS. 1997. The effects of matrix diffusion on solute transport and retardation in undisturbed peat in laboratory columns, J. Contam. Hydrol., **28**: 193–205.

Hobbs NB. 1986. Mire morphology and the properties and behaviour of some British and foreign peats. Q. J. Eng. Geol. **19**: 7-80.

Hogg EH. 1994. Climate and the southern limit of the western Canadian boreal forest. Can. J. Forest Res. **24**: 1835-1845.

Hooijer A, Page S, Jauhiainen J, Lee WA, Lu XX, Idris A, Anshari G. 2012. Subsidence and carbon loss in drained tropical peatlands. Biogeosci. **9**: 1053-1071.

Hopmans JW, Nielsen DR, Bristow KL. 2002. How useful are small-scale soil hydraulic property measurements for large-scale vadose zone modeling? Geophys. Mongraph-American Geophys. Union **129**: 247-258.

Houlahan JE, Keddy PA, Makkay K, Findlay CS. 2006. The effects of adjacent land use on wetland species richness and community composition. Wetlands **26**: 79-96.

Howell SG, Clarke AD, Freitag S, McNaughton CS, Kapustin V, Brekovskikh V, Jimenez J-L, Cubison MJ. 2014. An airborne assessment of atmospheric particulate emissions from the processing of Athabasca oil sands. Atmos. Chem. and Phys. **14:** 5073–5087.

Huat BK, Kazemian S, Prasad A, Barghchi M. 2011. State of an art review of peat: General perspective. Int. J. Phys. Sci. **6**: 1988–1996.

Hubbert MK. 1956. Darcy's law and the field equations of the flow of underground fluids, Petroleum Transactions. Am. Inst. Min. Mandal. Eng. **207**: 222-239.

Iden SC, Durner W. 2007. Free-form estimation of the unsaturated soil hydraulic properties by inverse modeling using global optimization, Water Resour. Res. **43**: 1-12.

Iden SC, Durner W. 2008. Free-form estimation of soil hydraulic properties using Wind's method. Eur. J. Soil Sci. **59**: 1228-1240.

Ingram HP. 1978. Soil layers in mires: function and terminology. J. Soil Sci. **29**: 224–227.

Jacobs L, Houlahan JE. 2011. Adjacent land-use affects amphibian community composition and species richness in managed forests in New Brunswick, Canada. Can. J. For. Res. **41**: 1687-1697.

Jacques D, Simunek J, Timmerman A, Feyen J. 2002. Calibration of Richard's and convection-dispersion equations to field scale water flow and solute transport under rainfall conditions. J. Hydrol. **259**: 15-31.

Jongedyk HA, Hickok RB, Mager ID, Ellis NK. 1950. Subsidence of muck soil in Northern Indiana. Bull. S.C. no. 366 Purdue Univ. Agric. Exp. Stn., Lafayette, Ind.

Kalia A. 1956. Determination of the degree of humification of peat samples. J. Sci. Agr. Soc. **28**: 18-35.

Karraker NE, Gibbs JP. 2011. Contrasting road effect signals in reproduction of long- versus short-lived amphibians. Hydrobiologia **664**: 213-218.

Kasimir-Klemedtsson A. 1997. Greenhouse gas emissions from farmed organic soils: a review. Soil Use Manage. **13**: 245-250.

Keddy P. 1999. Wetland Restoration: The potential for assembly rules In Service Of Conservation. Wetlands **19**: 716-732.

Kellner E, Halldin S. 2002. Water budget and surface-layer water storage in a sphagnum bog in central Sweden. Hydrol. Process. **16**: 87-103.

Kennedy GW, Price JS. 2004. Stimulating soil water dynamics in a cutover bog. Water Resour. Res. **40**: 1-13.

Kennedy GW, Price JS. 2005. A conceptual model of volume-change controls on the hydrology of cutover peats. J. Hydrol. **302**: 13-27.

Klute A, Dirksen C. 1986. Hydraulic conductivity and diffusivity: Laboratory methods. In Klute (ed.) Methods of soil analysis. Part 1. 2nd ed. Agron. Monogr, Madison, WI, 687-734.

Kool DM, Buurman P, Hoekman DH. 2006. Oxidation and compaction of a collapsed peat dome in Central Kalimantan. Geoderma **137**: 217-225.

Kool JB, Parker JC, van Genuchten MT. 1985. Determining soil hydraulic properties from one-step outflow experiments by parameters estimation: Theory and numerical studies. Soil Sci. Soc. Am. J. **49**: 1348-1354.

Kool JB, Parker JC, van Genuchten MT. 1987. Parameter estimation for unsaturated flow and transport models – A review. J. Hydrol. **91**: 255-293.

Kosugi K. 1996. Lognormal distribution model for unsaturated soil hydraulic properties. Water Resour. Res. **32**: 2697-2703.

Kuhry P, Nicholson BJ, Gignac DH, Vitt, Bayley SE. 1993. Development of Sphagnum dominated peatlands in boreal continental Canada. Can. J. Bot. **71**: 10-22.

Kutilek M, Novak V. 1998. Exchange of water in the soil-plant-atmosphere system. Agrophys. **12**: 28-33.

Kyziol, J. 2002. Effect of physical properties and cation exchange capacity on sorption of heavy metals onto peats. Pol. J. Environ. Stud. **11**: 713-718.

Leifeld J, Steffens M, Galego-Sala A. 2012. Sensitivity of peatland carbon loss to organic matter quality. Geophys. Res. Lett. **39**: L14704. doi:10.1029/2012GL051856.

Letts MG, Roulet NT, Comer NT. 2000. Parametrization of peatland hydraulic properties for the Canadian land surface scheme. Atmos. Ocean. **38**: 141-160.

Lewis KC, Zyvoloski GA, Travis B, Wilson C, Rowland J. 2011. Drainage subsidence associated with Arctic permafrost degradation. J. Geophys. Res. **117**: 1-18.

Lilly JP. 1981. The Blackland Soils of North Carolina: Their Characteristics and Management for Agriculture. N.C. Agric. Res. Ser. Tech. Bull. **270**: 1-70.

Long AJ, Waller MP, Stupples P. 2006. Driving mechanisms of coastal change: Peat compaction and the destruction of late Holocene coastal wetlands. Mar. Geol. **225**: 63-84.

Luken J. 1985. Zonation of Sphagnum mosses: interactions among shoot growth, growth form, and water balance. Am. Bryological and Lichenological Soc. **88**: 374-379.

Lukoshko ES, Bambalov NN, Smychnik TP. 1979. The changes in the composition of lignin in the process of peat formation. Khimiya Tverdogo Topliva **13**: 144-150.

Mammides C, Kadis C, Coulson T. 2014. The effects of road networks and habitat heterogeneity on the species richness of birds in Natura 2000 sites in Cyprus. Landscape Ecol. **30**: 67-75.

Marchand MN, Litvaitis JA. 2004. Effects of habitat features and landscape composition on the population structure of a common aquatic turtle in a region undergoing rapid development. Conservation Biol. **18**: 758-767.

Marshall IB, Schut P, Ballard M (compilers). 1999. Canadian Ecodistrict Climate Normals for Canada 1961–1990. A National Ecological Framework for Canada: Attribute Data. Environmental Quality Branch, Ecosystems Science Directorate, Environment Canada and Research Branch, Agriculture and Agri-Food Canada, Ottawa/Hull.

Mazerolle MJ. 2004. Amphibian road mortality in response to nightly variations in traffic intensity. Herpetologica **60**(1): 45-53.

McCarter CPR, Price JS. 2012. Ecohydrology of Sphagnum moss hummocks: mechanisms of capitula water supply and simulated effects of evaporation. Ecohydrol., DOI: 10.1002/eco.1313.

McCarter CP, Price JS. 2013. The hydrology of the Bois-des-Bel bog peatland restoration: 10 years post-restoration. Ecol. Eng. **55**: 73-81.

McLay CDA, Allbrook RF, Thompson K. 1992. Effect of development and cultivation on physical properties of peat soils in New Zealand. Geoderma **54**: 23-37.

McNeil P, Waddington JM. 2003. Moisture controls on Sphagnum growth and CO2 exchange on a cutover bog. J. Appl. Ecol. **40**: 354-367.

MEG Energy Corp. 2008. Environmental guidelines for facility construction.

Mesri G, Ajlouni M. 2007. Engineering properties of fibrous peat. ASCE J. Geotech. and Geoenviron. Eng. **133**: 850–866.

Miatkowski Z, Cieslinski Z, Turbiak J. 1999. Use of agroreclamation ploughing in reclamation of a deeply drained mineral-muckl soil. Agrophys. **23**: 97-105.

Miller B, Williams K, La Farge C, and Osko T. 2015. Occurences of bryophyte taxa on Firebag Pad 106 Road, unpublished.

Mitsch WJ, Gosselink JG. 2000. Wetlands. 3rd ed. Wiley, New York.

Moore TR, Knowles R. 1990. Methane emissions from fen, big and swamp peatlands in Quebec. Biogeochemistry. **11**: 45-61.

Moore PA, Morris PJ, Waddington JM. 2015. Multi-decadal water table manipulation alters peatland hydraulic structure and moisture retention. Hydrol. Process. DOI: 10.1002/hyp.10416

Mualem Y. 1976. A new model for predicting the hydraulic conductivity of unsaturated porous media. Water Resour. Res. **12**: 513-522.

National Wetlands Working Group. 1988. Wetlands of Canada. Ecological land classification series No.24. Environment Canada and Polyscience Publications: Ottawa; 452.

Nesterenko IM. 1976. Subsidence and wearing out of peat soils as a result of reclamation and agricultural utilization of marshlands. Proc. V Int. Peat Congr. Poznan. **1**: 218-232.

Neuman SP. 1990. Universal scaling of hydraulic conductivities and dispersivities in geologic media. Water Resour. Res. **26**: 1749-1758.

Nilsson B, Sidle RC, Klint KE, Bøggild CE, Broholm K. 2001. Mass transport and scale-dependent hydraulic tests in a heterogeneous glacial till-sandy aquifer system. J. Hydrol. **243**: 162-179.

Nugent C, Kanali C, Owende PO, Nieuwenhui M, Ward S. 2003. Characteristic site disturbance due to harvesting and extraction machinery traffic on sensitive forest sites with peat soils. Forest Ecology and Management. **180**: 85- 98.

Ojanen P, Lehtonen A, Heikkinen J, Penttila T, Minkkinen K. 2014. Soil CO2 balance and its uncertainty in forestry-drained peatlands in Finland. Forest Ecol. Manag. **325**: 60-73.

O'Kelly BC, Pichan SP. 2013. Effects of decomposition on the compressibility of fibrous peat – A review. Geomech. Geoeng. Int. J. **8**: 286-296.

O'Kelly BC, Orr TLL. 2014. Briefing: Effective-stress strength of peat in triaxial compression. Geotech. Eng. **167**: 417-420.

Okruszko HJ. 1993. Transformation of fen-peat soils under the impact of drainingage. Zzesz. Pprobl. pPost. nNauk rRol.n. **406**: 3-734.

Ours DP, Siegel DI, Glaser PH. 1997. Chemical dilation and the dual porosity of humified bog peat. J. Hydrol. **196**: 348-360.

Päivänen J. 1982. The effect of cutting and fertilization on the hydrology of an old forest drainage area. Folia For. **516**: 1-19.

Parent LE, Millette JA, Mehuys GR. 1982. Subsidence and erosion of a Histosol. Soil Sci. Soc. Am. J. **46**: 404-408.

Parker JC, Kool JB, van Genuchten MT. 1985. Determining soil hydraulic properties from one-step outflow experiments by parameter estimation: II. Experimental Studies. Soil Sci. Soc. Am. J. **49**: 1354-1360.

Patrick DA, Gibbs JP. 2010. Population structure and movements of freshwater turtles across a road-density gradient. Landscape Ecol. **25**(5): 791-801.

Peck AJ, Rabbidge RM. 1969. Design and performance of an osmotic tensiometer for measuring capillary potential. Soil Sci. Soc. Am. J. **33**: 196-202.

Peters A, Durner W. 2006. Improved estimation of soil water retention characteristics from hydrostatic column experiments. Water Resour. Res. **42**: 1-9.

Peters A, Durner W. 2008. Simplified evaporation method for determining soil hydraulic properties. J. Hydrol. **356**: 147-162.

Petranka JW, Francis RA. 2013. Effects of road salts on seasonal wetlands: Poor prey performance may compromise growth of predatory salamanders. Wetlands **33**(4): 707-715.

Petrone RM, Devito KJ, Silins U, Mendoza C, Kaufman SC, Price JS. 2007. Importance of seasonal frost to peat water storage in the Western Boreal Plains, Canada. In Abesser C, Wagener T, Nuetzmann G (eds.). Groundwater-Surface Water Interaction: Process Understanding, Conceptualization and Modelling, Proceedings of Symposium HS1002 at IUGG2007, Perugia, July 2007, IAHS Publication No 321, 61-66.

Petrone RM, Devito KJ, Silins U, Mendoza C, Brown SC, Kaufman SC, Price JS. 2008. Transient peat properties in two pond-peatland complexes in the sub-humid Western Boreal Plains, Canada. Mires Peat. **3**: 1-13.

Petrone R, Osko T. 2013. Suncor Firebag Road Removal Reclamation Study: 19 February 2013. Research Proposal.

Phillips MJ. 1997. Forestry best management practices for wetlands in Minnesota. In Trettin CC, Jurgensen MF, Grigal DF, Gale MR, Jeglum JK (eds.). Northern forested wetlands: Ecology and management. Lewis Publishers, New York, NY.

Pielke R, Vidale PL. 1995. The boreal forest and the polar front. J. Geophys. Res. **100**: 755-758.

Pojar J. 1996. Environment and biogeography of the Western boreal forest. Forest Chron. **72**: 51-58.

Prach K, Sandor B, Pysek P, van Diggelen R, Wiegleb G. 2001. The role of spontaneous vegetation succession in ecosystem restoration: a perspective. Applied Vegetation Sci. **4**: 111-114.

Price JS, Woo MK. 1988. Wetlands as waste repositories? Solute transport in peat. Proc. Nat. Student Conference on Northern Studies, 1986 Nov. 18-19, Association of Canadian Universities for Northern Studies, Ottawa, ON, 392-395.

Price JS. 1991. Evaporation from a blanket bog in a foggy coastal environment. Bound-Lay. Meteorol. **57**: 391-406.

Price JS, Schlotzhauer SM. 1999. Importance of shrinkage and compression in determining water storage changes in peat: the case of a mined peatland. Hydrol. Process. **13**: 2591-2601.

Price JS. 2003. The role and character of seasonal peat soil deformation on the hydrology of undisturbed and cutover peatlands. Water Resour. Res. **39**: 3-9.

Price JS, Healthwaite AL, Baird AJ. 2003. Hydrological processes in abandoned and restored peatlands: an overview of management approaches. Wetlands Ecology and Management **11**: 65-83.

Price JS, Cagampan J, Kellner E. 2005. Assessment of peat compressibility: is there an easy way? Hydrol. Process. **19**: 3469-3475.

Price JS, Whittington PN. 2008. A method to determine unsaturated hydraulic conductivity in living and undecomposed Sphagnum moss. Soil Sci. Soc. Am. J. **72**: 487.

Price JS, Whittington PN, Elrick DE, Strack M, Brunet N, Faux E. 2008. A method to determine unsaturated undecomposed Sphagnum moss. Soil Sci. Soc. Am. J. **72**: 487-491.

Price JS, Whittington PN. 2010. Water flow in sphagnum hummocks: mesocosm measurements and modeling. J. Hydrol. **381**: 333-340.

Pronger J, Schipper LA, Reece BH, Campbell DI, McLeod M. 2014. Subsidence Rates of Drained Agricultural Peatlands in New Zealand and the Relationship with Time since Drainage. J. Environ. Qual. **43**: 1442-1449.

Quinton WL, Gray DM, Marsh P. 2000. Subsurface drainage from hummock-covered hillslope in the Arctic Tundra. J. Hydrol. **237**: 113-125.

Quinton WL, Hayashi M, Carey SK. 2008. Peat hydraulic conductivity in cold regions and its relation to pore size and geometry. Hydrol. Process. **22**: 2829-2837.

Quinton WL, Elliot T, Price JS, Rezanezhad F, Heck R. 2009. Measuring physical and hydraulic properties of peat from X-ray tomography. Geoderma. **153**: 269-277.

Radforth NW, Brawner CO (eds.). 1977. Muskeg and the northern environmental in Canada. University of Toronto Press, 82-147.

Reeve MJ, Hall DGM, Bullock P. 1980. The effect of soil composition and environmental factors on the shrinkage of some clayey British soils. **31**: 429-442.

Reynolds WD, Elrick DE. 1991. Determination of hydraulic conductivity using a tensiometer infiltrometer. Soil Sci. Soc. Am. J. **55**: 633-639.

Rezanezhad F, Quinton WL, Price JS, Elrick D, Elliot TR, Heck RJ. 2009. Examining the effect of pore size distribution and shape on flow through unsaturated peat using computed tomography. Hydrol. Earth Syst. Sci. **13**: 1993-2002.

Rezanezhad F, Price JS, Craig JR. 2012. The effects of dual porosity on transport and retardation in peat. Can. J. Soil. Sci. **92**: 1-10.

Richards LA. 1948. Porous plate apparatus for measuring moisture retention and transmission by soils. Soil Sci. **66**: 105-110.

Rizzo B, Wiken E. 1989. Assessing the sensitivity of Canada's ecosystems to climatic change. In Koster EA, Boer MM. (compilers). Landscape Ecological Impacts of Climate Change on Boreal/(Sub)Arctic Regions with emphasis on Fennoscandia. LilC Project, 94-111.

Robroek BM, Limpens J, Breeuwer A, Ruijven JV, Schouten MC. 2007. Precipitation determines the persistence of hollow Sphagnum species on hummocks. Wetlands **27**: 979-986.

Rochefort L. 2000. Sphagnum—A Keystone Genus in Habitat Restoration. Bryologist **103**: 503-508.

Rodriguez-Iturbe I. 2000. Ecohydrology: a hydrologic perspective of climate-soil-vegetation dynamics. Water Resour. Res. **36**: 3-9.

Roulet N. 1990. Focus: aspects of the physical geography of wetlands. The Can. Geogr. **34**: 79-88.

Roulet N, Moore T, Bubier J, Lafleur P. 1992. Northern fens: methane flux and climate change. Tellus. **44**B: 100-105.

Rubec, CDA, Lynch-Stewart P, Wickware GM, Kessel-Taylor I. 1988. Wetland utilization in Canada. Montreal, Canada: Polyscience, 379-412.

Rydin H. 1985a. Effect of water level on desiccation of Sphagnum in relation to surrounding Sphagna. Oikos **45**: 374-379.

Rydin H. 1985b. Photosynthesis in Sphagnum at different water contents. J. Bryol. **13**: 579-584.

Rydin H. 1993. Interspecific competition between Sphagnum mosses on a raised bog. OIKOS **66**: 413-423.

Schindler U. 1980. A rapid method for measurement of hydraulic conductivity in partially saturated soil sample ring samples. Arch. Acker-Pflanzenbau Bodenkd. **24**: 1-7.

Schindler U, Mueller L, Behrendt A. 2004. Effect of drainage and land use on soil hydrological properties of peat soils. 8th International Drainage Symposium – Drainage VIII: 254-360.

Schindler U, Müller L. 2006. Simplifying the evaporation method for quantifying soil hydraulic properties. J. Plant Nutr. Soil Sci. **169**: 623-629.

Schindler DW, Lee PG. 2010. Comprehensive conservation planning to protect biodiversity and ecosystem services in Canadian boreal regions under a warming climate and increasing exploitation. Biol. Conserv. 143: 1571-1586.

Schindler U, Durner W, von Unold G, Müller L. 2010a. Evaporation method for measuring unsaturated hydraulic properties of soils: Extending the Measurement Range. Soil Sci. Soc. Am. J. **74**: 1071-1083.

Schindler U, Durner W, von Unold G, Müller L, Wieland R. 2010b. The evaporation method: Extending the measurement range of soil hydraulic properties using the air-entry pressure of the ceramic cup. J. Plant Nutr. Soil Sci. **173**: 563-572.

Schipperges B, Rydin H. 1998. Response of photosynthesis of Sphagnum species from contrasting microhabitats to tissue water content and repeated desiccation. New Phytol. **140**: 677-684.

Schlesinger WH. 1991. Biogeochemistry: An analysis of global change. Academic Press, Toronto.

Schlotzhauer SM, Price JS. 1999. Soil water flow dynamics in a managed cutover peat field, Quebec: Field and laboratory investigations. Water Resour. Res. **35**: 3675-3683.

Schneider K, Ippisch O, Roth K. 2006. Novel evaporation experiment to determine soil hydraulic properties. Hydrol. Earth Syst. Sci. **10**: 817-827.

Schothorst CJ. 1977. Subsidence of low moor peat soils in the western Netherlands. Geoderma **17**: 265-291.

Schulze-Makuch D, Carlson DA, Cherkauer DS, Malik P. 1999. Scale dependency of hydraulic conductivity in heterogeneous media. Ground Water **37**: 904-919.

Schwarzel K, Renger M, Sauerbrey R, Wessolek G. 2002. Soil physical characteristics of peat soils. J. Plant Nutr. Soil Sci. **165**: 479-486.

Schwarzel K, Simunek J, Stoffregen H, Wessolek G, van Genuchten MT. 2006. Estimation of the Unsaturated Hydraulic Conductivity of Peat Soils: Laboratory versus Field Data. Vadose Zone J. **5**: 628-640.

Shafiee A, Steward JP, Brandenberg SJ. 2015. Reset of Secondary Compression Clock for Peat by Cyclic Straining. J. Geotech. Geoenviron. Eng. DOI: 10.1061/(ASCE)GT.1943-5606.0001286

Silins U, Rothwell RL. 1998. Forest peatland drainage and subsidence affect soil water retention and transport properties in an Alberta peatland. Soil Sci. Soc. Am. J. **62**: 1048-1056.

Simunek J, Wendroth O, van Genuchten MT. 1998. Parameter estimation analysis of the evaporation method for determining soil hydraulic properties. Soil Sci. Soc. Am. J. **62**: 894-905.

Skaggs RW, Gilliam JW, Sheets T, Barnes J. 1980. Effect of agricultural land development on drainage waters in the north Carolina tidewater region. N.C. Water Resour. Res. **159**: 1-161.

Soluk DA, Zercher DS, Worthington AM. 2011. Influence of roadways on patterns of mortality and flight behavior of adult dragonflies near wetland areas. Biol. Conserv. **144**: 1638-1643.

Sonnleitner MA, Abbaspour KC, Schulin R. 2003. Hydraulic and transport properties of the plant-soil system estimated by inverse modeling. Eur. J. Soil Sci. **54**: 127-138.

Spatt PD, Miller MC. 1981. Growth conditions of vitality of Sphagnum in a tundra community along the Alaska pipeline haul road. Arctic **34**: 48-54.

Spiers GS, Dudas MD, Muehlenbachs KM, Turchenek LT. 1983. Mineralogy and oxygen isotope geochemistry of clays from surficial deposits in the Athabasca Tar Sands area. Can. J. Earth Sci. **21**: 53-60.

Steen DA, Gibbs JP. 2004. Effects of roads on the structure of freshwater turtle populations. Conserv. Biol. **18**(4): 1143-1148.

Strack M, Waddington JM. 2007. Response of peatland carbon dioxide and methane fluxes to a water table drawdown experiment. Global Biogeochem. Cy. **21**: 1-13.

Sun Y, Liu HL, Yang G, Xiao Y. 2013. Formulation of cross-anisotropic failure criterion for soils. Water Sci. Eng. **6**: 456-468.

Surridge BWJ, Baird AJ, Heathwaite AL. 2005. Evaluating the quality of hydraulic conductivity estimates from piezometer slug tests in peat. Hydrol. Process. **19**: 1227-1244.

Tarnocai C, Kettles IM, Ballard M. 1995. Peatlands of Canada. Geological Survey of Canada map. Open File 3152.

Tarnocai C. 2009. The impact of climate change on Canadian peatlands. Can. Water Res. J. **34**: 453-465.

Tashiro M, Nguyen SH, Inagaki M, Yamada S, Noda T. 2015. Simulation of large-scale deformation of ulta-soft peaty ground under test embankment loading and investigation of effective countermeasures against residual settlement and failure. Soils and Found. **55**: 343-358.

Terzaghi K. 1943. Theoretical Soil Mechanics. Wiley: New York.

Thompson DK, Waddington JM. 2008. Sphagnum under pressure towards an ecohydrological approach to examining Sphagnum productivity. Ecohydrology. **1**: 299-308.

Thompson DK, Waddington JM. 2013. Peat properties and water retention in boreal forested peatlands subjected to wildfire. Water Resour. Res. **49**: 3651-3658.

Tindal JA, Kunkel JR. 1999. Unsaturated zone hydrology for scientists and engineers. Prentice Hall, Upper Saddle River, NJ, 64 pages.

Todorova SG, Siegeland DI, Costello AM. 2005. Microbial Fe(III) reduction in a minerotrophic wetland – geochemical controls and involvement in organic matter decomposition. Appl. Geochem. **20**: 1120-1130.

Tromboulak SC, Frissell CA. 2000. Review of the ecological effects of roads on terrestrial and aquatic communities. Biol. Conserv. **14**: 18-20.

Turetsky MR, Wieder RK, Williams CJ, Vitt DH. 2000. Organic matter accumulation, peat chemistry, and permafrost melting in peatlands of boreal Alberta. Ecoscience. **7**: 379-392.

Turetsky MR, St. Louis VL. 2006. Disturbance in boreal peatlands. Pages 359-372 iIn R.K. Wieder and D.H. Vitt, (editors.). Boreal peatland ecosystems. Springer- Verlag, Berlin, Germany, 359-372.

Turetsky MR, Crow SE, Evans R, Vitt DH, Wieder K. 2008. Trade-offs in resource allocation among moss species control decomposition in boreal peatlands. J. Ecol. **96**: 1297-1305.

Turunen J, Tomppo E, Tolonen E, Reinikainen A. 2002. Estimating carbon accumulation rates of undrained mires in Finland-application to boreal and subarctic regions. The Holocene **12**: 69-80.

Tyner JS, Arya LM, Wright WC. 2006. The dual gravimetric hot air method for measuring soil water diffusivity. Vadose Zone J. **5**: 1281-1286.

UMS HYPROP-Fit User Manual. 2015. UMS GmBH, Gmun- der Str. 37, 81379 Munchen, Germany. URL: http://www.ums.muc.de/static/Manual_HYPROP-FIT.pdf

van Asselen S, Stouthamer E, van Asch Th.WJ. 2009. Effects of peat compaction on delta evolution: A review on processes, responses, measuring and modeling. Earth-Sci Rev. **92**: 35-51.

van Asselen. 2010. The contribution of peat compaction to total basin subsidence: Implications for the provision of accommodation space in organic-rich deltas. Basin Res. **23**: 239-255.

Van Cleve K, Oechel WE, Hom JL. 1990. Response of black spruce (Picea mariana) ecosystems to soil temperature modifications in interior Alaska. Can. J. Forest Res. **20**: 1530-1535.

van der Ploeg MJ, Gooren HPA, Bakker G, de Rooij GH. 2008. Matric potential measurements by polymer tensiometers in cropped lysimeters under water-stressed conditions. Vadose Zone J. **7**: 1048-1054.

van der Ploeg MJ, Gooren HPA, Bakker G, Hoogendam CW, Huiskes C, Koopal LK, Kruidhof H, de Rooij GH. 2009. Polymer tensiometers with ceramic cones: Performance in drying soils and comparison with water filled tensiometers and time domain reflectometry. Hydrol. Earth Syst. Sci. Discuss. **6**: 4349-4377.

van der Schaaf S. 1999. Analysis of the hydrology of raised bogs in the Irish Midlands. A case study of Raheemore Bog and Clara Bog. PhD Thesis. Wageningen University, 375.

van der Schaaf S. 2004. A single well pumping and recovery test to measure in situ acrotelm transmissivity in raised bogs. J. Hydrol. **290**: 152-160.

van Genuchten MT, Wierenga PJ. 1976. Mass-transfer studies in sorbing porous media: Analytical Solutions. Soil Sci. Soc. Am. J. **40**: 473-480.

van Genuchten, MT. 1980. A closed-form equation for predicting the hydraulic conductivity of unsaturated soils. Soil Sci. Soc. Am. J. **44**: 892-898.

Vargas-Salinas F, Cunnington GM, Amézquita A, Fahrig L. 2014. Does traffic noise alter calling time in frogs and toads? A case study of anurans in Eastern Ontario, Canada. Urban Ecosystems **17**: 945-953.

Varosio G. 2000. Peat Subsidence due to Ground Water Movements. In Edil TB and Fox PJ (eds.), Geotechnics of High Water Content Materials, ASTM STP 1374, American Society for Testing and Materials, West Conshohocken, PA. 375-386

Verry ES, Boelter DH. 1978. Peatland hydrology. Wetlands, 389-402.

Verry ES, Brooks KN, Barten PK. 1988. Streamflow response from an ombrotrophic mire. Symp. Hyd. of Wetlands in the temperate and cold regions. **1**: 52-59.

Viraraghavan T, Ayyaswami A. 1989. Batch studies on septic tank effluent treatment using peat. Can. J. Civ. Eng. **16**: 157-161.

Vitt DH, Halsey LA, Thormann M, Martin T. 1996. Peatland Inventory of Alberta. Prepared for the Alberta Peat Task Force, National Center of Excellence in Sustainable Forest Management, University of Alberta, Edmonton.

Vogel T, Cislerova M. 1988. On the reliability of unsaturated hydraulic conductivity calculated from the moisture retention curve. Transport Porous Med. **3**: 1-15.

Waddington JM, Kellner E, Strack M, Price JS. 2010. Differential peat deformation, compressibility, and water storage between peatland microforms: implications for ecosystem function and development. Water Resour. Res. **46**: *W07538, doi: 10.1029/2009WR008802.*

Walczak R, Rovdan E, Witkowska-Walczak B. 2002. Water retention characteristics of peat and sand mixtures. Agrophys. **16**: 161-165.

Wardenaar, EPC. 1987. A new hand tool for cutting peat profiles. Can. J. Bot. **65**: 1772-1773.

Weiss R, Alm J, Laiho R, Laine J. 1998. Modeling moisture retention in peat soils. Soil Sci. Soc. Am. J. **62**: 305-313.

Wendroth O, Rogasik H, Koszinski S, Ritsema CJ, Dekker LW, Nielsen DR. 1999. State-space prediction of field scale soil water content time series in a sandy loam. Soil Tillage Res. **50**: 85-93.

Whalley WR, Clark LJ, Take WA, Bird NA, Leech PK, Cope RE, Watts CW. 2006. A porous-matrix sensor to measure the matric potential of soil water in the field. Eur. J. Soil Sci. **58**: 18-25.

Whisenant SG. 1999. Repairing damaged wildlands: a process- orientated, landscape-scale approach. Cambridge University Press, Cambridge.

White JS, Bayley SE, Curtis PJ. 2000. Sediment storage of phosphorus in a northern prairie wetland receiving municipal and agro-industrial wastewater. Ecol. Eng. **14**: 127-138.

White JS, Bayley SE. 2001. Nutrient retention in a northern prairie marsh (Frank Lake, Alberta) receiving municipal and agro-industrial wastewater. Water Air and Soil Poll. **126**: 63-81.

Williams CJ, Yavitt JB, Wieder RK, Cleavitt NL. 1998. Cupric oxide oxidation products of northern peat and peat forming plants. Can. J. Bot. **76**: 51-62.

Williams TJ, Quinton WL, Baltzer JL. 2013. Linear disturbances on discontinuous permafrost: Implications for thaw-induced changes to land cover and drainage patterns. Environ. Res. Lett. **8**: 1-12.

Wind GP. 1966. Capillary conductivity data estimated by a simple method, in Proc. Symp. "Water in the Unsaturated Zone," Wageningen, Tthe Netherlands, 181-191.

Wind GP. 1968. Capillary conductivity data estimated by a simple method. P.E. Rijtema and H. Wassink (eds.). Water in the unsaturated zone. Proc. Wageningen Symp. June 1966. Gentbrugge, Belgium, 181-191.

Wong LS, Hashim R, Ali FH. 2009. A review on hydraulic conductivity and compressibility of peat. J. Appl. Sci. **9**: 3207–3218.

Wosten JHM, Ismail AB, van Wijk ALM. 1997. Peat Subsidence and its practical implications: a case study in Malaysia. Geoderma **78**: 25-36.

Yamaguchi H, Ohira Y, Kogure, K, Mori S. 1985. Undrained shear characteristics of normally consolidated peat under triaxial compression and extension conditions. Jpn. Soc. Soil Mech. Found. Eng. **25**: 1–18.

Young MH, Sisson JB. 2002. Tensiometry. In J.H. Dane and G.C. Topp (eds.). Methods of soil analysis. Part 4. SSSA Book Ser. 5. SSSA, Madison, WI., 575-608.

Yuan Y, Zeng G, Liang J, Li X, Li Z, Zhang C,… Yu X. 2014. Effects of landscape structure, habitat and human disturbance on birds: A case study in East Dongting Lake wetland. Ecol. Eng. **67**: 67-75.

Zachmann DW, Duchateau PC, Klute A. 1981. Simultaneous approximation of water capacity and soil hydraulic conductivity by parameter identification. Soil Sci. **134**: 157-163.

Zanello F, Teatini P, Putti M, Gambolati G. 2011. Long term peatland subsidence: Experimental study and modeling scenarios in the Venice coastland. J. Geophys. Res. **116**: 1-14.

Zhang L, O'Kelly, BC. 2013. Constitutive models for peat – a review, Proceedings of the 12th International Conference on Computational Plasticity – Fundamentals and Applications (COMPLAS XII). 1294-1304.

Zhang L, O'Kelly BC. 2014. The principle of effective stress and triaxial compression testing of peat. Geotech. Eng. **167**: 40-50.

Zuidhoff FS. 2003. Physical Pproperties of the surface peat layer and the influence on thermal conditions during the development of palsas. Permafrost,In M. Phillips, SM Springman & LU Arenson (eds.)., Permafrost, Swets & Zeitlinger, Lisse, 1313-1317.

Zwanenburg C, Barends FBJ. 2007. The Influence of Anisotropic Stiffness On The Consolidation of Peat. Soils Found. **47**: 507-516.

Appendices

Appendix 1

Pad 106 Pipeline Photograph

Appendix 2

Civil Engineering Road Material Data and Calculations

Let: W_M = weight of the moisture, %M = weight % that is moisture, M = million, P = pressure, and F = Force.

Moisture Weight

$$W_M = \frac{\%M}{100} \times \frac{kg\ H_20}{kg\ total} \times \frac{1\ kg\ total}{\left(1 - (\frac{\%M}{100})\right)} \times \rho_D \times volume$$

$$W_M = \frac{\%M}{100 - \%M} \times \rho_D \times vol$$

$$W_{moisture} = \frac{(11.5550725)\left(\frac{1908.42029\ kg}{m^3}\right)(6034m^3)}{88.449} = 1,504,385.3\ kg$$

Volume Percent

1.5M kg = 1.5M L (*assuming density of water = 1kg/L*)

$$\frac{Moisture\ weight\ in\ litres}{Road\ volume\ in\ litres} = \frac{1,504,385.3\text{M L}}{6034\text{M L}} = 0.24931803 = 25\%\ Moisture\ Content$$

Pressure and Total Weight

$$Weight_{total} = Weight_{dry} + Weight_{moisture}$$

$$Weight_{total} = (1908.42029 \times 6034) + 11.5550725 = 11,515,419.58\ kg$$

$11,515,419.58kg \times 9.81 = 1.129 \times 10^8\ \text{N}\ or\ \frac{1.129 \times 10^8\ kg \cdot m}{s^2}$

$$P = \frac{F}{A} = \frac{1.129 \times 10^8\ N}{4784.617774}$$

$$P = \frac{23,599\ N}{m^2}$$

Location	Position	Depth	Moisture (%)
1	1	1	9.6
1	1	2	11.1
1	1	3	9.5
1	1	4	10.3
1	1	5	12.6
1	1	6	11.9
1	2	1	8.3
1	2	2	10.5
1	2	3	11.8
1	2	4	11.8
1	2	5	10.9
1	2	6	12
1	3	1	9.4
1	3	2	13.7
1	3	3	10.9
1	3	4	13.2
1	3	5	12.6
1	3	6	13.3
2	1	1	8.9
2	1	2	9.8
2	1	3	10.2
2	1	4	11.6
2	1	5	12.4
2	1	6	14.2
2	2	1	8.6
2	2	2	9.4
2	2	3	11.6
2	2	4	12.4
2	2	5	12
2	2	6	12.1
2	3	1	12.1
2	3	2	11.8
2	3	3	13.3
2	3	4	13
2	3	5	13.2
2	3	6	-
3	1	1	8.8
3	1	2	11.8
3	1	3	10.2
3	1	4	12.6
3	1	5	11.5

3	1	6	10.9
3	2	1	10.4
3	2	2	11.3
3	2	3	11.6
3	2	4	11.2
3	2	5	11.5
3	2	6	11.5
3	3	1	11.8
3	3	2	14.1
3	3	3	11.3
3	3	4	13.2
3	3	5	12.5
3	3	6	13.5
4	1	1	10.4
4	1	2	11
4	1	3	10.2
4	1	4	12.9
4	1	5	12.9
4	1	6	-
4	2	1	8.6
4	2	2	10.7
4	2	3	12.2
4	2	4	11.6
4	2	5	11.7
4	2	6	13
4	3	1	8.1
4	3	2	11.2
4	3	3	11.4
4	3	4	12.1
4	3	5	12.5
4	3	6	13.5

(Source: Terry Osko)

Pad 106 Access Road Average dry density (Kg/m^3)	1908.42029
Pad 106 Access Road Average moisture (%)	11.5550725
Pad 106 Access Road dimensions:	
Length (m):	228.183934
Width (m) at well 1-4:	19.526
Width (m) at well 2-4:	21.253
Width (m) at well 3-4:	20.255
Width (m) at well 4-4:	22.839
Average width (m):	20.96825
Road Volumes (m^3)	
Clay	4866
Mud and organics	987
Gravel	181

(Source: Terry Osko)

THURBER ENGINEERING LTD.
GEOTECHNICAL • ENVIRONMENTAL • MATERIALS

#200, 9638 - 51 Avenue, Edmonton, AB T6E 6A5 Phone (780) 438-1460 Fax (780) 437-7125

MOISTURE DENSITY REPORT

Client: CIRCLE T CONSULTING INC

Project Number: 19-6496-0

Project: PEATLAND ROAD REMOVAL - MATERIALS

Date Tested: 01-Oct-13

Date Sampled: N/A

Sample Source: 1. West, 1. Mid, 1. East

Sample Description: Combined samples, Clay

Oversized material:
2.6% retained on the 4.75 mm sieve

As-Received Moisture Content: 11.6%

Thurber Lab Series #: 21483

Wet Density - kg/m³	2012	2143	2156	2116			
Dry Density - kg/m³	1844	1930	1907	1840			
Moisture Content- %	9.1	11.0	13.0	15.0			
Pocket Pen. (kg/cm²)	>4.5	>4.5	3.3	1.3			

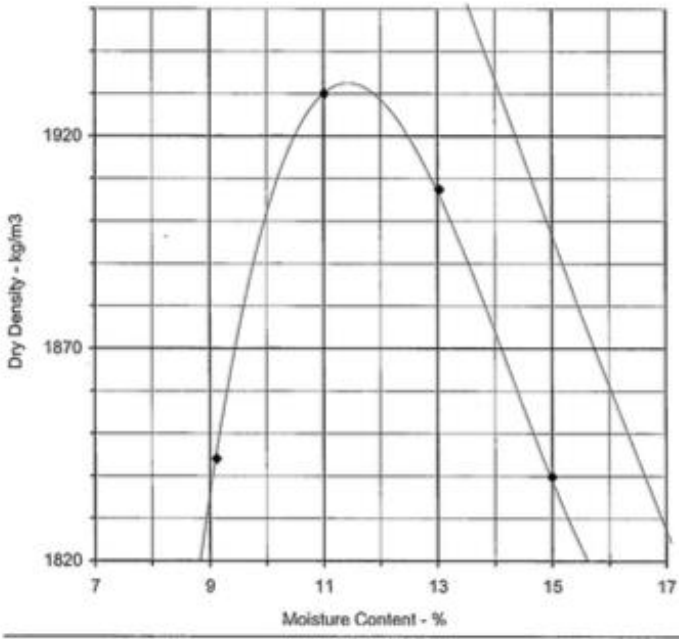

Proctor Results
Max. Dry Density: **1933 kg/m³**
Optimum Moisture: **11.3%**

Preparation: Moist
Compaction Std.: ASTM D698
Method: A
Rammer Type: Manual

Sampled By: Client

Tested By: SRA

Project Eng.: YCL

Zero Air Voids Curve plotted for a Specific Gravity of 2.65

Comments:

Report Checked: _____

Tested In accordance with ASTM Designation D698 unless otherwise noted

(Source: Terry Osko)

Thurber Engineering Ltd.
Suite 200, 9636 - 51 Avenue, Edmonton, Alberta T6E 6A5 Phone: (780) 438-1460 Fax: (780) 427-7125

CLIENT: Circle T Consulting **FILE:** 19-6496-0
PROJECT: Peatland Road Removal **DATE:** 23-Aug-13

TEST HOLE LOCATION	DEPTH (m)	LIQUID LIMIT	PLASTIC LIMIT	PLASTIC INDEX	FIELD MOISTURE CONTENT (%)	M.C. above OMC	LIQUID INDEX	EST. OMC* (%)	SPMDD ** (kg/m^3)	SOIL CLASS
1-West	50 - 75	33	14	19	10.9	-2.9	-0.16	**13.8**	**1850**	CI
1-Middle	0 - 25	32	14	18	8.3	-5.3	-0.32	**13.6**	**1855**	CI
1-East	75-100	33	14	19	10.3	-3.5	-0.19	**13.8**	**1850**	CI
2-West	50 - 75	32	14	18	13.3	-0.3	-0.04	**13.6**	**1855**	CI
2-Middle	100-125	32	14	18	12.0	-1.6	-0.11	**13.6**	**1855**	CI
2-East	125 - 150	32	15	17	14.2	-0.2	-0.05	**14.4**	**1819**	CI
3-West	125 - 150	32	14	18	10.9	-2.7	-0.17	**13.6**	**1855**	CI
3-Middle	75 - 100	31	15	16	11.2	-3.0	-0.24	**14.2**	**1824**	CI
3-East	25 - 50	34	14	20	8.8	-5.1	-0.26	**13.9**	**1845**	CI
4-West	75 - 100	33	14	19	12.1	-1.7	-0.10	**13.8**	**1850**	CI
4-Middle	125 - 150	31	15	16	13.0	-1.2	-0.13	**14.2**	**1824**	CI
4-East	100 - 125	33	14	19	12.9	-0.9	-0.06	**13.8**	**1850**	CI
Average SPMDD								**13.8**	**1844**	CI
Maximum SPMDD								**13.6**	**1855**	CI
Minimum SPMDD								**14.4**	**1819**	CI

* Estimated optimum moisture content (OMC) based on Alberta Transportation (AT) correlations
** Estimated Standard Proctor Maximum Dry Density (SPMDD) based on Alberta Transportation (AT) correlations

(Source: Terry Osko)

Appendix 3

Forb/Shrub and Tree Survey

Forbs/Shrubs			Trees			
Plot	**Species**	**Cover (%)**	**Species**	**Class**	**Circum.**	**Count**
1-1	*Chamaedaphne calyculata* *Eriophorum angustifolium* *Kalmia polifolia* *Smilacina trifolia* *Oxycoccus microcarpus* *Rubus chamaemorus* *Sphagnum spp*		*Picea mariana*	9-12	12	1
1-2	*Eriophorum angustifolium* *Chamaedaphne calyculata* *Betula glandulosa* *Betula pumila* *Sphagnum spp* *Kalmia polifolia*	75 30 <5 <5 <5 5				
1-3	*Smilacina trifolia* *Eriophorum angustifolium* *Kalmia polifolia* *Chamaedaphne calyculata* *Oxycoccus microcarpus* *Sphagnum spp* *Eriophorum angustifolium* *Salix ssp*	30 60 20 70 15 70 <5 <5				
1-5	*Epilobium angustifolium* *Picea mariana* *Ledum groenlandicum* *Rubus chamaemorus* *Smilacina trifolia* *Chamaedaphne calyculata* *Eriophorum vaginatum* *Salix ssp* *Oxycoccus microcarpus* *Carex ssp* *Sphagnum spp*	50 <5 25 20 5 <5 <5 30 5 10 70	*Populus tremuloides* *Picea mariana*	Sapling Sapling		1 2
1-6	*Ledum groenlandicum* *Picea mariana* *Rubus chamaemorus* *Vaccinium vitis-idaea* *Oxycoccus microcarpus* *Betula glandulosa* *Smilacina trifolia* *Chamaedaphne calyculata* *Andromeda polifolia* *Sphagnum spp*		*Picea mariana* *Picea mariana* *Picea mariana* *Picea mariana* *Picea mariana* *Picea mariana*	Sapling 3-6 6-9 9-12 12-15 15+		
1-7	*Ledum groenlandicum* *Picea mariana* *Rubus chamaemorus* *Smilacina trifolia* *Vaccinium vitis-idaea*	45 15 10 5 15	*Picea mariana* *Picea mariana* *Picea mariana* *Picea mariana* *Picea mariana*	Saplings 3-6 6-9 9-12 12-15	 5 9.2 12.1 13.4	11 7 7 8 5

Forbs/Shrubs			Trees			
Plot	**Species**	**Cover (%)**	**Species**	**Class**	**Circum.**	**Count**
2-1	*Rubus chamaemorus*	20				
	Smilacina trifolia	40				
	Ledum groenlandicum	15				
	Chamaedaphne calyculata	40				
	Oxycoccus microcarpus	20				
	Vaccinium vitis-idaea	5				
	Andromeda polifolia	5				
	Picea mariana	5				
	Betula glandulosa	<5				
	Eriophorum vaginatum	<5				
	Eriophorum angustifolium	<5				
	Sphagnum spp	100				
2-2	*Chamaedaphne calyculata*		*Picea mariana*	Sapling		8
	Ledum groenlandicum		*Picea mariana*	3-6	5	3
	Rubus chamaemorus		*Picea mariana*	6-9	8.2	3
	Andromeda polifolia		*Picea mariana*	9-12		0
	Picea mariana		*Picea mariana*	12-15	11.1	3
	Eriophorum vaginatum		*Picea mariana*	15+	27	12
	Smilacina trifolia					
	Vaccinium vitis-idaea					
	Oxycoccus microcarpus					
	Kalmia polifolia					
	Sphagnum spp					
2-3	*Smilacina trifolia*	20				
	Eriophorum angustifolium	10				
	Eriophorum vaginatum	<5				
	Chamaedaphne calyculata	60				
	Salix ssp	<5				
	Kalmia polifolia	<5				
	Rubus chamaemorus	<5				
	Sphagnum spp	100				
2-5	*Ledum groenlandicum*	35	*Picea mariana*	Sapling		3
	Epilobium angustifolium	20	*Larix laricina*	Sapling		2
	Rubus chamaemorus	12	*Betula papyrifera*	Sapling		1
	Larix laricina	5				
	Eriophorum vaginatum	5				
	Smilacina trifolia	<5				
	Salix ssp	<5				
	Picea mariana	<5				
	Carex ssp	60				
	Sphagnum spp	40				

Forbs/Shrubs			Trees			
Plot	**Species**	**Cover (%)**	**Species**	**Class**	**Circum.**	**Count**
2-6	*Ledum groenlandicum*	80	*Picea mariana*	Sapling		6
	Picea mariana	5	*Picea mariana*	3-6	7	0
	Vaccinium vitis-idaea	50	*Picea mariana*	6-9		4
	Rubus chamaemorus	5	*Picea mariana*	9-12	13.2	0
	Smilacina trifolia	5	*Picea mariana*	12-15	41.2	3
	Sphagnum spp	75	*Picea mariana*	15+		20
2-7	*Ledum groenlandicum*	55	*Picea mariana*	Sapling		10
	Rubus chamaemorus	30	*Picea mariana*	3-6	3.8	2
	Vaccinium vitis-idaea	35	*Picea mariana*	6-9	8.6	2
	Chamaedaphne calyculata	25	*Picea mariana*	9-12		0
	Smilacina trifolia	10	*Picea mariana*	12-15	16.6	4
	Picea mariana	10	*Picea mariana*	15+	32.9	6
	Oxycoccus microcarpus	<5	<5			
	Betula glandulosa	<5	<5			
	Sphagnum spp	80				
3-1	*Andromeda polifolia*	75	*Larix laricina*	Sapling		6
	Eriophorum angustifolium	20	*Picea mariana*	Sapling		7
	Chamaedaphne calyculata	15	*Picea mariana*	3-6	6.4	4
	Smilacina trifolia	25	*Picea mariana*	6-9	9.5	1
	Larix laricina	<5	*Picea mariana*	9-12	12.6	1
	Oxycoccus microcarpus	10	*Picea mariana*	12-15		
	Sphagnum spp	100	*Picea mariana*	15+		
3-2	*Betula pumila*	10	*Picea mariana*	Sapling		
	Picea mariana	20	*Picea mariana*	3-6	5	
	Ledum groenlandicum	30	*Picea mariana*	6-9		2
	Rubus chamaemorus	50	*Picea mariana*	9-12		
	Smilacina trifolia	20	*Picea mariana*	12-15		
	Kalmia polifolia	30	*Picea mariana*	15+		
	Chamaedaphne calyculata	10				
	Eriophorum angustifolium	5				
	Eriophorum vaginatum	<5				
	Oxycoccus microcarpus	<5				
	Vaccinium vitis-idaea	10				
	Sphagnum spp	100				
3-3	*Chamaedaphne calyculata*	20	*Picea mariana*			
	Andromeda polifolia	20	*Larix laricina*			
	Eriophorum vaginatum	10	*Betula papyrifera*			
	Smilacina trifolia	50				
	Ledum groenlandicum	10				
	Rubus chamaemorus	<5				
	Eriophorum angustifolium	50				
	Sphagnum spp	100				
	Oxycoccus microcarpus	30				

Forbs/Shrubs			Trees			
Plot	**Species**	**Cover (%)**	**Species**	**Class**	**Circum.**	**Count**
3-5	*Chamaedaphne calyculata*	40	*Picea mariana*			
	Ledum groenlandicum	25	*Picea mariana*			
	Rubus chamaemorus	60	*Picea mariana*			
	Eriophorum vaginatum	<5	*Picea mariana*			
	Epilobium angustifolium	5	*Picea mariana*			
	Picea mariana	<5	*Picea mariana*			
	Carex ssp	<5				
	Kalmia polifolia	10				
	Andromeda polifolia	<5				
	Oxycoccus microcarpus	<5				
	Vaccinium vitis-idaea	<5				
3-6	*Smilacina trifolia*	75	*Picea mariana*	Sapling		12
	Ledum groenlandicum	40	*Picea mariana*	3-6	4.5	2
	Chamaedaphne calyculata	10	*Picea mariana*	6-9	7	2
	Rubus chamaemorus	30	*Picea mariana*	9-12		0
	Picea mariana	15	*Picea mariana*	12-15		0
	Vaccinium vitis-idaea	30	*Picea mariana*	15+	28	5
	Oxycoccus microcarpus	<5				
	Andromeda polifolia	5				
	Carex ssp	<5				
3-7	*Ledum groenlandicum*	40	*Picea mariana*	0.5-3		8
	Kalmia polifolia	<5	*Picea mariana*	3-6	7	7
	Vaccinium vitis-idaea	25	*Picea mariana*	6-9	12.7	6
	Oxycoccus microcarpus	<5	*Picea mariana*	9-12	12.1	1
	Smilacina trifolia	5	*Picea mariana*	12-15	11.5	5
	Rubus chamaemorus	<5	*Picea mariana*	15+	27.4	4
	Picea mariana	20				
	Sphagnum spp	100				
4-1	*Ledum groenlandicum*	20	*Picea mariana*	Sapling		17
	Smilacina trifolia	40	*Picea mariana*	3-6	6	5
	Chamaedaphne calyculata	30	*Picea mariana*	6-9	7.3	4
	Kalmia polifolia	40	*Picea mariana*	9-12		
	Picea mariana	<5	*Picea mariana*	12-15	16.1	1
	Eriophorum angustifolium	<5	*Picea mariana*	15+	26.1	1
	Oxycoccus microcarpus	10				
	Andromeda polifolia	5				
	Sphagnum spp	100				
4-2	*Ledum groenlandicum*	60	*Picea mariana*	Sapling		12
	Kalmia polifolia	10	*Picea mariana*	3-6	6.5	4
	Eriophorum vaginatum	<5	*Picea mariana*	6-9		
	Rubus chamaemorus	30	*Picea mariana*	9-12	11.3	1
	Smilacina trifolia	10	*Picea mariana*	12-15	16.1	2
	Andromeda polifolia	5	*Picea mariana*	15+	26.1	6
	Picea mariana	<5				
	Oxycoccus microcarpus	10				
	Sphagnum spp	100				

Forbs/Shrubs			Trees			
Plot	**Species**	**Cover (%)**	**Species**	**Class**	**Circum.**	**Count**
4-3	*Eriophorum vaginatum*	20				
	Chamaedaphne calyculata	10				
	Ledum groenlandicum	35				
	Kalmia polifolia	25				
	Andromeda polifolia	20				
	Smilacina trifolia	50				
	Rubus chamaemorus	5				
	Oxycoccus microcarpus	<5				
	Vaccinium vitis-idaea	<5				
	Sphagnum spp	100				
	Eriophorum angustifolium	10				
4-5	*Ledum groenlandicum*	50	*Larix laricina*	Sapling		12
	Larix laricina	5				
	Smilacina trifolia	80				
	Vaccinium myrtilloides	5				
	Chamaedaphne calyculata	15				
	Rubus chamaemorus	<5				
	Oxycoccus microcarpus	30				
	Epilobium angustifolium	5<				
	Kalmia polifolia	<5				
	Andromeda polifolia	<5				
	Juncus bufonius	20				
	Eriophorum vaginatum	<5				
4-6	*Ledum groenlandicum*	15	*Picea mariana*	Sapling		7
	Kalmia polifolia	<5	*Picea mariana*	3-6	7.7	13
	Vaccinium myrtilloides	50	*Picea mariana*	6-9	8.8	5
	Cornus canadensis	<5	*Picea mariana*	9-12	12.8	2
	Rosa acicularis	<5	*Picea mariana*	12-15	15	7
	Carex ssp	<5	*Picea mariana*	15+		0
	Vaccinium vitis-idaea	<5				
	Equisetum arvense	<5				
4-7	*Ledum groenlandicum*	30	*Larix laricina*	Sapling		1
	Picea mariana	35	*Larix laricina*	15+	22.1	1
	Vaccinium myrtilloides	65	*Picea mariana*	Sapling		11
	Vaccinium vitis-idaea	20	*Picea mariana*	3-6	5.9	13
	Kalmia polifolia	15	*Picea mariana*	6-9	8.5	8
	Betula glandulosa	5	*Picea mariana*	9-12	16	5
			Picea mariana	12-15	21.5	4
			Picea mariana	15+	20	4

(Source: Jenna K. Pilon, Tristan Gingras-Hill and Terry Osko)

Appendix 4

Peat Core Lab Observations

Core ID	Field Length (cm)	Lab Length (cm)	Lab Observations
1-1	**72**	**70**	Small webs upper 10cm Bottom 8cm same small fibrous webs Organic material transition into clayey material ~30cm 40cm-79cm very fine organic decomposed material, small quantity of visible vegetation
1-2	**81**	**80**	Bottom 7cm compressed; crushed and in pieces Plant material distinct and complete up to 33cm From 1-43cm plant material easily recognizable 1-43cm: light yellowish brown 43-75cm: Medium dark brown 43-70cm: plant material recognizable 70-80cm: brown black; little to no distinctive plant material
1-3	**83**	**83**	Intact green mosses @core top Top (0cm)-50cm: plant structures identifiable 75-83cm: plant structure vaguely recognizable Top-10cm: light (spongy) brown; plant structures easily identified 10-52cm: medium brown; easily identifiable bits of plant material 52-65cm: dark brown; twigs easily identified- fibrous bits and pieces of vegetation 65-78cm: very dark brown; starting at 65cm, mulched fibrous vegetation strands (hair like) become less obvious 78-83cm: black brown; muddy texture Cluster of wood chips present at 48cm
1-4	**70**	**60**	organic layer ends at 38.5cm Mineral layer broken in pieces Upper 11cm very dry, distinguishable decomposed vegetation Compressed – Moisture loss 0-24cm range= distinguishable decomposed vegetation, disappears at 24cm 0-11cm= dry, yellow brown distinguisable peat 11-24cm= light brown, visibly compressed vegetation 24-38.5cm= dark brown, little to no visible vegetatio
1-5	**100**	**100**	Great condition Bottom appeared to be slightly crumbled Moist Top 40cm: compressed peat, spongy texture, easily distinguishable Top 20cm: medium brown, visible leaves, twigs, roots, & mulched bits of vegetation- easily recognizable 20-30cm: light yellow/tan- same texture at the top 20cm range 30-40cm: lighter brown, visible twigs, same spongy/texture, somewhat yellow in colour, fibrous 40-50cm: dark brown, muddy texture, few visble & identifiable bits/pieces of moderately decomposed 60-75cm: black brown, muddy texture, little distinctive plant material 75-100cm: black, small fibrous strands (as seen throughout the entire core), indistinctive plant structures 60-100cm range: small pieces of decomposed woody material

Core ID	Field Length (cm)	Lab Length (cm)	Lab Observations
1-6	**106**	**95**	Compact bottom Overall good condition
1-7	**90**	**90**	Bottom 12cm detached- pieces broke off most likely during transport, loss of moisture versus upper profile Small white specks- possible mold or other bacteria growth in 20-23cm range (8 visible specks total) Small white fibrous webbing- upper 9cm Mosses distinctive- upper 9cm Living moss layer ~4cm in thickness Bottom 30cm (60-90cm range) very dark- black brown 10-60cm range- medium dark brown Top 4cm living moss layer
2-1	**104**	**97**	Good condition 0-19cm: yellow brown peat with visible green mosses, clearly visible & distinguishable vegetation 19-35cm: medium brown, few distinguishable bits of vegetation 35-56cm: dark brown, small scattered bits of in-distinguishable decomposed plant material, muddy texture 56-97cm: black brown, barely any visible pieces of decomposed plant structure, small pieces of decomposed wood near bottom @66-97cm
2-2	**100**	**99**	Upper 15cm contains green mosses Twigs visible up until ~70cm Upper 10cm very fibric, spongy, yellow with some green mosses, discernible leaves, grasses, vegetation easily recognizable 15-60cm: medium brown, yellowish. Vege still identifiable, spongy texture 60cm zone (+/- 10cm): transition from spongy to muddy texture 70-80cm: medium dark brown- some bits of mulched vegetation, recognizable but vague, muddy texture 80-99cm: black brown, muddy, thick, no visible vegetation, if there is any vegetation it's not easily recognizable 85-95cm: large cobbles
2-3	**92**	**86**	Top: spongy upper layer slightly compressed Upper 13cm spongy texture, green mosses, light yellow peat, easily distinguishable vegetation 13-36cm: light brown, distinguishable plant structure 36-78cm: medium dark brown, fewer visible strands of distinguishable plant material, large pieces of decomposed wood Bottom slightly crumbled- overall good condition
2-4	**62**	**35**	Dark brown/black thick mud/clayey material Consistent geologic material throughout Few distinguishable organics- bottom intact 10cm, upper 10cm slightly lighter brown, more dominance of distinguisable wood chips Bottom crumbled
2-5	**76**	**76**	Good condition
2-6	**106**	**94**	Upper 10cm of peat compressed, Some living mosses at the top of core, top- abundance of twigs & leaves Upper 10cm- peat layer- visble and easily distinguised decomposed vegetation 10-26cm: slightly more decomposed, medium dark brown, not easily identifiable plant structures 26-61cm: dark brown, few visble indistinctive pieces of decomposed plant material 61-86cm: black brown, some distinct plant (stringy, thin, yellow, hair like fibrous material) matter and silica grains Large break in core at 72cm 70-90cm: severe loss of moisture, bottom 30cm (70-90range) broken into blocks due to mositure loss Mineral layer starting at ~93cm
2-7	**25**	**21**	Compact bottom Moisture loss

Core ID	Field Length (cm)	Lab Length (cm)	Lab Observations
3-1	**120**	**114.3**	Good condition Bottom 20cm compact but still intact
3-2	**88**	**83.5**	Bottom slightly compressed Smells like freshly chopped wood/fresh pine needles Upper 15cm visible green mosses, recognizable plant matter Peat, roots, plant matter clearly visible up to 75cm At 70-83.5cm: dark brown to brown black At 60-70cm: Medium dark brown At 50-20cm: light brown At 20-10cm: distinctive plant matter, green moss, twigs, roots, leaves
3-3	**110**	**96**	Bottom 9cm compact
3-4	**40**	**39.5**	Bottom compact
3-5	**81**	**75**	40-75cm range: pieces broke off most likely from travel- easily reconstructed 1-40cm: Intact Upper 6cm: light fibrous brown peat, with green mosses- excellent condition 54-75cm range: geologic material layer- coarse grained sand, some roots Geologic material very soft, easily squished Break in core at 40cm Mineral layer dark at Interface, entire layer itself light brown in colour and covered in silica grains 10-20cm: medium dark brown 20-40cm: dark brown 40-48cm: very dark medium brown 48-75cm: brown black
3-6	**77**	**30**	Bottom ~2cm of core- visible decomposed plant fibres Beige coarse grained silca grains at bottom Compressed upper 1cm of core (core most likely slid down to the 'top' end of the box during transport, compressed upper 1cm) Top 4cm clearly distinguisable plant material- visible moss, roots, leaves and twigs 4-13cm: light brown with little visible, intact plant material- not easily identifiable 13-18cm: medium dark brown, no distinct plant material18-30cm: black/brown- no visible plant material 22-24cm: small white specks of mold or other baterial growth (8 total)- forming along break in core Overall great condition, good condition after travel
3-7	**35**	**32**	Compressed bottom

Core ID	Field Length (cm)	Lab Length (cm)	Lab Observations
4-1	**91**	**90**	Upper 10cm very spongy, yellow mosses, vegetation intact Upper 5cm- dominated by yellow/light brown spongy moss, some green vegetation 10-40cm profile: light brown, not as much yellow colour, still spongy 40-70cm: medium brown- more compact, slightly more muddy, thick texture, slight spongy feel, vegetation still identifiable 70-90cm: medium dark brown, dominant pasty muddy texture, very slight spongy texture vegetation mulched into bits: fibers (roots?) and wood pieces 50cm: strip of yellow grass layer- bright goldish yellow in colour
4-2	**108**	**108**	Upper 1-15cm, fibrous yellow brown peat, very light, soft & spongy 20-65cm: medium dark brown 1-20cm: easily identifiable plant organic matter 20-80cm: scattered pieces of grasses and roots, few visible/easily identifiable plant pieces 65-78cm: dark brown- very few easily seen grass bits/roots/decomposed material 78-108cm: black brown- no visible plant material 100-108cm: pieces of decomposed wood cluclumped together wood pieces at bottom ranged in length from 6.5 to 12cmmped together
4-3	**111**	**96**	Compact bottom
4-4	**45**	**42**	White spots dominated the bottom half of the core Top half dominated with small blueish/green spots- mold?
4-5	**77**	**64**	Bottom crumbled off- most likely from transport Upper 60cm of profile good condition- fully intact -no breaks Upper 10cm fully distinguishable decomposed peat No living moss at the top of profile top 10cm= light brown/yellowish brown 10-31cm range= light brown, visible vegetation 31-45cm range= medium dark brown- little to no decomposed vegetation 45-64cm range= brown black, no clearly seen/ visible pieces of decomposed vegetation
4-6	**30**	**11**	Only upper 11cm of core intact Bottom- coarse grained sand, visible grains, completely crumbled Top of the core covered in green reindeer lichen Sand: yellow/tan/beige in colour
4-7	**33**	**24**	soil layer: upper 20cm pure plant material, shallow peat Very compact few pieces split off bottom

4-4 (extra)	**60**	**60**	Highly compact throughout Upper 5cm (0-5cm): clear vegetation, compact, yellow, brown, white in colour, very dry, not distinguishable 30cm down- pieces crumbled, easily reassembled 0-25cm: white patches- mildew?- highly concentrated in 5cm-15cm zone colouration very consistent light brown: 0-4cm medium brown: 4-23cm dark brown: 23-60cm 6-60cm: very little plant/fibrous material, little observable distinct vegetation, some wood chunks @ 29cm & 60cm Severe loss of moisture

Appendix 5

Von Post Scale of Humification

Von Post Scale of Humification: Transect 1							
Depth (cm)	**1-1**	**1-2**	**1-3**	**1-4**	**1-5**	**1-6**	**1-7**
10	H1	H1	H2	H3	H1	H2-H3	H3
20	H2	H1	H2	H3	H1	H3	H3
30	H2	H1	H2	H3	H2	H3	H3
40	H3	H1	H2	H3	H2	H3	H3
50	H4	H2	H2	H4	H3	H3	
60	H6	H4	H3	H4	H3	H3	
70			H4		H5	H4	
80			H5		H5	H4	
90					H6		
100					H7		

Von Post Scale of Humification: Transect 2							
Depth (cm)	**2-1**	**2-2**	**2-3**	**2-4**	**2-5**	**2-6**	**2-7**
10	H1	H1-H2	H1	H3	H1	H1	H1
20	H3	H2	H2	H3	H3	H3	H2
30	H3	H2	H2	H4	H3	H3	
40	H4	H2	H3		H4	H5	
50	H4	H2-H3	H3		H4	H5	
60	H4	H4	H4		H5	H6	
70	H4	H5	H4		H6	H6	
80	H4	H6	H5			H7	
90	H5	H6					
100							

Von Post Scale of Humification: Transect 3							
Depth (cm)	**3-1**	**3-2**	**3-3**	**3-4**	**3-5**	**3-6**	**3-7**
10	H2	H1	H1-H2	H6	H2	H2	H1
20	H2	H1	H2	H7	H3	H3	H1
30	H2	H2	H3	H7	H3	H5	H2-H3
40	H2	H2	H3		H3		
50	H3	H3	H4		H5		
60	H3	H4	H5		Mineral		
70	H3	H5	H6		Mineral		
80	H7	H6	H7				
90	H8						
100							

Von Post Scale of Humification: Transect 4							
Depth (cm)	**4-1**	**4-2**	**4-3**	**4-4**	**4-5**	**4-6**	**4-7**
10	H2	H1-H2	H3	H3	H3	H2	H1-H2
20	H2	H2	H3	H3	H3-H4		H2
30	H2	H2	H3	H4	H4		
40	H2-H3	H2	H3	H4	H4		
50	H3	H3	H4	H6	H4		
60	H4	H4	H4-H5	H6	H5		
70	H4-H5	H4	H5				
80	H7	H4	H5				
90	H7	H4					
100		H4					

Appendix 6

Fort McMurray Precipitation Data

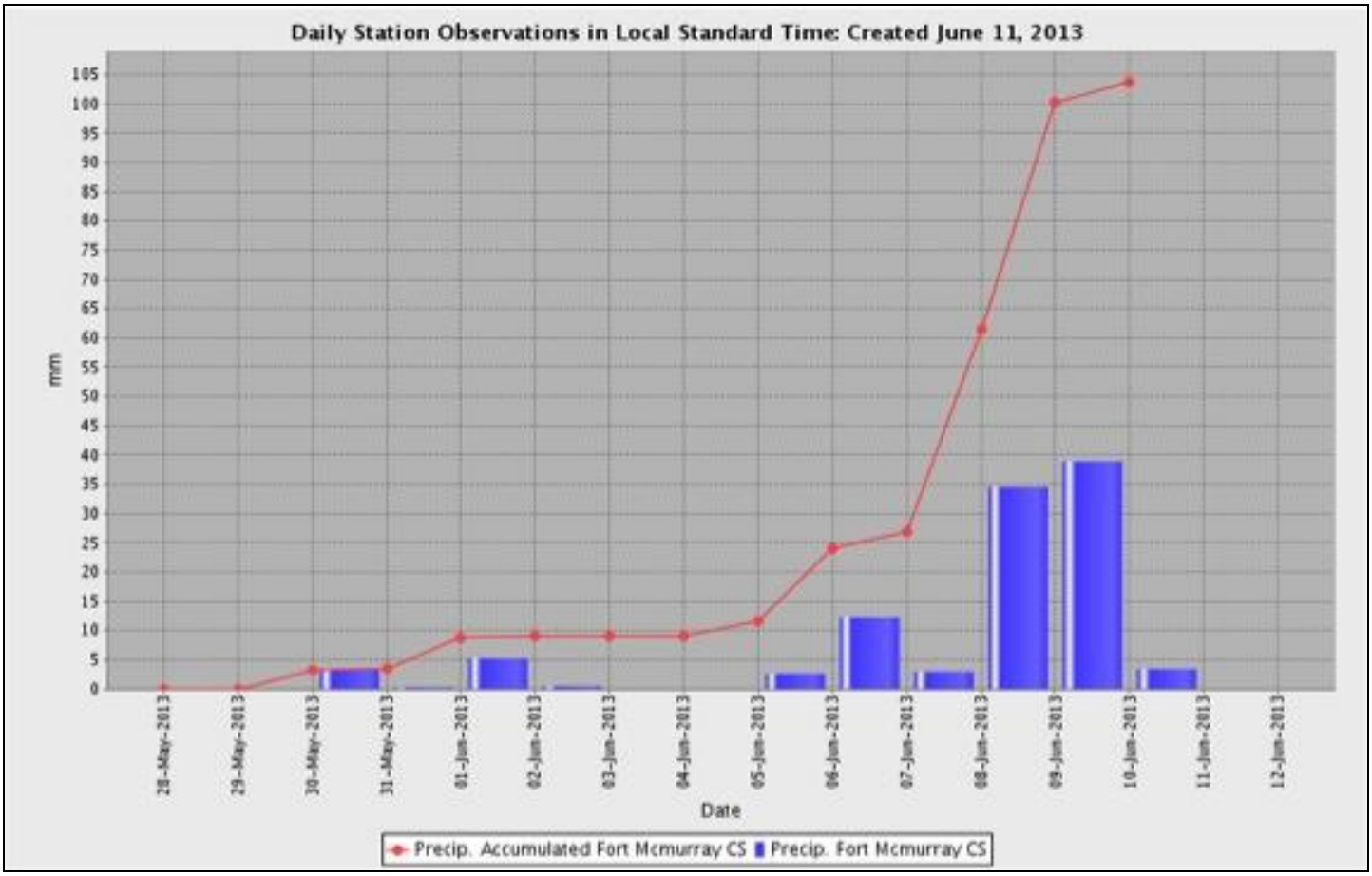

(Source: Fort McMurray Airport Weather Station; Environment Canada)

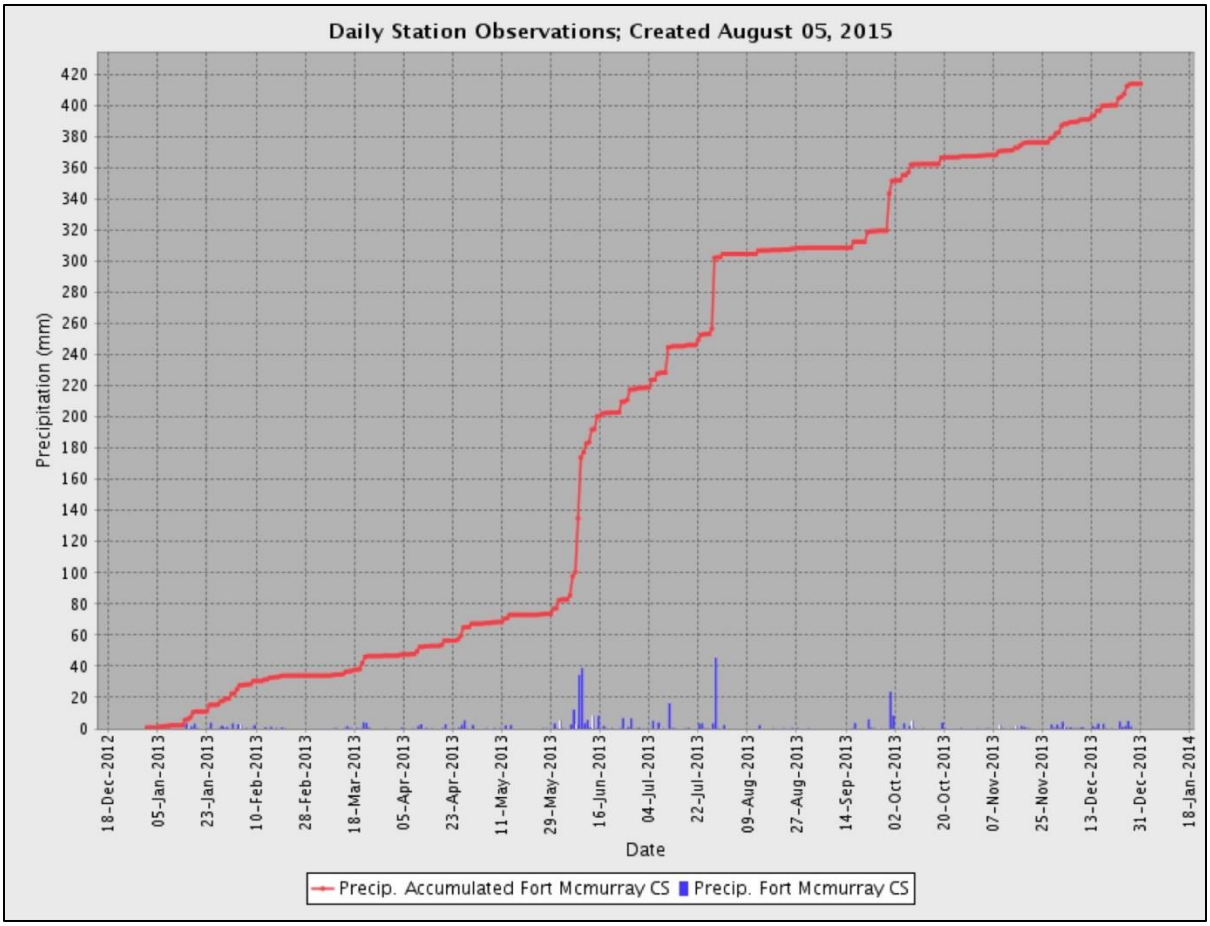

(Source: Fort McMurray Airport Weather Station; Environment Canada)

Appendix 7

Anisotropy: Values and Ratios

		K_v	K_h	Anisotropic Ratio
Road	1_4	0.00283	0.000744	3.8
	2_4	0.0000751	0.00113	0.066
	3_4	0.00363	0.00000631	575
	4_4	0.00154	0.00079	1.9
West	1_1	0.000399	0.00011	3.6
	1_2	0.000554	0.00689	0.080
	1_3	0.000625	0.00101	0.62
	2_1	0.000393	0.00321	0.12
	2_2	0.00457	0.00245	1.9
	2_3	0.00223	0.000412	5.4
	3_1	0.0000701	0.000696	0.10
	3_2	0.0000552	0.0000481	1.1
	3_3	0.0000619	0.0000991	0.62
	4_1	0.000155	0.000319	0.489
	4_2	0.000401	0.000589	0.68
	4_3	0.0021	0.000275	7.6
East	1_5	0.0000404	0.00056	0.072
	1_6	0.000499	0.0000254	19
	1_7	0.00371	0.000219	17
	2_5	0.000479	0.000349	1.4
	2_6	0.000147	0.000574	0.26
	2_7	0.0055	0.00229	2.4
	3_5	0.00138	0.0013	1.1
	3_6	0.0000696	0.000557	0.12
	3_7	0.0000896	0.00188	0.048
	4_5	0.00201	0.000394	5.1
	4_6	0.0059	0.00381	1.5
	4_7	0.000647	0.00453	0.14